MECHANISTIC STUDIES OF PHOTOELECTROCHEMICAL SYSTEMS

by

John Philip Davies

A thesis submitted for the degree of Doctor of Philosophy of the University of London and for the Diploma of Membership of Imperial College

Chemistry Department
Imperial College
London
SW7 2AY

February 1985

ABSTRACT

This thesis is concerned with the study of photogalvanic cells based on two types of photosensitiser; water-soluble thiazine dyes and metalloporphyrins. Kinetic parameters for both of these systems have been studied using the Optical Rotating Disc Electrode (ORDE) and the theory for this technique has been further developed.

ORDE results for the water-soluble thiazine dye DMST2 have been compared to results obtained using flash photolysis, flash electrolysis and stopped flow. A complete description of the iron-DMST2 system is given in terms of quantum efficiencies for the production of semithiazine and leucothiazine and rate constants for the reactions of these species.

Studies of the water-soluble metalloporphyrin $ZnTMPyPCl_4$ using the ORDE technique allowed us to calculate rate constants for the electron transfer quenching reaction and for reverse reaction of the photoproducts. An unexpected feature of the work on $ZnTMPyCl_4$ was that increasing the concentration of quencher decreases the yield of photoproducts above an optimum quencher concentration. A mechanism involving the formation of a complex between the photo-excited metalloporphyrin and quencher species is proposed which is shown to be consistent with the experimental observations.

The results obtained for both the thiazine system and the metalloporphyrin system are considered in the light of requirements for an ideal photogalvanic cell.

For Mary

ACKNOWLEDGEMENTS

I would like to thank:

John Albery for providing encouragement, supervision and much food for thought.

All of the research group and, in particular:-

Steven Fisher

Andrew Foulds

Philip Bartlett

Rob Hillman

Steve Wilson

Mike Pritchard

Jack Porter

Lionel Milgrom

Peter Tebbut and

Nick Goddard

Richard Compton for help with units.

Jim Darwent, while at the Royal Institution and at Birkbeck College for help with all of the flash photolysis experiments.

Gail Craigie for typing the manuscript.

The SRC for their financial support.

CONTENTS

FIGURES

TABLES

Chapter 1

INTRODUCTION

In 1839, Bequerel[1] found that a current flows when two identical electrodes immersed in a dilute acid solution are illuminated. This was the first observation of a photoelectrochemical effect and since then many other systems have been investigated which show an electrochemical change on illumination. These systems may be divided into three main groups according to where the light is absorbed:

(1) Absorption by an electrode (e.g. at a semiconductor-electrolyte interface) - photovoltaic cells[2,3].

(2) Absorption at the surface of an electrode (e.g. in a dye layer attached to the surface of an electrode) - dye sensitised electrodes[4,5].

(3) A homogeneous photochemical reaction yields electroactive products which diffuse to and react at an electrode - photogalvanic cells[6].

This thesis is principally concerned with the third of these categories - photogalvanic cells.

In a typical photogalvanic cell (figure 1.1), light enters through a transparent electrode and is absorbed by a dye, A. Electron transfer quenching then occurs between the excited dye molecule and a species Z, producing electroactive products B and Y.

The reaction schemes for the dye couple A/B and the quencher couple Y/Z are shown below.

Figure 1.1. A typical photogalvanic cell.

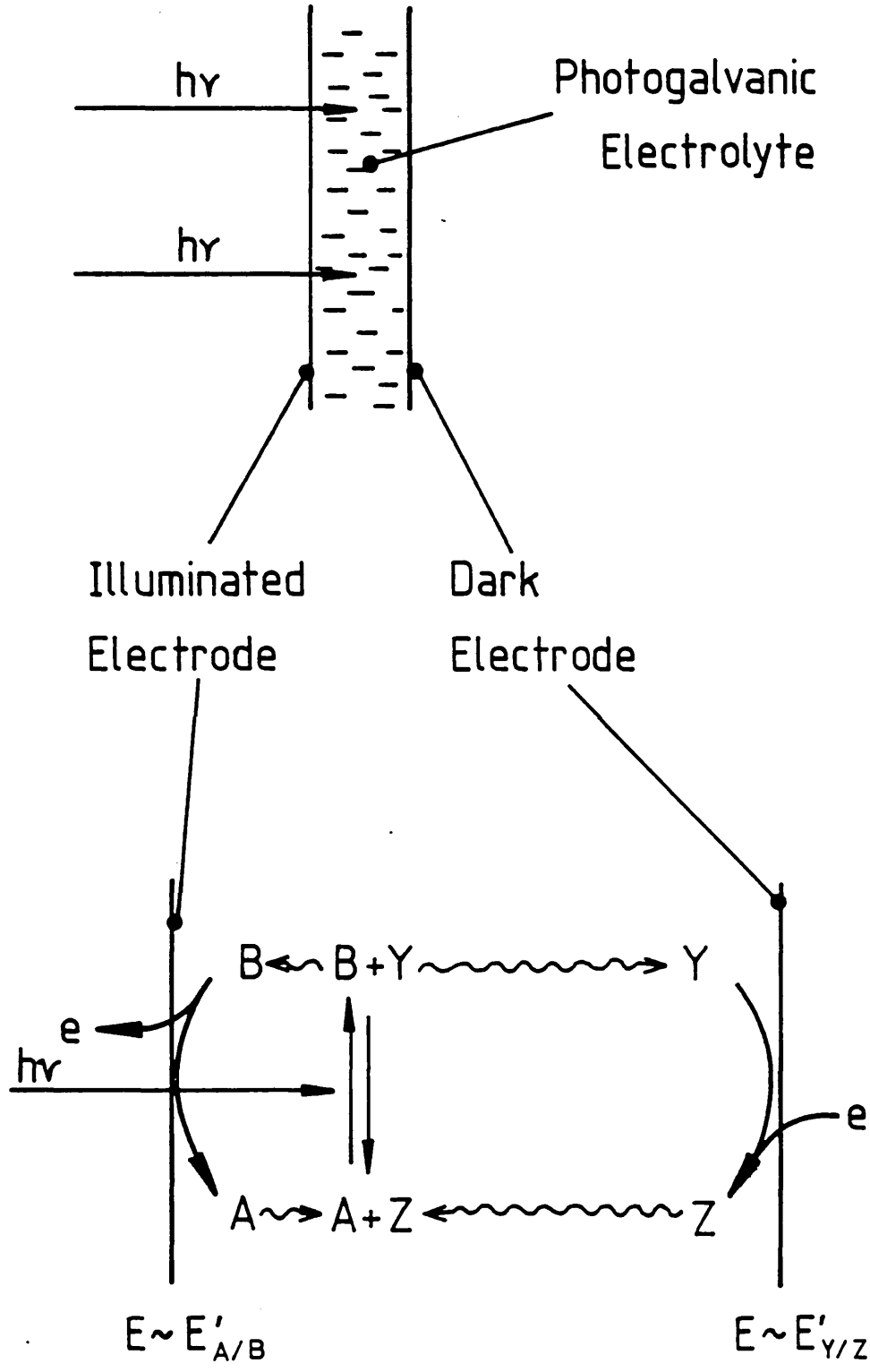

Figure 1.2. Operation of a photogalvanic cell.

In the dark $A + Z \rightleftharpoons B + Y \quad K << 1$

Under illumination

$$A \xrightarrow{h\nu} A^*$$

$$A^* + Z \xrightarrow{K_Q} B + Y$$

At the electrodes

$$B \longrightarrow A \pm e^-$$

$$Y \pm e^- \longrightarrow Z$$

Thermal back reaction

$$B + Y \xrightarrow{k_{-2}} A + Z$$

1.1. Essential Features of a Photogalvanic Cell

For the cell to work, the reaction at the electrodes supplying power to an external load must be exergonic. It follows then that the photolysis reaction forming the electroactive products must be an endergonic process. A second requirement of the system is that the products of the photolysis reaction must be completely returned to their starting materials in a cyclic fashion.

A photogalvanic cell based on an aqueous electrolyte will have a high ionic strength. This means that any electric field effects will be negligible and that transport of species within the solution will be by diffusion. However, the electroactive products B and Y can diffuse to either electrode and so the cell must have differential

electrode kinetics if the electrodes are not merely to catalyse the back-reaction.

There are sixteen combinations in which the two couples are reversible (active) or irreversible (inactive) at the two electrodes. Of these, eight combinations have both couples irreversible at one or both of the electrodes. With this situation no current could flow and so the cell will not produce any power. In a further four of the combinations, the Y/Z couple is reversible at both electrodes. No voltage is produced in this arrangement because of the proportionately small change in concentration of the species in the Y/Z couple upon illumination. The remaining four combinations are shown in table 1.1 and are described below.

Case 1

We can reject case 1 because both couples are reversible at the illuminated electrode. The electrode can catalyse the back reaction and no net electron transfer occurs.

Case 2

In this arrangement, both electrodes are selective for the A/B couple. This would be the case if both electrodes were made of the same material. The device works as a concentration cell, that is, by differences in the concentration of the A/B couple at the two electrodes. Albery and Archer[7] have shown that a large potential can be achieved at open circuit, but when a load is applied the potential will only be $\simeq RT/F$, i.e. about 59 mV. Under open circuit conditions a large difference can be maintained between the concentrations of B at the two electrodes, but when a current passes it lowers this difference

Table 1.1

Possible Combinations of Reversible (R) and Irreversible (I) Electrode Kinetics for a Photogalvanic Cell

	Illuminated Electrode		Dark Electrode		
Couple	A/B	Y/Z	A/B	Y/Z	
Case 1	R	R	R	I	Reject
Case 2	R	I	R	I	concentration cell
Case 3	R	I	I	R	Differential Electrode Kinetics
Case 4	R	I	R	R	Differential Electrode Kinetics

and the voltage is considerably reduced. A photogalvanic cell with both electrodes selective for the A/B couple would thus have a maximum efficiency of less than 0.3%.

Case 3

The electrodes can discriminate between the two couples so that B and Y may be separated. This means that the cell voltage is simply the difference in the electrode potentials of the two couples, and $N_{h\nu}$ (the photoelectrochemical collection efficiency) approaches the value of ϕ, the quantum efficiency for generation of B and Y. The electrode selectivity of this system gives a theoretical maximum efficiency of 18%[8] for conversion of light into electrical energy.

Case 4

In an ideal cell, all of the light will be absorbed close to the transparent electrode and none will reach the other side of the cell. The cell is then said to be differentially illuminated. Species B is generated close to the illuminated electrode and so it does not have to diffuse far to react. However, B cannot reach the dark electrode as it will be destroyed by reaction with Y. As a result, for a differentially illuminated cell, case 4 is effectively the same as case 3 - there is no need to differentiate between the two couples at the dark electrode because none of the species B reacts there.

The differential electrode kinetics in cases 3 and 4 means that B must only diffuse a relatively short distance to the illuminated electrode where it can react. Y must diffuse right across the cell to the dark electrode and because of this, the cell must be thin to prevent concentration polarisation which would reduce the current.

If the dye is not strongly absorbing, B is generated at a considerable distance from the illuminated electrode and will be destroyed by reaction with Y before reaching the electrode. Having a thin cell also helps to reduce ohmic losses.

These requirements suggest that an efficient photogalvanic system should consist of a strongly absorbing dye species A, between two closely spaced electrodes with differential electrode kinetics. A cell working according to these principles is shown in figure 1.2.

The conditions required for an efficient photogalvanic cell have been worked out by Albery and Archer[7-9] and their findings are discussed below.

1.2. Theoretical Analysis of the Photogalvanic Cell

The steady state concentration profile for B in a working photogalvanic cell is

$$\frac{D\partial^2[B]}{\partial x^2} + g - k_{-2}[B][Y] = 0 \qquad (1.1)$$

Diffusion — Photochemical generation — Back reaction

where

$$g = \phi I \varepsilon [A] \qquad (1.2)$$

and

D is the diffusion coefficient

x is the distance across the cell

ϕ is the quantum efficiency for generation of B

ε is the natural extinction coefficient of A

I is the flux of photons

k_{-2} is the back reaction rate constant

The first term describes transport of B by diffusion, the second term photochemical generation of B and the third term loss of B by reaction with Y. No convective term is included because we assume that the electrode spacing is too small for natural convection to occur. In this treatment it is assumed that the irradiance obeys the Beer-Lambert law,

$$I = I_0 \exp(-\varepsilon[A]x) \tag{1.3}$$

where

$I_0 = I$ at $x = 0$

The cell is best described in terms of the four characteristic lengths depicted in figure 1.3 and listed in table 1.2.

Detailed analysis[7-9] shows that the requirements for an efficient cell, based on the characteristic lengths, are as follows:

$$10X_\varepsilon \simeq 2X_k \simeq X_G < \tfrac{1}{2}X_\ell \tag{1.7}$$

X_k must be greater than X_ε, so that B is generated close enough to the illuminated electrode to reach it before being destroyed by reaction

Table 1.2

Characteristic Lengths in a Photogalvanic Cell

Name	Description	Symbol and Equation	
Cell Length	Distance between electrodes	X_ℓ	
Absorption length	Distance over which the light is absorbed	$X_\varepsilon = 1/\varepsilon[A]$	(1.4)
Generating length	Distance over which A can diffuse in the light flux I_o before being converted to B	$X_G = (D/\phi\varepsilon I_o)^{\frac{1}{2}}$	(1.5)
Kinetic length	Distance over which B can diffuse before being destroyed by reaction with Y	$X_k = (D/k_{-2}[Y])^{\frac{1}{2}}$	(1.6)

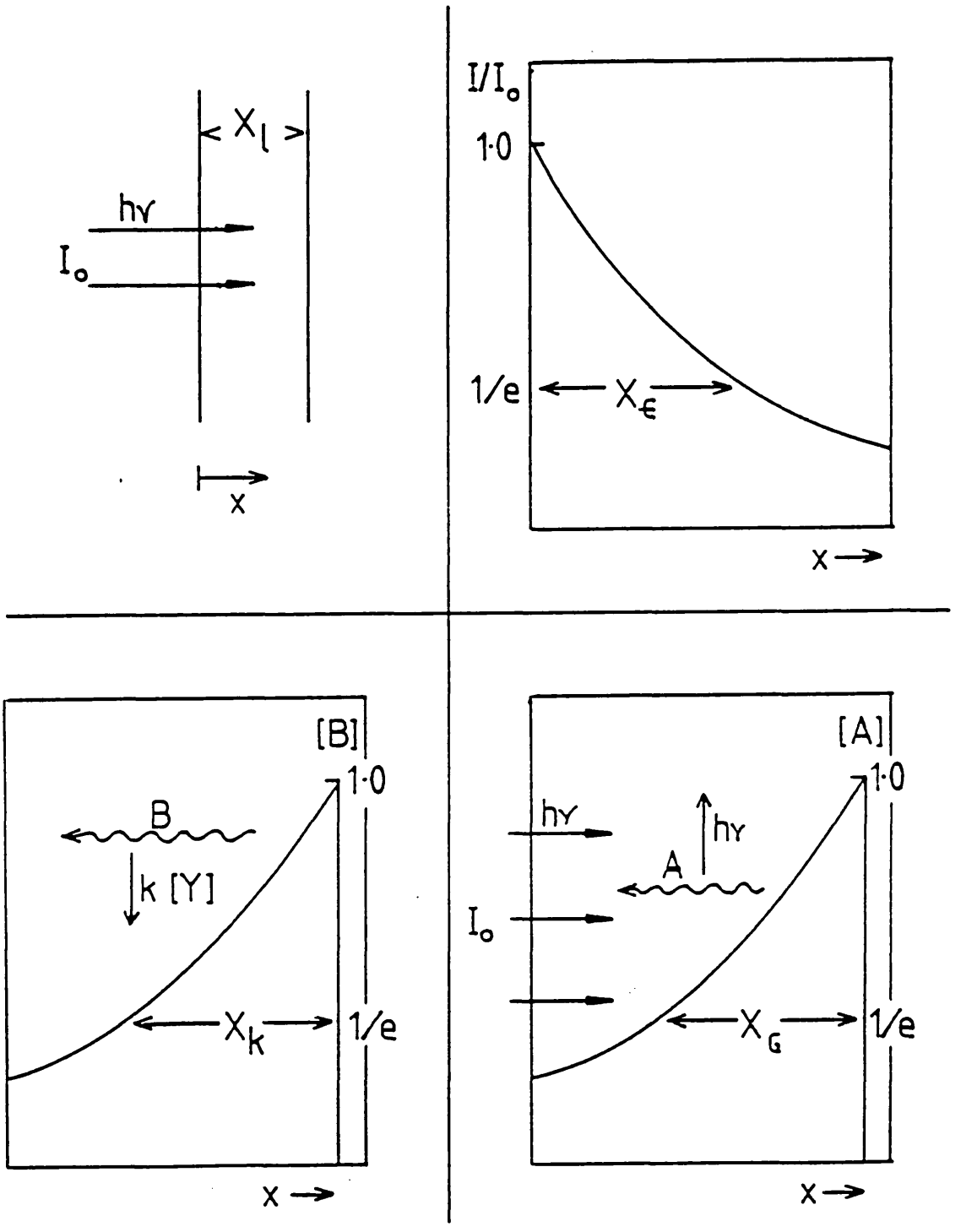

Figure 1.3. The characteristic lengths in table 1.2.

with Y. X_ε has to be an order of magnitude smaller than X_G to ensure that all of the light is absorbed without the solution becoming bleached and X_ℓ must be at least 20 times greater than X_ε so that B can only react at the illuminated electrode. This last condition also ensures that all of the processes occur within the length of the cell.

If we take a typical value for the solar irradiance, $I_o = 1.6 \times 10^{-7}$ mol cm^{-2} s^{-1}, and rather optimistic values for the system of $D = 10^{-5}$ cm^2 s^{-1}, $\varepsilon = 10^8$ cm^2 mol^{-1} and $\phi = 1$[8], we find that

$$X_G = 10^{-3} \text{ cm} \tag{1.8}$$

from which it follows that the ideal cell will have

$$X_k = 4 \times 10^{-4} \text{ cm} \tag{1.9}$$

$$X_\varepsilon = 10^{-4} \text{ cm} \tag{1.10}$$

$$X_\ell \geq 2 \times 10^{-3} \text{ cm} \tag{1.11}$$

From the value of X_k we find that $k_{-2}[Y] = 60$ s^{-1}.

The concentration of Y is fixed because Y must carry current across the cell without causing concentration polarisation at the dark electrode. Using the electron flux that would be flowing in an efficient cell we calculate that

$$[Y] \simeq 10^{-2}\ M \tag{1.12}$$

which means that $k_{-2} < 6000\ M^{-1}\ s^{-1}$.

An excited molecule of the dye A* may be subject to electron transfer quenching with Z, or to a thermal deactivation process.

$$A^* \xrightarrow{k_T} A$$

$$Z + A^* \xrightarrow{k_q} B + Y$$

If the electron transfer process is to predominate a high concentration of quencher is required such that

$$[Z] > k_T/k_q \tag{1.13}$$

In a working cell, however, a low concentration of Z is desirable to provide the maximum voltage difference between the two electrodes. For many systems a quencher concentration of 10 mM is enough to efficiently quench the dye. Therefore in a working cell we have

$$[Z] = 10^{-2}\ M \tag{1.14}$$

1.3. Concentration Profiles in a Cell

Concentration profiles for the ideal photogalvanic cell are shown in figure 1.4.

The diffusion of Y and Z across the cell in opposite directions requires that the concentration gradients of Y and Z at the dark electrode should be equal to the concentration gradient of B at the illuminated electrode. The concentration gradient of B extends over the absorption length which is shorter than the cell length, over which the concentration gradients of Y and Z occur. The concentrations of both Y and Z must therefore be significantly greater than the concentration of photo-generated B. This leads again to the requirement that

$$[Y] \simeq [Z] \simeq 10^{-2}\ M \tag{1.15}$$

1.4. Ideal Power Output

The ideal power conversion efficiency for a photogalvanic cell is about 18%. The maximum power output is given by[8]

$$W_m = 0.8F\phi I_o \Delta E^o \simeq 140\ Wm^{-2} \tag{1.16}$$

Before this efficiency can be achieved, the following, rather severe constraints must be satisfied.

(i) A must be a very soluble dye ($\simeq$ 0.1 M) with a high extinction coefficient.

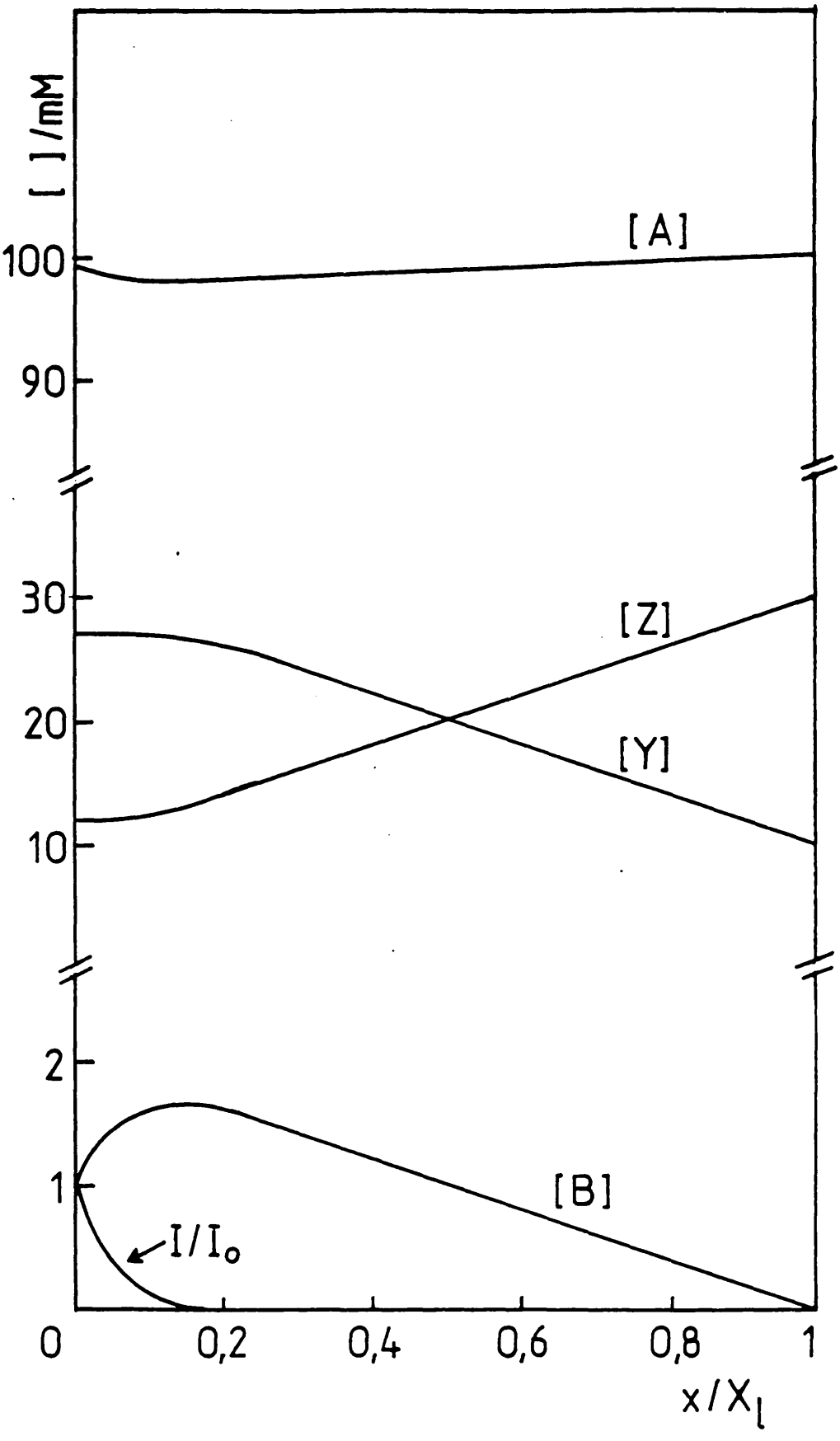

Figure 1.4. Concentration profiles in a photogalvanic cell. Note the changes in scale on the y-axis.

(ii) The electrode kinetics of the A/B couple at the illuminated electrode must be rapid ($k_B^{\prime} > 0.1$ cm s^{-1}).

(iii) The electrode kinetics of the Y/Z couple at the illuminated electrode must be very slow ($k_Y^{\prime} < 10^{-12}$ cm s^{-1}).

(iv) Despite the large thermodynamic driving force of $\simeq$ 1.1 V, back reaction between B and Y must be very slow ($k_{-2} < 6000\ M^{-1}\ s^{-1}$).

(v) The rate constant for quenching of A* by Z must be high, so that as much of the excited dye as possible can be converted to electroactive products. This means that $(k_q\tau)^{-1} < 10$ mM, where τ is the natural lifetime of A*.

1.5. Photogalvanic Systems

Systems based on the quenching of ruthenium complexes by Fe(III) have been studied by several workers[10-12]

$$\underset{A}{Ru(II)L_3} + \underset{Z}{Fe(III)} \rightleftharpoons \underset{B}{Ru(III)L_3} + \underset{Y}{Fe(II)}$$

where L is a ligand, e.g. 2,2'-bipyridine.

These systems have the advantage that ϕ, the quantum efficiency for production of B is close to unity but at present there are no electrodes available which are selective towards ruthenium complexes. Also, the back reaction, k_{-2}, is too fast to satisfy the condition required for X_k. By choosing different ligands, k_{-2} can be reduced but unfortunately this also lowers the cell voltage[31].

An efficiency of 0.3% has been reported for an iron-iodine photogalvanic system

$$2Fe^{II} + I_3^- \underset{\longleftarrow}{\overset{h\nu}{\longrightarrow}} 2Fe^{III} + 3I^-$$

In this cell the back reaction is very slow - the photostationary state takes several hours to decay, and a degree of selectivity is available, n-SnO_2 being selective for the Fe^{II}/Fe^{III} couple and glassy carbon for the iodine couple. However the power available from the cell is limited by the small difference between the standard electrode potentials of the two couples ($\Delta E^0 \simeq 236$ mV). Cells with rhodamine B as the dye species have also been investigated. In one system the excited dye is quenched by hydroquinone. The illuminated electrode is made of SnO_2, and this is partially selective towards the dye couple, the quinone/hydroquinone couple reacts at a gold electrode. In another system Fe(III) acts as the quencher but because Fe(III) is fairly irreversible on SnO_2, both of the electrodes must be made of gold. The low efficiency of these cells is thought to be due to a high rate constant for the back reaction and to irreversible reactions of the oxidised and reduced dye species.

1.6. The Iron Thiazine Photogalvanic System

Thionine and its one electron and two electron reduction products, semithionine and leucothionine are shown in figure 1.5.

The photobleaching of aqueous acidic solutions of thionine in the presence of ferrous salts was first observed by Weiss[43]. The system was first used to convert light into electricity in a photogalvanic cell

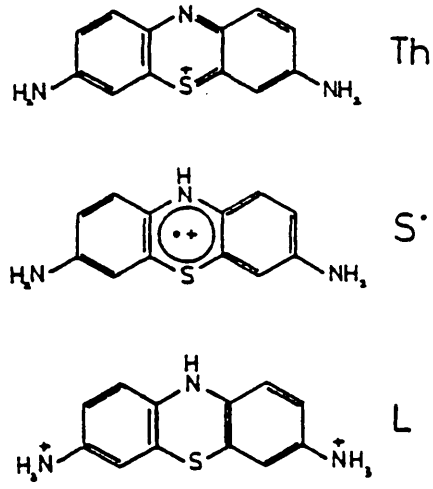

Figure 1.5 The structures of thionine, semithionine and leucothionine

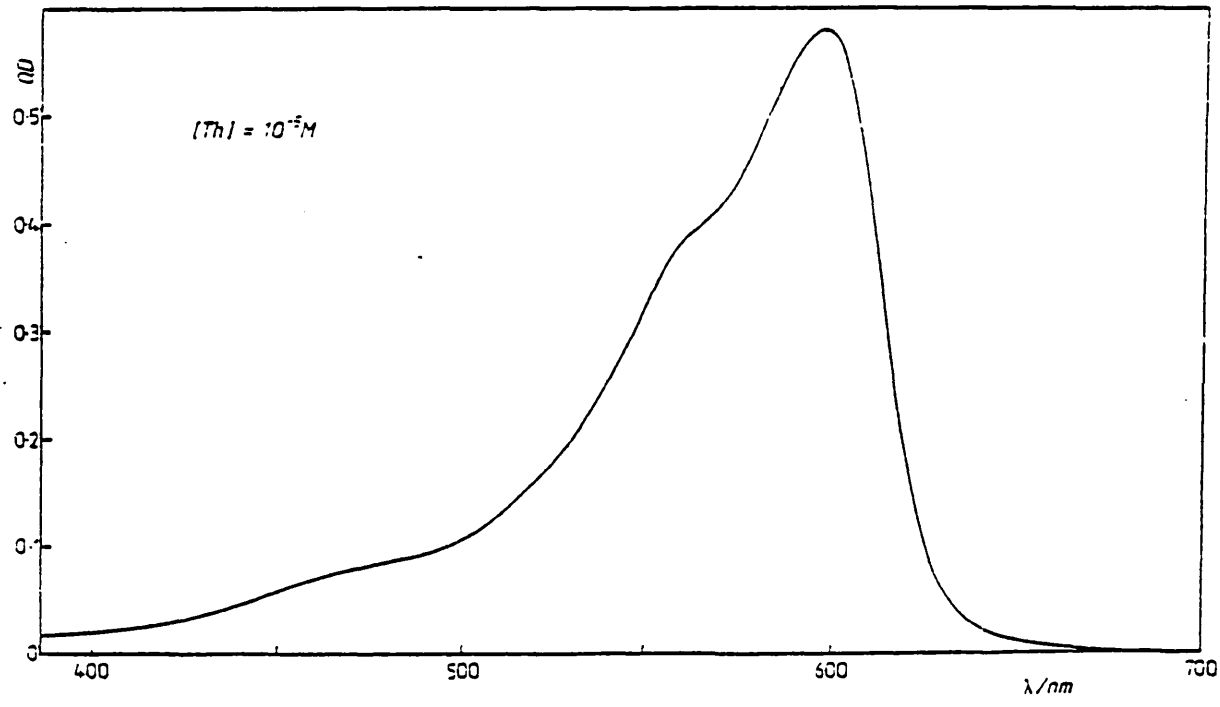

Figure 1.6 Absorption spectrum of thionine

by Rabinowitch[14]. The visible spectrum of thionine is shown in figure 1.6, the absorption is a singlet-singlet transition. In sulphate medium, the fluorescence lifetime is 345ps[15] and the fluorescence yield is 0.047[15].

The excited singlet undergoes efficient intersystem crossing to a triplet with a lifetime of 20 μs[16], and in the presence of ferrous ions this triplet state is subject to electron transfer quenching to produce ferrous, and the semithionine radical ($S^{\cdot}$). These reactions are summarised below

$$Th \xrightarrow[599\ nm]{h\nu} {}^1Th^* \qquad \varepsilon = 5.6 \times 10^4\ dm^3\ mol^{-1}\ cm^{-1}$$

$${}^1Th^* \xrightarrow{k_{isc}} {}^3Th^*$$

$${}^3Th^* + Fe(II) \xrightarrow{k_Q} S + Fe(III) \qquad k_Q = 3.5\ (\pm 0.7) \times 10^9\ dm^3\ mol^{-1}\ s^{-1}\ (16,17)$$

The iron-thionine system is more complicated than the schematic A,B/Y,Z system because of the rapid disproportionation of the semithionine radical to form thionine and leucothionine[16,17].

The kinetic scheme may be conveniently depicted as follows[14,18,19]:

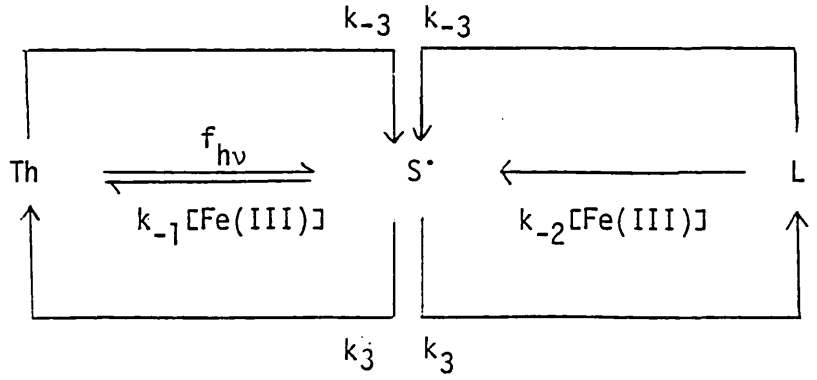

where

$$k_{-1} = 7.9 \times 10^4 \text{ dm}^3 \text{ mol}^{-1} \text{ s}^{-1} \quad (17)$$

$$k_{-2} = 2.6 \times 10^2 \text{ dm}^3 \text{ mol}^{-1} \text{ s}^{-1} \quad (17)$$

$$k_{-3} = 1.0 \times 10^4 \text{ dm}^3 \text{ mol}^{-1} \text{ s}^{-1} \quad (19)$$

$$k_3 = 2.4 \times 10^9 \text{ dm}^3 \text{ mol}^{-1} \text{ s}^{-1} \quad (16,17)$$

At moderate light intensities, when an appreciable amount of $S^{\cdot}$ is produced the dismutation is so rapid that most of the photoproduct is present as leucothionine.

One of the main problems with the iron-thionine system is the low solubility of thionine ($\simeq$ 50 μM in 50 mM H_2SO_4). In the ideal cell the dye has a concentration of about 0.1 M and the electrodes are differently illuminated - one electrode receives the full incident light intensity and the other electrode receives no irradiation. Because of the low solubility of the dye, Lichtin has investigated a cell using thionine in which both electrodes receive approximately the same irradiance, the totally illuminated-thin layer (or TI-TL) cell. For the cell to operate efficiently, both electrodes must be selective, because the dye couple is now available to react at both electrodes and not at one, as is the case with the differentially illuminated-thin layer cell. This type of cell is inefficient however, because the low dye concentration increases the likelihood of bleaching, with a consequent reduction in current[8].

Several different approaches have been suggested to increase the solubility of the dye couple. Another thiazine dye, new methylene blue is soluble up to approximately 10^{-1} M in aqueous solution[20], and this dye has been investigated by Albery and Foulds using the optical rotating disc (ORDE) technique[21]. The dye was found to dimerize at concentrations as low as 10^{-4} M and the action spectrum showed that the photoredox reaction is driven only by the monomer. ORDE experiments also showed that the

photoexcited dye is subject to diffusion controlled self-quenching by both the monomer and the dimer.

In another approach, Bowen[22] solubilised thionine in micellar sodium dodecyl sulphate solution. The surfactant increases the dye concentration from 50 μM to about 3 mM, however the micellar system was found to increase the back reaction rate constant from 430 $dm^3\ mol^{-1}\ s^{-1}$ to 1 x 10^6 $dm^3\ mol^{-1}\ s^{-1}$, and the quantum efficiency for leucothionine production was significantly reduced. The rate constant for the reaction of the dye couple at the illuminated electrode was also found to decrease.

Lichtin and co-workers have investigated the iron-thionine system in mixed aqueous-organic solvents. The solubility of thionine is increased to about 1 mM in 50% H_2O/MeCN solution. An increased rate constant for electron transfer quenching of the triplet dye is observed[23] in these systems, possibly caused by the complexation of Fe(II) leading to an anionic bridge between the dye and Fe(II).

Several approaches have been used to lower the rate constant for the back reaction in the iron-thionine system. Shigehara and co-workers[24,25] have studied a thin-layer cell in which thionine is bound to a cationic polymer. It is proposed that the back reaction is slowed by electrostatic repulsion between the polymer and Fe(III), although this will depend on the state of complexation of the ferric ion. The power available from the device was again lower than that for a simple iron-thionine cell because of the high internal resistance of the cell and slow diffusion of electroactive species within the gel medium.

It has been found that the addition of anions such as fluoride, citrate and 2-aminopropionate, which complex Fe(III) more strongly than Fe(II) can increase the power output from a thin-layer cell by as much as 500 times. The reasons for this are not fully understood, but it has been suggested that the rate of the back reaction is reduced by the

complexation. The standard electrode potential of the Fe(II)/Fe(III) couple will be reduced, leading to a greater cell voltage, and the electrochemical rate constant for the Fe(II)/Fe(III) couple will also be affected.

Recent studies of the reaction between leucothionine and Fe(III) have produced disagreement over the processes which are involved. Several workers[27-29] have shown that in the presence of excess ferric, the pseudo-first order rate of oxidation of leucothionine approaches a limiting value with increasing [Fe(III)]. This has been ascribed to the rapid, reversible formation of a complex between the two species. Brokken-Zijp and co-workers[19] have shown however, that the rate of reappearance of thionine depends on the concentration of thionine present in the solution. They emphasize the importance of the synproportionation reaction between thionine and leucothionine and the oxidation of semithionine by Fe(III), and suggest that the assumption of complex formation is not required to explain the non-pseudo first order behaviour.

The amount of incident radiation which can be utilized by a photogalvanic cell is limited by the relatively narrow absorption band of the photoreactive dye. The absorption efficiency can be increased by using several absorbing dyes. The added dye species may be photoreactive, e.g. other thiazine dyes, or they may be sensitisers which, although not photoreactive themselves are capable of absorbing light and transferring excitation energy to the photoreactive dyes. Lichtin and co-workers[30] found that the power output of a TI-TL cell can be increased if rhodamine 6G is added as a sensitiser.

Chapter 2

APPARATUS AND EXPERIMENTAL

2.1. Electronics

The controlling system of electronics used for the dark electrochemistry and ORDE experiments was based on designs by Chadwick[32] and Hillman[33].

2.2. Electronics for Flash Electrolysis

A potentiostat was constructed to a design by Goddard[34] which enabled the potential of the working electrode to be kept constant over the timescale of charging and discharging of the electrical double layer capacitance. The response time of the potentiostat was about 10 μs. A diagram of the circuit is shown in figure 2.1.

The potentiostat was housed in an aluminium box which included a compartment for the electrochemical cell. The voltage supply and charger arrangement for the potentiostat are shown in figure 2.2. To reduce interference from electromagnetic noise which might be caused by an external a.c. power source, a battery of rechargeable cells was mounted onto a printed circuit board and fixed within the box of the potentiostat. These cells were charged by an external 9 mA, 55 V d.c. constant current source, which could be completely disconnected from the potentiostat before use. The voltage output from the rechargeable cells to the electronics of the potentiostat was mediated by a pair of ± 15 V voltage regulators (type 7815-R.S. 305-901 and type 7915-R.S. 305-923). Using this arrangement the potentiostat unit could be charged overnight and used continuously for about seven hours before it was necessary to recharge the batteries.

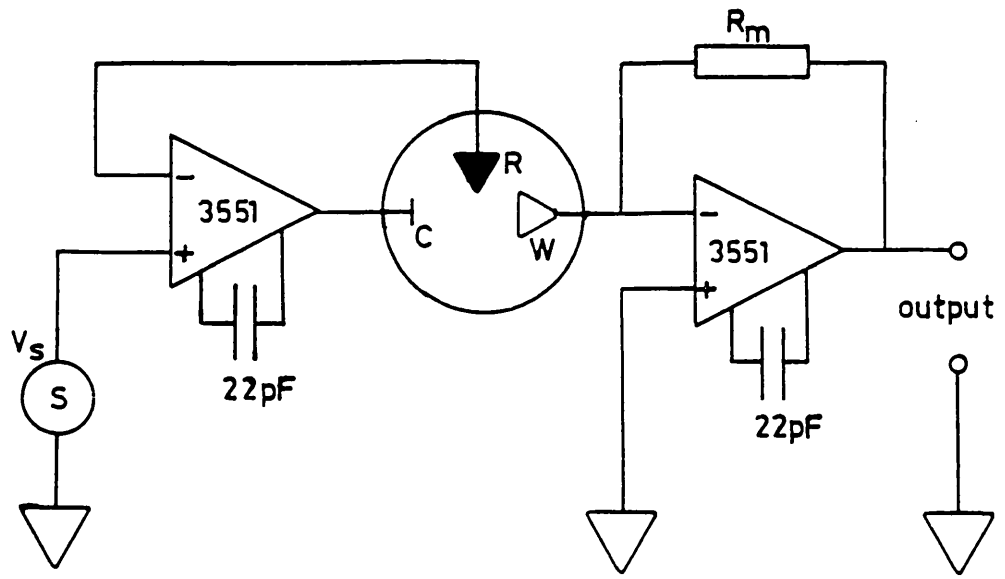

R_m= 10kΩ or 100kΩ

Figure 2.1. Circuit diagram for the rapid response potentiostat.

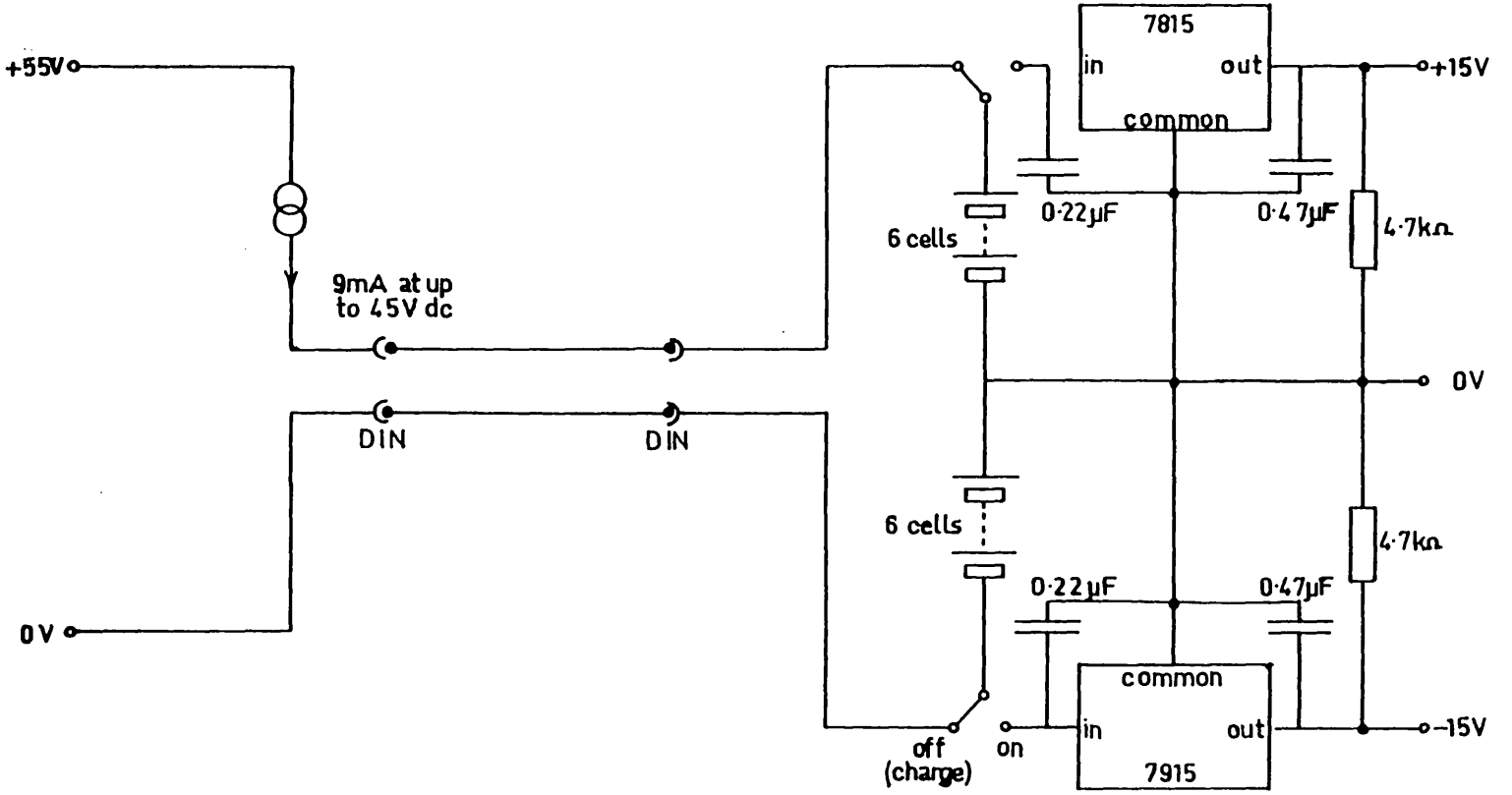

Figure 2.2. Voltage supply and charger arrangement for the rapid response potentiostat.

For some flash electrolysis experiments we considered double layer charging effects in the presence of a faradaic current. Under these conditions the high impedance saturated calomel reference electrode used for the ORDE experiments resulted in a long rise time and damped oscillations of the current signal. To allow information to be gathered within the first few milliseconds after the flash, the dual electrode system[35] shown in figure 2.3 was used.

This system combines a wire and an SCE coupled to each other and to the potentiostat reference input. The values of the elements in the coupling circuit are chosen so that the potentiostat effectively sees only this impedance. The coupling circuit behaves such that two paths are provided through which the current may pass. The capacitor provides a relatively low impedance, through which current flows for the first 10 μs. At longer times, and under d.c. conditions the standard reference electrode is controlling. An additional feature of the dual reference is that the system acts as a filter for power-line frequency noise.

2.3. Electrodes

The platinum rotating disc electrodes used were set in a mantle of either teflon or araldite. Any major abrasions to the surface were removed using 6 μm and then 3 μm diamond lapping compounds (Engis) on a purpose built polishing machine. A mirror finish was achieved by hand polishing with a slurry of 1 μm and then 0.3 μm alumina (Banner Scientific) in deionised, doubly distilled water (DDW) on cottol wool. Polishing with 0.3 μm alumina was repeated before each experiment.

The semitransparent electrodes used in ORDE and flash electrolysis experiments were prepared in the following manner. Spectrosil Quartz rods (4 mm diameter, 120 mm long, Thermal Syndicate) were

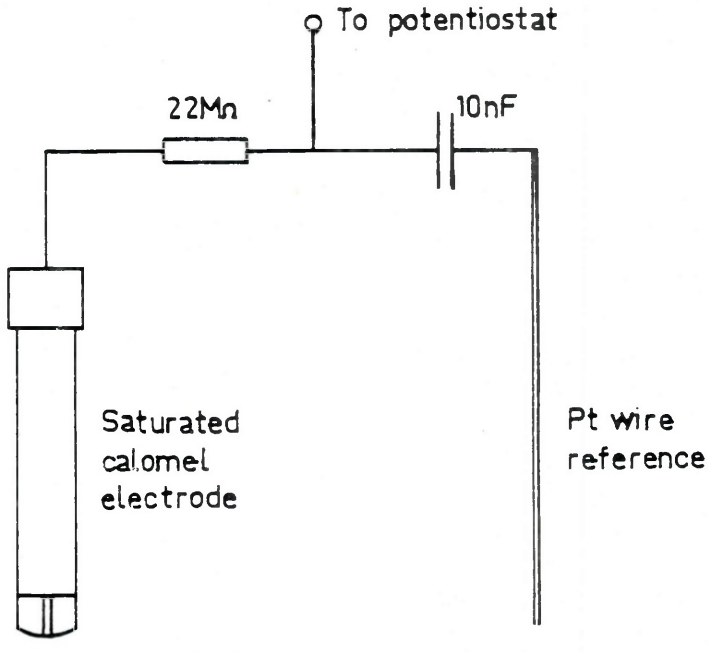

Figure 2.3 The dual reference

Plate 2.1 An ORDE

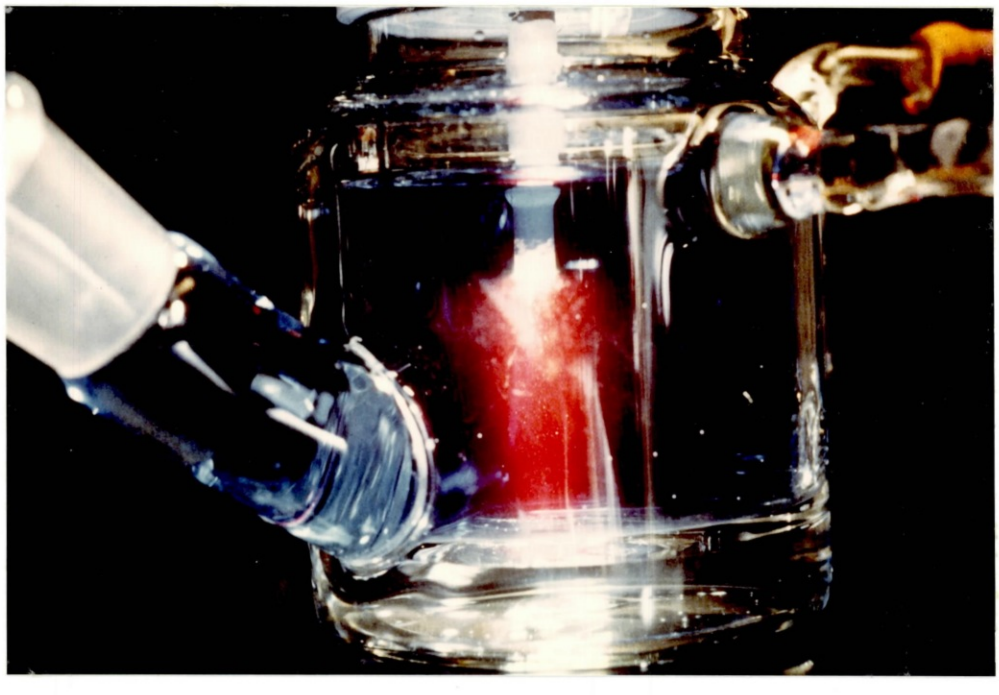

mechanically polished at each end until free from scratches and optical distortion. Polishing began with 180, 320 and then 600 grade carbonundum discs (Engis) with water as lubricant. The final polishing was with a slurry of Tecepol (III) in DDW (Abrafact) on a Hyprocell Pellon polishing pad (Engis).

The polished rods were cleaned by soaking in Decon 90 (BDH) and thoroughly dried. A coat of platinum paint (Johnson Matthey PBC 2532) was applied to one end of the rod for a length of 2 cm and a small overlap (about 0.5 mm) was made as a ring on the face to allow electrical contact. The paint was fired in a carbolite MF3 furnace according to the manufacturer's instructions to remove the organic components and leave a thin layer of platinum.

Tin oxide was deposited on the face of the electrode by spraying a solution of $SnCl_4$ and $SbCl_5$ in ethyl acetate onto the rod. The spraying solution was prepared by dropwise addition of 16.7 cm^3 of $SnCl_4$ (Koch Light) and 1 cm^3 of $SbCl_5$ (BDH) to 33.3 cm^3 of ice-cold ethyl acetate (BDH). The molar ratio of Sn:Sb = 95:5 provides the maximum conductivity for the film[36]. The solution was allowed to age for one month, during which time it changed in colour from straw yellow to black. When applying the spraying solution, the quartz rod was rotated at 5 Hz and heated to red heat using an oxygen/natural gas flame. The solution was applied to the heated rod with a De Vilbis spray gun (No. 1 nozzle, using compressed air). Sprayed rods were tested for optical and electrical properties and only those with a resistance of less than 100 Ω between the edge and centre of the optical face were used. Interference fringes created by the tin oxide film indicated that the thickness of the film was 400-700 nm. The prepared rods were fitted into brass sheaths using heat shrink tubing (Radio Spares 399.940 9.5 mm diam.) and electrical contact made to the

brass with silver-loaded paint (Johnson Matthey FSP 51). Finally three coats of enamel paint (Humbrol) were applied over the silver-loaded paint to give the finished electrode. Electrodes prepared in this manner were characterised by capacitance measurements (by Hillman and Bartlett[37]) and by cyclic voltammetry and were found to be reproducible.

A travelling microscope was used to measure electrode diameters. To calculate the electrode area, the mean value of twelve evenly spaced diameters was used. An ORDE under illumination is shown in plate 2.1.

Potentials were measured with respect to home-made saturated calomel electrodes (SCEs). The potentials of these electrodes were periodically checked against a commercial SCE (Radiometer) and agreement was always found to be better than ± 1 mV.

The counter and generating electrodes used were large area platinum gauzes. These were regularly cleaned in Decon 90 solution.

2.4. The Rotation System

The experimental arrangement is shown in plate 2.2. The light source and bearing assembly were mounted above the electrochemical cell on two stainless steel rods. The electrodes were supported in a bearing block containing a sealed mercury contact designed by Heslop[38]. Because of the need to illuminate through the electrode shaft it was not possible to use a direct drive system between the motor and the electrode. Therefore a toothed drive belt (Aurora) was used to couple the motor to the bearing assembly. The assembly was driven by a printed armature d.c. servo motor and an Oxford Electrodes motor controller. The rotation speed was continuously measured by a slotted opto-switch (Radio Spares 306.061) connected to the motor shaft, and was displayed on a digital readout. The system provided rotation speeds between 1 Hz and 50 Hz, which were stable to ± 0.1 Hz.

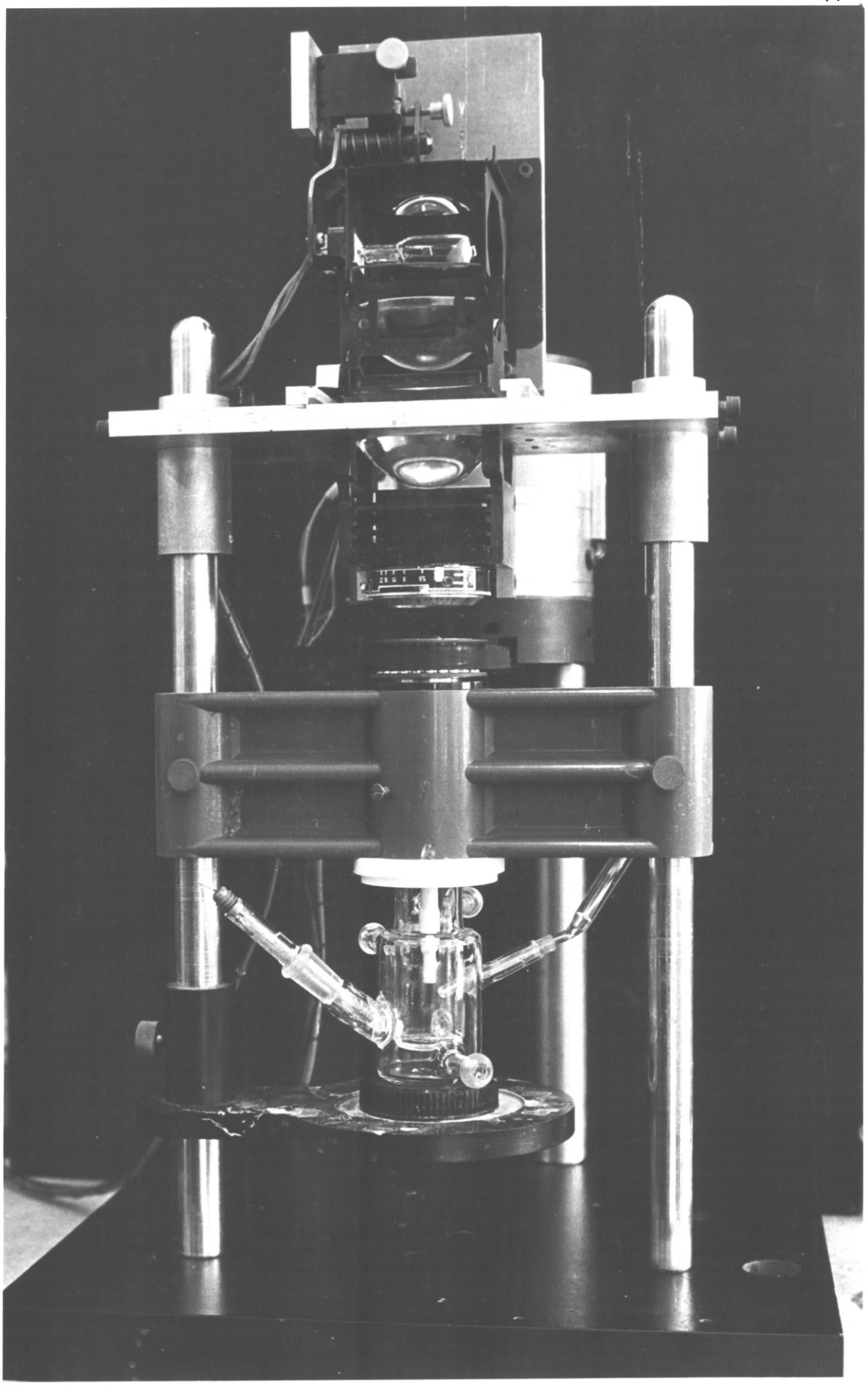

Plate 2.2

2.5. Cell Assembly

The electrochemical cell assembly is shown in figure 2.4. The cells were purpose built double-walled glass vessels thermostatted at 25.0 (± 0.2)^{o}C by circulating water through the outer jacket. The counter electrode was held in a side-arm behind a grade 3 glass frit to prevent contamination of the solution by products of the reaction at the counter electrode. The cell was mounted on a platform supported above the baseplate, so that it could be readily lowered and removed to allow the electrode to be changed without disturbing the light source and bearing block. All solutions were degassed with white spot nitrogen which had previously been purged of any traces of oxygen by a train of dreschel bottles containing a caustic solution of anthraquinone-2-sulphonate in contact with amalgamated zinc.

2.6. Solutions and Chemicals

All solutions were freshly prepared using doubly distilled water (DDW) and were deoxygenated for at least 15 minutes before use.

All simple inorganic chemicals were AnalaR grade and were used without further purification. Thionine was supplied by Fluka and Aldrich. Insoluble impurities were removed by filtration, and the resulting solutions shown to be free from dye impurities by chromatography on alumina. The concentration of thionine solutions was determined spectrophotometrically at 599 nm (ε_{599}/mol dm^{-3} cm^{-1} = 56000[15]).

2.7. Light Sources

The light source for ORDE experiments was an A1/223, 250 W, 24 V quartz iodine projector lamp bulb with a filament temperature of 3350 K.

Light intensity measurements using a photodiode showed that there was a 5 to 10% variation in the light intensity using an a.c. source.

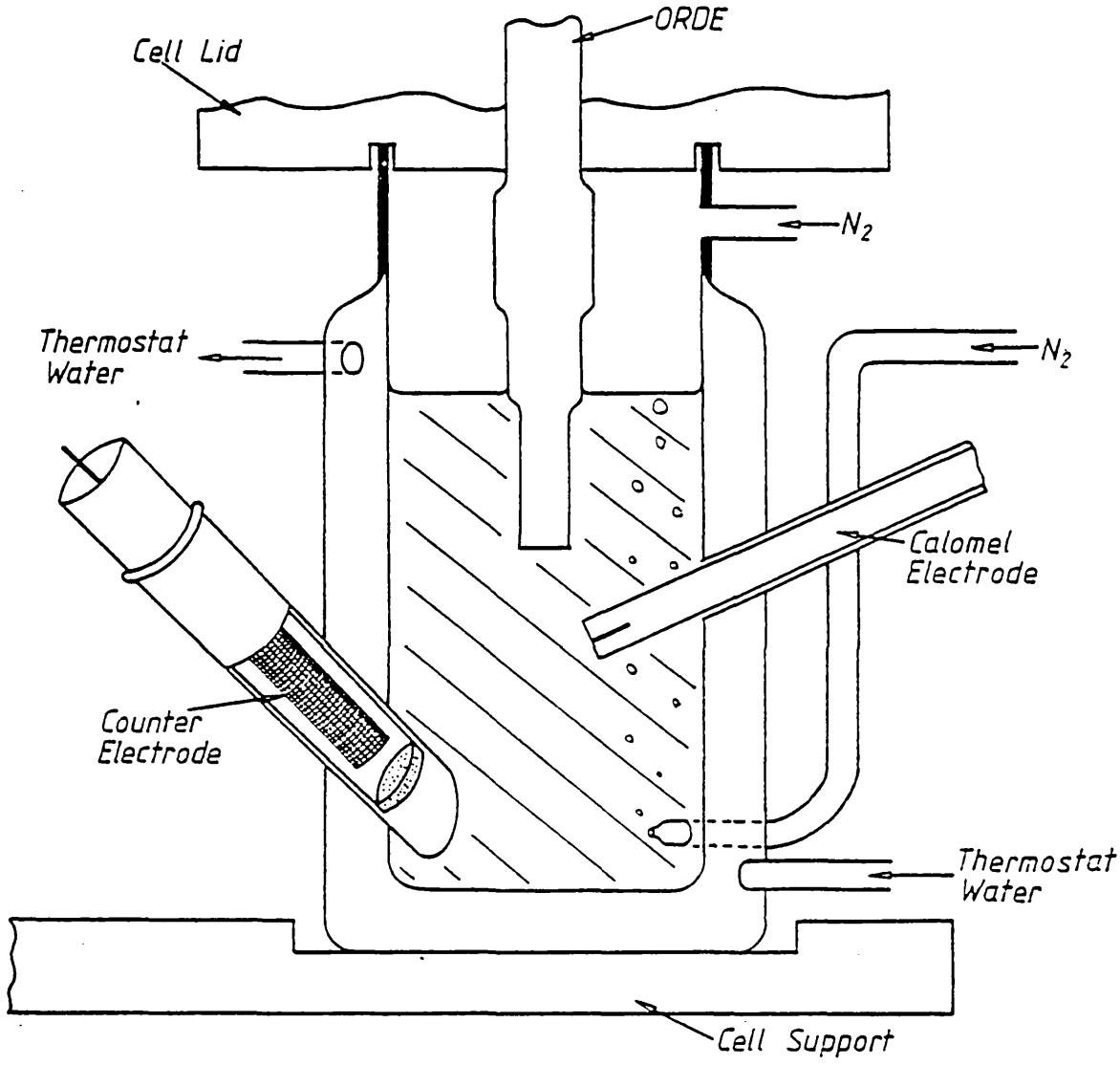

Figure 2.4. An electrochemical cell.

This was unacceptable for steady-state ORDE experiments, so a d.c. source, designed by Fisher[11] was used to power the lamp. A circuit diagram for the lamp power supply is shown in figure 2.5. 10 nm band pass interference filters (Ealing IRI 25 mm) were used to monochromate the light and the intensity was varied using Ealing neutral density filters. In shutter experiments a GB Kershaw 450 camera shutter and cable release were used. The rise time of the shutter was about 2.5 ms.

The light source used in the flash electrolysis experiments was a Prinz 770c camera flashgun. The flash tube in this unit is a "colour coated Xenon tube with a colour temperature of 5600 K". The unit is powered by Nickel-Cadmium rechargeable batteries which are used to charge a capacitor. Discharge of the capacitor across the flash tube creates the photolysis flash for the experiment, but also causes a considerable amount of electromagnetic noise. To prevent this noise from interfering with the controlling electronics, the flashgun unit was housed in a die-cast aluminium box and the light delivered to the photolysis cell via a light pipe (Dolan-Jenner Industries, 61 cm long, 0.33 cm diameter).

Figure 2.6 shows a block diagram of the flash electrolysis apparatus. The semitransparent electrode was held stationary and the current transient was recorded on a Gould OS4000/1 digital storage oscilloscope, triggered by a photodiode. The response time of the photodiode was about 250 ns. Once stored, transients were 'rolled out' at a lower speed on a Bryans 29000 chart recorder.

Stopped flow experiments were performed using a Nortech 5F 2A stopped flow spectrophotometer fitted with a grating monochromator and the control system from the SF 3A model. All experiments were conducted under pseudo-first order conditions. The solution reservoirs were modified so that air sensitive compounds could be electrogenerated *in situ*.

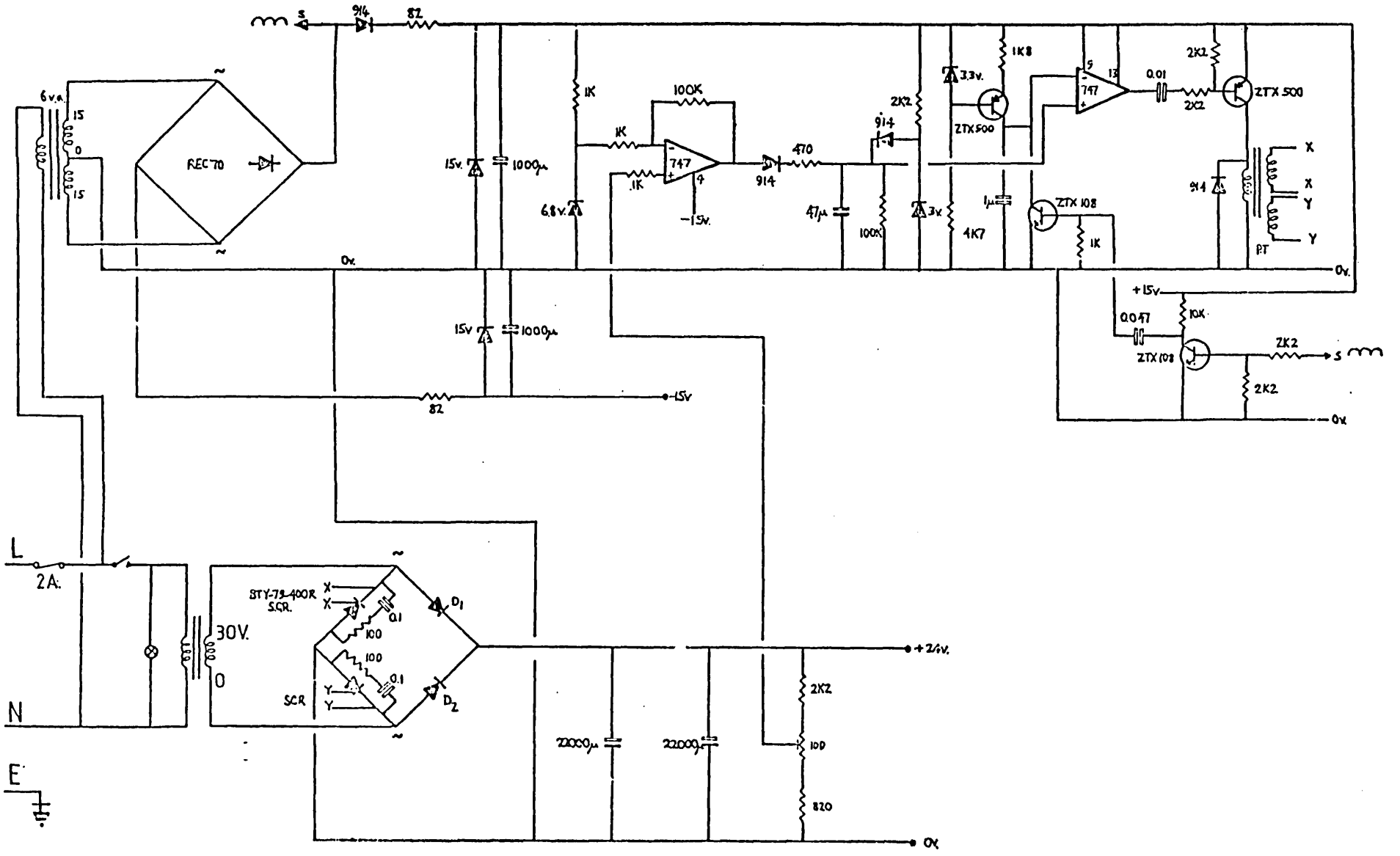

Figure 2.5. 250 W Lamp power supply unit.

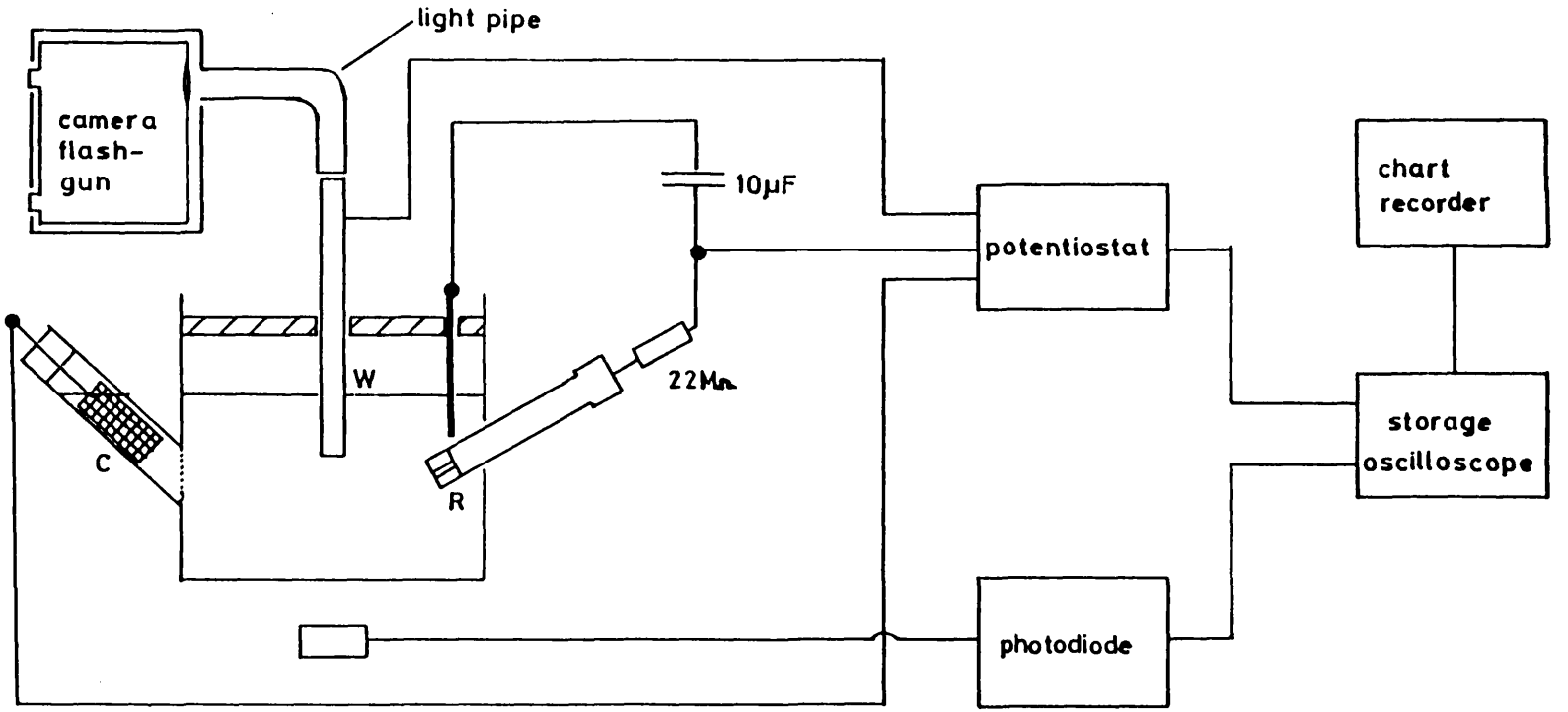

Figure 2.6. Apparatus used in flash electrolysis experiments.

Thiazine dyes were produced in the leuco form by electrogeneration at a platinum gauze. A useful feature of the apparatus was the 'ratio arm' which allowed the reactant syringes to be driven in various volume ratios, so that the concentrations of the reactants could be varied without making up solutions at each concentration.

Solutions for flash photolysis were outgassed by repeated freeze-thaw cycles. Conventional microsecond flash photolysis measurements were made with an Applied Photophysics K200 system, using a dichromate filter to remove excitation wavelengths < 550 nm as described by West[67].

Chapter 3

THEORY

The Rotating Disc Electrode and Optical Rotating Disc Electrode Techniques

The measurement of electrochemical currents in an unstirred solution provides irreproducible results. The composition of the solution at the electrode surface is changed as soon as any current flows, and stray convection may be caused by thermal gradients and mechanical shock. A system with reproducible mass transport is required to eliminate these effects and so a number of forced convection systems have been developed. These include the dropping mercury[39], tube[40], wall jet[41] and bubbling gas electrodes[42], as well as the rotating disc electrode[43] which has been used in this work.

3.1. The Rotating Disc Electrode (RDE)[43,44]

We first consider the hydrodynamics of a rotating electrode in solution. The system may be described in terms of cylindrical polar coordinates ϕ, r and x as shown in figure 3.1. The exact pattern of flow set up in the solution by the spinning disc was calculated by von Karman in 1921[41]. The velocities of flow along the three coordinates are given by:

$$v_\phi = r\omega G(\chi_H) \tag{3.1}$$

$$v_r = r\omega F(\chi_H) \tag{3.2}$$

$$v_x = (\omega\nu)^{\frac{1}{2}} H(\chi_H) \tag{3.3}$$

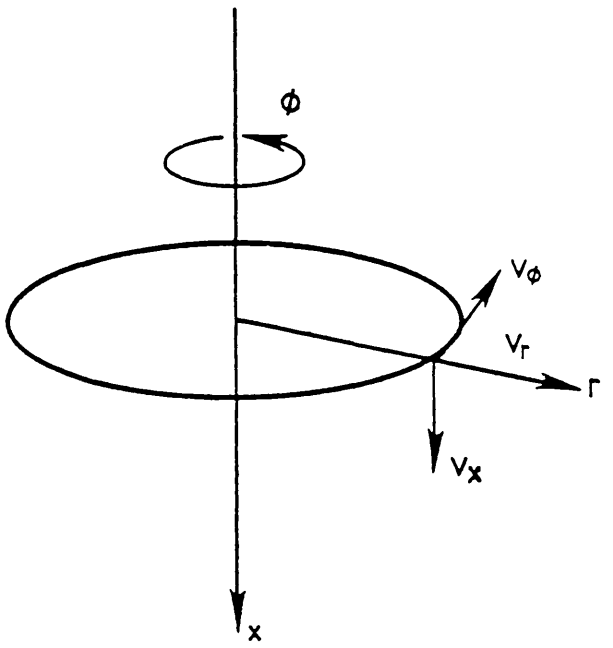

Figure 3.1. Co-ordinate system and fluid velocity components for the RDE.

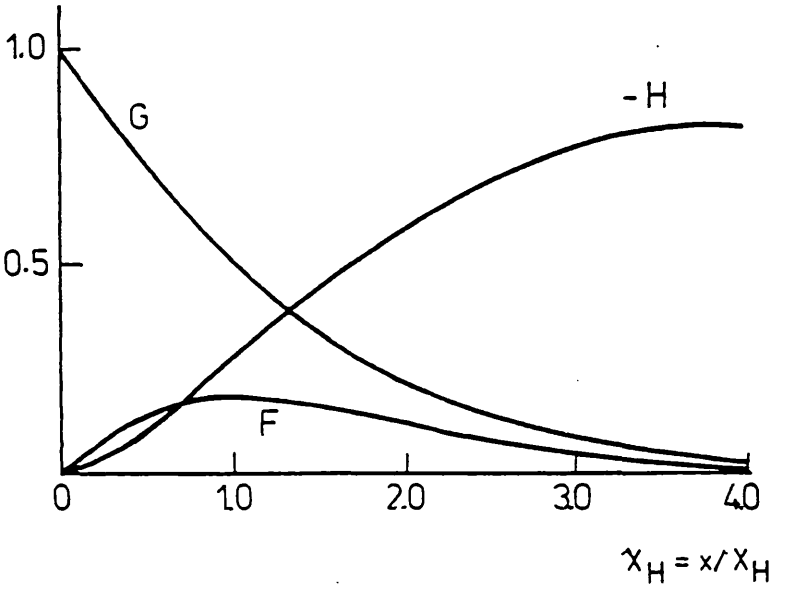

Figure 3.2. The functions F, G and H describing the fluid flow at the RDE.

where

v is in cm s^{-1}

ω is the rotation speed in radians s^{-1}

ν $(= \eta/\rho)$ is the kinematic viscosity in cm^2 s^{-1}

and
$$\chi_H = x/X_H \tag{3.4}$$
$$X_H = (\nu/\omega)^{\frac{1}{2}} \tag{3.5}$$

X_H is the hydrodynamic length, which is characteristic of the system and is typically 0.1 - 1 mm.

The functions F, G and H are plotted against χ_H in figure 3.2. It is important to note that v_x is independent of r_1 which means that transport to the disc is uniform across its surface. The equations provide a mathematical description of the flow of solution below the disc. The angular velocity of the solution increases as it is drawn up towards the electrode and as the solution gets near to the disc it is thrown out centrifugally. Very close to the disc however, there is a stagnant layer called the diffusion layer which rotates with the disc.

The mathematical model for hydrodynamic flow to a disc allowed Levich[46] to calculate the mass transport to a disc electrode. The full differential equation contains terms for both migration and diffusion but the migrational term may be omitted when background electrolyte is added to the solution. Under these conditions the differential equation simplifies to

$$D\frac{\partial^2 c}{\partial x^2} = v_x\frac{\partial c}{\partial x} \tag{3.6}$$

Diffusion Transport

where

C is the concentration of electroactive species in mol cm^{-3}, and

D is the diffusion coefficient in $cm^2\ s^{-1}$.

Solving equation (3.6) using the boundary condition that $C \to C_\infty$ as $x \to \infty$, we find that j, the flux of electroactive species to the electrode is given by:

$$j = D\left(\frac{\partial C}{\partial x}\right)_o = \frac{C_\infty - C_o}{X_D} \tag{3.7}$$

where X_D is the thickness of the diffusion layer in cm given by

$$X_D = 0.643\ \nu^{1/6}\ D^{1/3}\ W^{-1/2} \tag{3.8}$$

where j is in mol $cm^{-2}\ s^{-1}$, W is the rotation speed of the electrode in Hz and C_o is the surface concentration in mol cm^{-3}.

The profile of concentration with distance from the electrode is shown in figure 3.3.

The distance X_D divides the concentration profile into two regions. When $x < X_D$ transport is diffusion-controlled and there is a linear concentration gradient between $x = 0$ and $x = X_D$ but when $x > X_D$ there is sufficient motion of the fluid for the solution to be well stirred and the concentration is uniform.

To calculate the current which flows at the electrode we must consider not only mass transport to the electrode surface but also the rate of reaction of the electroactive species at the electrode - the electrode

Figure 3.3. Variation of concentration with distance from an RDE.

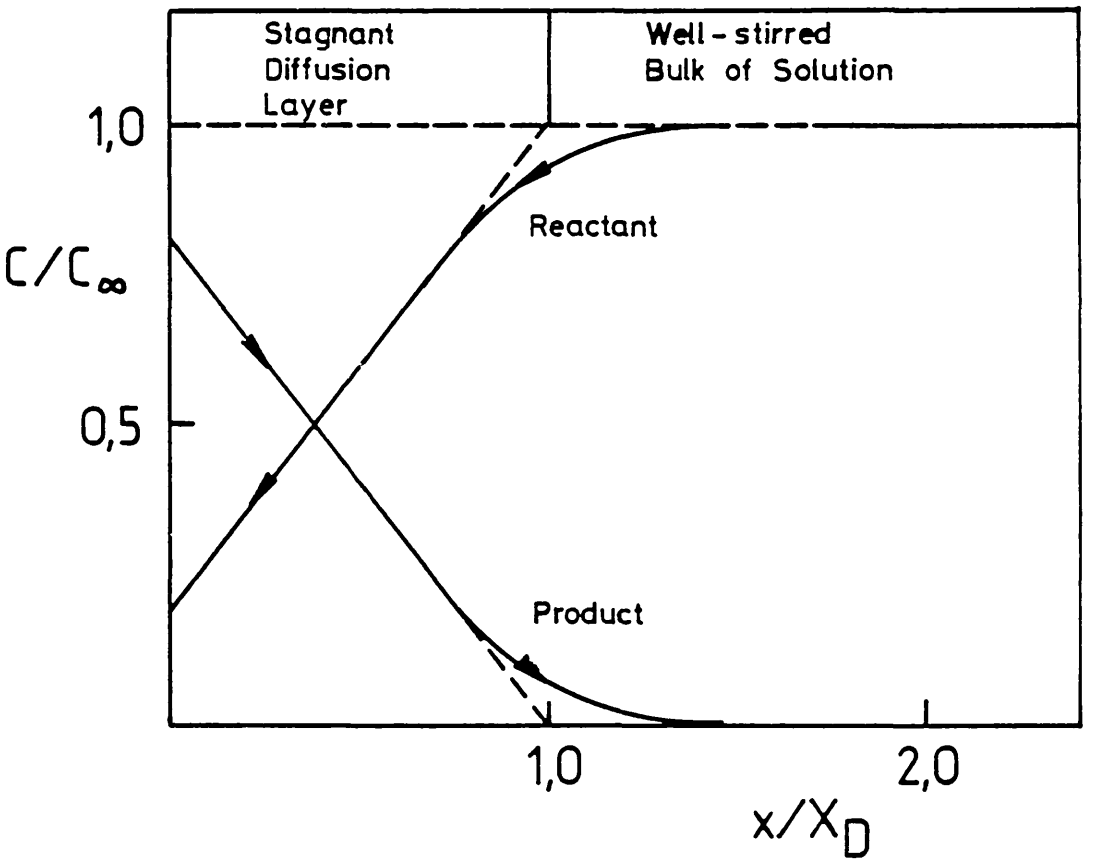

kinetics. For the reduction of a species at the electrode the rate constant k' is given by:

$$k' = k'_{E'} \exp(-\alpha F(E - E')/RT) \tag{3.9}$$

where

α is the electron transfer coefficient, and

$k'_{E'}$ is the standard electrochemical rate constant.

In the steady state, the flux of material reacting at the electrode surface must be equal to the flux transported through the diffusion layer. The flux at the electrode is given by:

$$j = k'C_o \tag{3.10}$$

and substituting for C_o from equation (3.7) we obtain

$$\frac{1}{j} = \frac{1}{k'C_\infty} + \frac{1}{k_D C_\infty} \tag{3.11}$$

where k_D is the diffusional rate constant given by

$$k_D = \frac{D}{X_D} \tag{3.12}$$

Equation (3.11) has two limiting forms:

(a) When $k_D >> k'$, $j = k'C_\infty$ and $C_0 = C_\infty$, the flux is controlled by the electrode kinetics and

(b) When $k_D << k'$, $j = k_D C_\infty$ and $C_0 << C_\infty$, the flux is controlled by transport to the electrode and is independent of potential. This is shown in figure 3.4.

When transport is the controlling factor, the limiting flux is given by:

$$j_L = k_D C_\infty = DC_\infty / X_D \tag{3.13}$$

Converting the flux to the electrode into a current

$$i_L = nAFj_L \tag{3.14}$$

and using equation (3.8) we obtain the familiar Levich equation

$$i_L = 1.554\ nFAD^{2/3}\ \nu^{-1/6}\ C_\infty\ W^{1/2} \tag{3.15}$$

where A is the electrode area.

This expression predicts that the limiting current i_L, varies linearly with the square root of rotation speed, and allows us to calculate the diffusion coefficient of a species in a solution of known concentration.

The shape of an irreversible current-voltage curve may be obtained by combining equations (3.11) and (3.13):

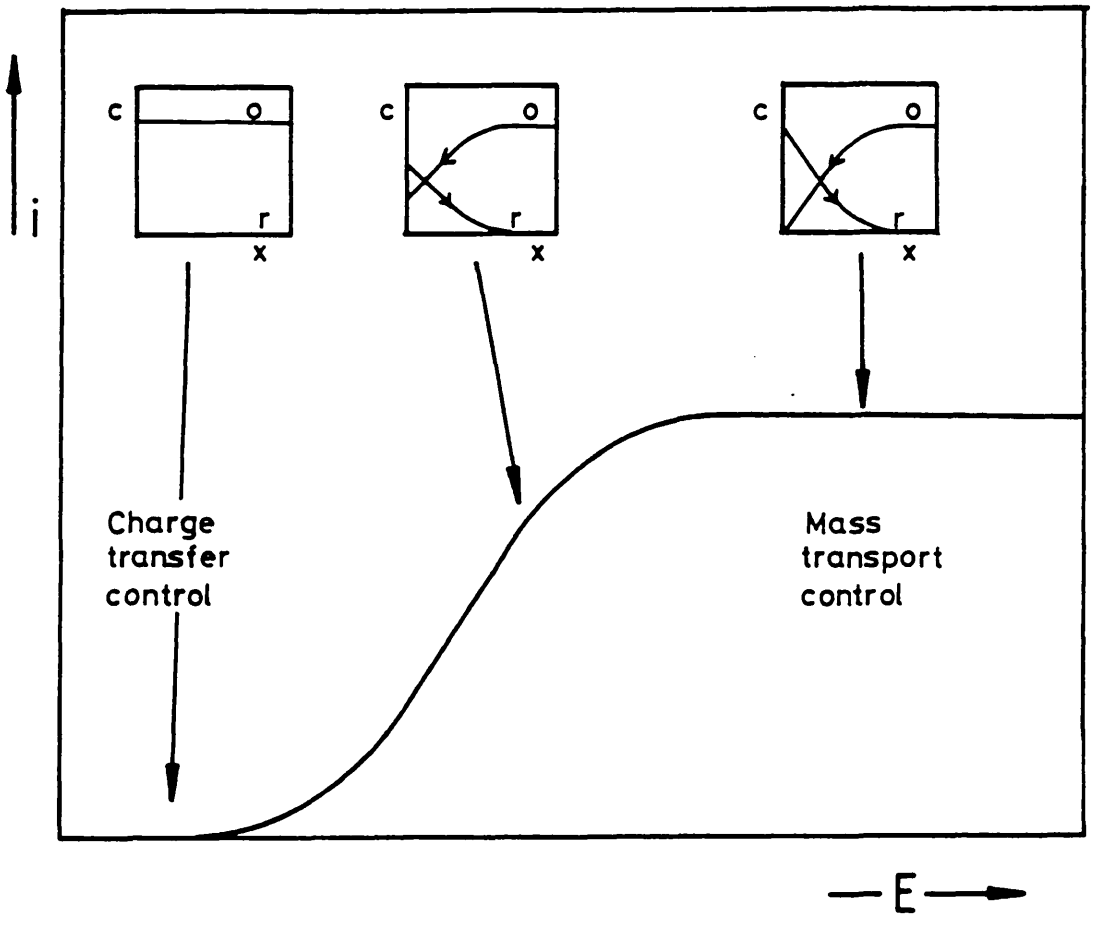

Figure 3.4. Schematic polarogram for the reduction of an electroactive species at an RDE. Schematic concentration profiles are shown inset.

$$\frac{j}{j_L} = \frac{i}{i_L} = \frac{k'}{k_D + k'} = \frac{1}{1 + k_D/k'} \tag{3.16}$$

Substitution from equations (3.9) and (3.13) gives the Tafel equation

$$-\ln\left(\frac{j_L}{j} - 1\right) = -\ln\left(\frac{j_L}{C_\infty}\right) + \ln k'_{E'} - \frac{\alpha F(E - E')}{RT} \tag{3.17}$$

from which we can calculate the standard electrode potential for a reversible couple.

3.2. Optical Rotating Disc Electrode Theory

In the steady-state ORDE[47-50], the solution is illuminated by a uniform, parallel beam of light through a semitransparent rotating disc electrode. The photoproduct B is generated with a quantum efficiency ϕ in the reaction

$$A + Z \underset{k_{-2}}{\overset{h\nu,\phi}{\rightleftharpoons}} B + Y$$

The following assumptions are made to construct the differential equation for convective diffusion of B:

(i) The light makes only a small perturbation to the concentration of A. This means that the solution does not bleach and that the light has a Beer-Lambert profile.

$$I = I_0 e^{-\varepsilon[A]x} \tag{3.18}$$

where

ε is the natural extinction coefficient of A,

x is the distance from the electrode and

I is the irradiance. $I = I_0$ when $x = 0$.

(ii) $[Y] >> [B]$, so that the back reaction is pseudo-first order with a rate constant given by

$$k = k_{-2}[Y] \tag{3.19}$$

(iii) The electrode is at a potential such that the Y/Z couple is inactive whilst all of the photoproduct B arriving at the electrode is converted to A.

Using these assumptions the convective diffusion equation for B is[48]

$$D\frac{\partial^2 b}{\partial x^2} + V_x\frac{\partial b}{\partial x} + \phi I_0 \varepsilon a e^{-\varepsilon a x} - kb = 0 \tag{3.20}$$

Diffusion Convection Generation Back Reaction

where a and b are the concentrations of A and B respectively and v_x is the velocity of flow towards the electrode. This equation is the same as the usual equation for the rotating disc electrode, eqn (3.6) except for the addition of terms for the generation and loss of B.

The system is characterised by the lengths introduced previously, namely:

the hydrodynamic length $X_H = (2\pi\nu/W)^{1/2}$ (3.5)

the diffusion length $X_D = 0.643\ W^{-1/2}\ \nu^{1/6}\ D^{1/3}$ (3.8)

the kinetic length $X_k = (D/k)^{1/2}$ (1.6)

the absorption length $X_\varepsilon = 1/\varepsilon a$ (1.4)

Solving equation (3.20) we obtain the following result for the photoelectrochemical collection efficiency[48,49]

$$\frac{N_{h\nu}}{\phi} = \operatorname{cosech}(\kappa') \left\{ \frac{\cosh(\kappa') - \frac{\zeta}{\kappa'} \sinh(\kappa') - \left(\frac{\zeta}{\kappa'}\right)^2 e^{-\zeta}}{\kappa'/\zeta - \zeta/\kappa'} - \frac{\exp(-\zeta - \frac{1}{2}(\kappa')^2)}{\kappa'/\zeta} \left[1 - \frac{\exp\left(-\frac{1.3\ X_H}{X_\varepsilon}\right)}{1 + X_{G,k}^2\ X_*^{-2}} \right] \right\} \quad (3.21)$$

where

$\kappa' = X_D/X_{G,k}$ (3.22)

$X_* = (X_D^3\ X_\varepsilon/3.7\ X_H^2)^{\frac{1}{2}}$ (3.23)

$X_{G,k}^{-2} = X_G^{-2} + X_k^{-2}$ (3.24)

$\zeta = X_D/X_\varepsilon$ and (3.25)

$N_{h\nu}$ = (flux of electrons)/(flux of photons) (3.26)

Thankfully, simplified forms of the equation for $N_{h\nu}$ are obtained when the relative sizes of the characteristic lengths are considered. Equations for $N_{h\nu}$ under different conditions are shown in figure (3.5).

When X_G is large, no bleaching occurs, and for region A of figure (3.5) the collection efficiency is equal to unity. $X_\varepsilon < X_D$ so the light is absorbed close to the electrode and because $X_\varepsilon < X_k$, all of the photogenerated B reaches the electrode before it is destroyed. In region B the back reaction is sufficiently fast to destroy the material on its passage across the diffusion layer and only material generated within X_k can reach the electrode.

In zones C, D and E the back reaction is sufficiently slow to allow material from outside the diffusion layer to reach the electrode. In region C, light does not penetrate far outside the diffusion layer and the amounts of material reaching the electrode from inside and outside the diffusion layer are roughly equal. In region D, light penetrates beyond the hydrodynamic layer and the collection efficiency becomes constant. In region E the kinetics are so rapid that the loss of photogenerated species is caused by the back reaction rather than by convection.

For zones A and B the photocurrent is independent of rotation speed since all of the material reaching the electrode originates within the diffusion layer. In zone D an increase in rotation speed increases both convective dilution and mass transport. These two effects cancel each other out and the photocurrent is again independent of rotation speed. In zone C the photocurrent varies with $W^{-\frac{1}{2}}$ and so an increase in rotation speed decreases the photocurrent. This is most unusual - the normal behaviour at a rotating disc electrode is for the limiting current to increase with increasing rotation speed, as the diffusion thickness

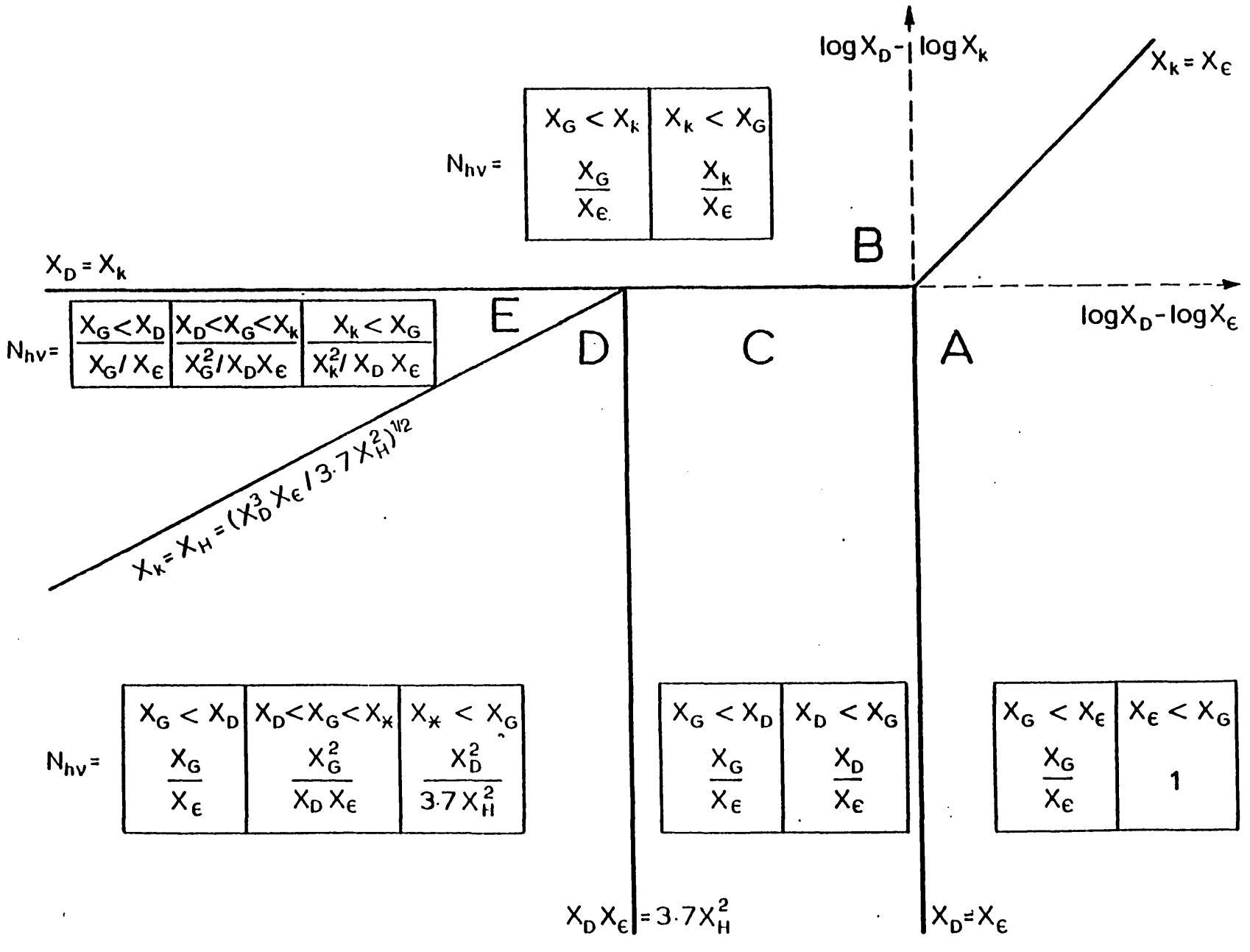

Figure 3.5

Expression for $N_{h\nu}$ as a function of X_D, X_k and X_ϵ. In each zone the last expression refers to the unbleached case and the first expression to the most bleached case.

becomes smaller. In this case however, as the diffusion layer becomes narrower, there is less space for species to be generated without risk of them being swept away by radial convection.

3.3. ORDE for DMST2

The iron-thionine system is more complicated than the A,B/Y,Z system because of the intermediacy of S$^{\cdot}$. The mechanism may be described thus:

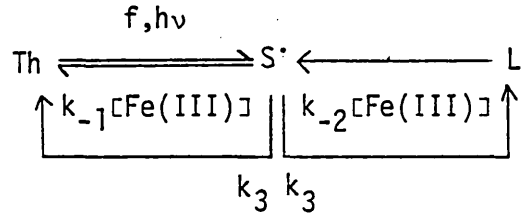

(3.27)

Characteristic lengths defined in section 1.2 must be redefined to include the behaviour of the semi-reduced species.

$$X_G = (D/\phi_1\phi_2\Phi I_{\Phi = 1}\,\varepsilon)^{\frac{1}{2}} \text{ and} \tag{3.28}$$

$$X_k = (D/(1 - \phi_2)k_{-2}[Fe(III)])^{\frac{1}{2}} \tag{3.29}$$

where

Φ is the fraction of light transmitted by the neutral density filter

$I_{\Phi = 1}$ is the flux of photons per unit area for $\Phi = 1$

ϕ_1 is the quantum efficiency for production of S$^{\cdot}$ and

ϕ_2 is the fraction of S$^{\cdot}$ that is converted into L .

In equation (3.21) ϕ is now given by

$$\phi = \phi_1\phi_2 \tag{3.30}$$

In the generating length, the term $\phi_1\phi_2$ arises because bleaching the solution requires the conversion of thiazine to leucothiazine. For similar reasons the factor of $(1 - \phi_2)$ appears in the definition of X_k because this is the fraction of semithiazine forming thiazine.

ORDE for DMST2 with no Added Ferric

In the case where $X_{G,k}$ is the longest of the characteristic lengths and X_ε is large we have

$$X_D < X_G < X_\varepsilon < X_{G,k} \tag{3.31}$$

In the ORDE experiment for DMST2 with no added ferric the concentration of A used in the experiment is low and so the concentration of photogenerated Y will be correspondingly low. Also the rate of the back reaction is quite low. We therefore assume that photogenerated Y has a negligible effect on the concentration of species B.

The system has characteristics of both zones C and D in figure (3.5) and equation (3.21) reduces to

$$\frac{N_{h\nu}}{\phi} = \frac{X_D}{X_\varepsilon}\left[1 + \frac{X_G^2}{X_D^2}\left(\frac{\exp(-1.3\ X_H/X_\varepsilon)}{1 + 3.7(X_G^2X_H^2/X_\varepsilon X_D^3}\right)\right] \tag{3.32}$$

If we now assume that

$$\exp(-\ 1.3\ X_H/X_\varepsilon) \simeq 1 \tag{3.33}$$

and that when $X_{G,k} >> X_D$

$$3.7\ X_G^2X_H^2/X_\varepsilon X_D^3 >> 1 \tag{3.34}$$

Equation (3.32) becomes

$$\frac{N_{h\nu}}{\phi} = \frac{X_D}{X_\varepsilon} + \frac{X_D^2}{3.7\ X_H^2} \tag{3.35}$$

In terms of measured currents

$$\frac{N_{h\nu}}{\phi} = \frac{i}{AFI_o} = \frac{i}{i_{h\nu}} \tag{3.36}$$

or

$$\frac{N_{h\nu}}{2(\frac{1}{2})\phi_1} = \frac{i}{(i_{h\nu})_{\Phi = 1}\ \Phi} \tag{3.37}$$

where the factor of $\frac{1}{2}$ appears because in the absence of added ferric, the reaction of semithiazine with ferric is negligible and $\phi_2 = \frac{1}{2}$. The factor of 2 arises because two electrons are transferred when a molecule of leucothiazine reacts at the electrode.

Thus we have

$$\frac{i}{\Phi\phi_1(i_{h\nu})_{\Phi = 1}} = \frac{X_D}{X_\varepsilon} + \frac{X_D^2}{3.7\ X_H^2} \tag{3.38}$$

or

$$\frac{i}{\Phi} = \phi_1 i_{h\nu} \left\{ \frac{X_{D,1}}{X_\varepsilon W^{\frac{1}{2}}} + \frac{1}{3.7} \left(\frac{0.643\ \nu^{1/6}\ D^{1/3}}{2\pi\nu} \right) \right\} \tag{3.39}$$

ORDE for DMST2 with Added Ferric

For DMST2, when ferric is added to the solution, the length $X_{G,k}$ becomes shorter and

$$X_D < X_{G,k} \simeq X_k < X_\varepsilon \tag{3.40}$$

X_ε is large and the system shows characteristics of zones B, C and D in figure (3.5). Equation (3.21) may be re-written as

$$\frac{N_{h\nu}}{\phi} = \frac{X_{G,k}}{X_\varepsilon} \left\{ \frac{\cosh\left(\frac{X_D}{X_{G,k}}\right) - \exp\left(-\frac{X_D^2}{2X_{G,k}^2}\right) [1 - H]}{\sinh\left(\frac{X_D}{X_{G,k}}\right)} \right\} \tag{3.41}$$

With $X_\varepsilon > X_H$, this equation has two forms depending on the relative sizes of X_D and $X_{G,k}$.

(i) At low rotation speeds, when $X_D > X_{G,k}$ the $[1 - H]$ term is negligible and

$$\frac{N_{h\nu}}{\phi} \to \frac{X_{G,k}}{X_\varepsilon} = \frac{N_{lim}}{\phi} \tag{3.42}$$

where N_{lim} is obtained from the limiting value of the graph in figure (5.20).

(ii) At high rotation speeds, when $X_D < X_{G,k}$ the [1 - H] term dominates, and

$$\frac{N_{h\nu}}{\phi} = \left(1 + \frac{X_\varepsilon X_D}{3.7\ X_H^2}\right) \frac{X_D}{X_\varepsilon} \tag{3.43}$$

For a particular ferric concentration, ϕ_2 is constant and, returning to the full expression for the photoelectrochemical collection efficiency (eqn. (3.41)) we can write

$$F = \frac{N_{h\nu}}{N_{lim}} = \frac{\cosh(\kappa') - \exp(-\frac{1}{2}(\kappa')^2)}{\sinh(\kappa')} \Bigg/ \left(1 + \frac{X_\varepsilon X_D(\kappa')^2}{3.7\ X_H^2}\right) \tag{3.44}$$

In the reaction scheme (3.27), f is the photogenerated flux of semithiazine and is given by

$$f = \frac{\phi_1\ I_{\Phi = 1}\ \Phi}{X_\varepsilon} \tag{3.45}$$

Using this reaction scheme and employing the steady-state approximation for [S$^\cdot$], [L] and [Th] respectively we obtain

$$f + k'_{-2}[L] = 2k_3[S^\cdot]^2 + k'_{-1}[S^\cdot] \tag{3.46}$$

$$k_3[S^\cdot]^2 = k'_{-2}[L] \tag{3.47}$$

$$f = k_3[S^\cdot]^2 + k'_{-1}[S^\cdot] \tag{3.48}$$

The quantum efficiency for production of L from S$^{\cdot}$ is given by

$$\phi_2 = \frac{k_3[S^{\cdot}]^2}{k'_{-1}[S^{\cdot}] + 2k_3[S^{\cdot}]^2} \tag{3.49}$$

Thus

$$\frac{1}{1 - 2\phi_2} = 1 + \frac{2k_3[S^{\cdot}]}{k'_{-1}} \tag{3.50}$$

and from the definition of f and equation (3.48)

$$\frac{1}{(1 - 2\phi_2)^2} - 1 = \frac{4fk_3}{k^2_{-1}[Fe(III)]_o} \tag{3.51}$$

Rearrangement of this expression generates an expression for ϕ_2

$$\phi_2 = \tfrac{1}{2}\left[1 - \left(\frac{1}{1 + 4k_3 f/(k_{-1}[Fe(III)]_o)^2}\right)^{\frac{1}{2}}\right] \tag{3.52}$$

where $[Fe(III)]_o$ is the ferric concentration at the electrode surface.

3.4. ORDE for the $ZnTMPyP^{4+}$/Fe System

In the ORDE experiments with $ZnTMPyP^{4+}$, the back reaction is very fast and

$$X_G \simeq X_\varepsilon \simeq X_D > X_k$$

The results fall into zone B of figure (3.5) with

$$N_{h\nu} = X_k/X_\varepsilon \qquad (3.53)$$

The concentration of A is quite large in the experiment and for this system the back reaction is rapid. The concentration of photogenerated species Y is therefore important. For the porphyrin system we must consider the situation where the two photogenerated species react with second order kinetics and where species B is electroactive but Y is not[49].

When there is no added species Y, increasing the rotation speed increases the photocurrent. This is because the distance over which Y must diffuse to escape the diffusion layer is reduced. The concentration of Y near to the electrode decreases and there is less Y available to react with B and so decrease the flux of B reaching the electrode. If a significant concentration of species Y is added to the solution the concentration of photogenerated Y is negligible compared to the concentration in the bulk. The photocurrent is therefore independent of rotation speed.

3.5. Flash Electrolysis Theory[11,51,52,53]

The flash electrolysis technique allows us to follow the homogeneous reaction kinetics of species B (leuco dye in the case of the thiazines). A short pulse of uniform, parallel light is passed through a stationary semi-transparent electrode which is set at a potential where B is electroactive. Deviation of the measured current transient from the transient in the absence of the perturbing reaction allows a rate constant for the perturbing reaction to be measured.

The differential equation for transport of B to the electrode is derived using the following assumptions:

(i) The flash is of infinitely short duration and occurs at t = 0.

(ii) The optical density of the solution is low, so that the concentration of B at t = 0, b_0, is uniform with distance from the electrode. This condition becomes redundant if the solution is bleached by the flash.

(iii) The back reaction is pseudo-first order in the bulk solution. That is $b_0 >> [Y]$ and one of the boundary conditions is

$$b = b_0 e^{-kt} \quad \text{as } x \to \infty \tag{3.54}$$

where

$$k = k_{-2}[Y] \tag{3.19}$$

(iv) The electrode is at a potential where the Y/Z couple is inactive but all the B reaching the electrode is converted to A. This gives the second boundary condition:

$$\text{When } x = 0,\ b = 0 \tag{3.55}$$

With these assumptions the differential equation for transport of B to the electrode is

$$\frac{\partial b}{\partial t} = D\frac{\partial^2 b}{\partial x^2} - kb \tag{3.56}$$

Diffusion Back Reaction

Using the dimensionless variables

$$m_t = (b_o e^{-kt} - b)/b_o \tag{3.57}$$

$$\tau = kt \tag{3.58}$$

$$\chi_k = x/X_k \tag{3.59}$$

we obtain

$$\frac{\partial m_t}{\partial \tau} = \frac{\partial^2 m_t}{\partial \chi_k^2} - m_t \tag{3.60}$$

with boundary conditions

$$m_t = 0 \text{ at } \tau = 0 \tag{3.61}$$

$$m_t = e^{-\tau} \text{ at } \chi_k = 0. \tag{3.62}$$

$$m_t = 0 \text{ as } \chi_k \to \infty \tag{3.63}$$

Solution by Laplace transform[54] then gives

$$\left(\frac{\partial m_t}{\partial \chi_k}\right)_o = -\frac{e^{-\tau}}{(\pi\tau)^{\frac{1}{2}}} \tag{3.64}$$

and thus

$$j = (D/\pi)^{\frac{1}{2}} b_o t^{-\frac{1}{2}} e^{-k/t} \tag{3.65}$$

or

$$\ln(it^{\frac{1}{2}}) = -kt + \text{constant} \tag{3.66}$$

Equation (3.66) predicts that the current will tend to infinity at $t = 0$, which experimentally is impossible. In practice the transient is initially dominated by charging and discharing effects of the double layer capacitance at the working electrode, which can be described mathematically by Dawson's Integral[11,53,54]. The observed photocurrents are thus due to a combination of three effects: double layer charging, diffusion and pseudo-first order decay of photocurrent.

Chapter 4

THIAZINE DYES

This chapter describes the electrochemistry and photochemistry of some water-soluble thiazine dyes and the pH and temperature variation of the back reaction in the iron-thionine system.

4.1. pH and Temperature Variation of k_{-2} for Thionine[55]

The voltage developed by a photogalvanic cell can be increased by shifting the $E^{\ominus}$ of the dye system to more negative potentials. The pH variation of the standard electrode potential for the thionine-leucothionine couple has been measured by Lichtin[56] and by Albery *et al*[57]. These investigations show that below pH 3, $E^{\ominus}$ for the couple decreases by 90 mV per pH unit. The shift in $E^{\ominus}$ will also affect k_{-2} however, and thus the variation of k_{-2} with $[H_2SO_4]$ which might occur in an operating cell has been investigated for the iron-thionine system. A solar cell is likely to operate at temperatures greater than 25°C, and so the variation of k_{-2} with temperature was also investigated.

The rate determining step in the oxidation of leucothionine by ferric ions is the generation of $S^{\cdot}$. The reaction was therefore monitored by following the reappearance of thionine, produced by the rapid disproportionation of $S^{\cdot}$, using the stopped flow technique. Figure (4.1) shows a typical stopped flow transient as a plot of transmittance against time under pseudo-first order conditions. Figure (4.2) shows the data plotted according to equation (4.1).

$$\ln[\lg(I_0/I_t)] = -kt + \text{constant} \qquad (4.1)$$

Figure 4.1. Typical stopped flow transient. In this case [H_2SO_4]/M = 0.5, [Fe(III)]/mM = 5.0, T = 308.6 K.

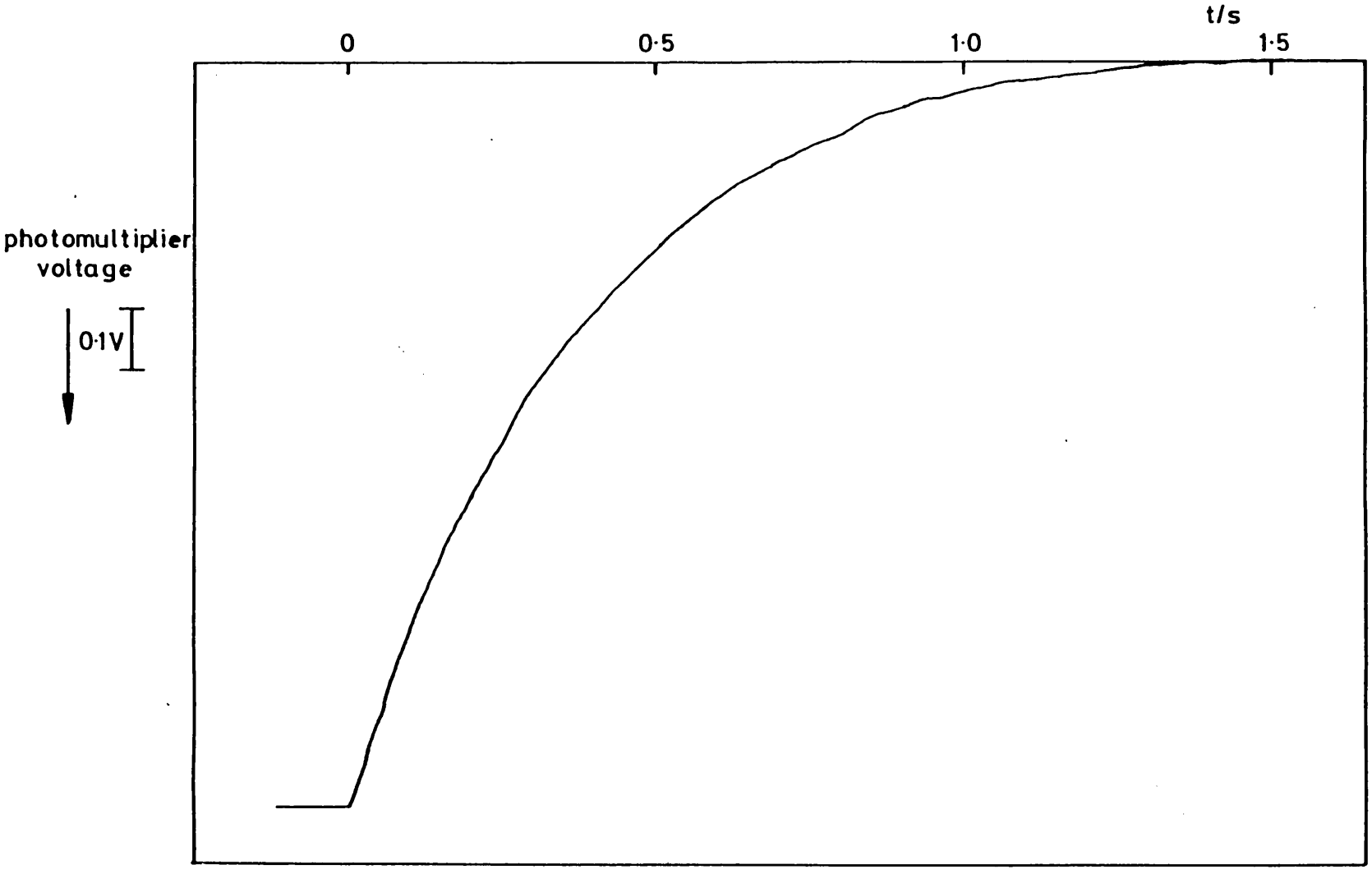

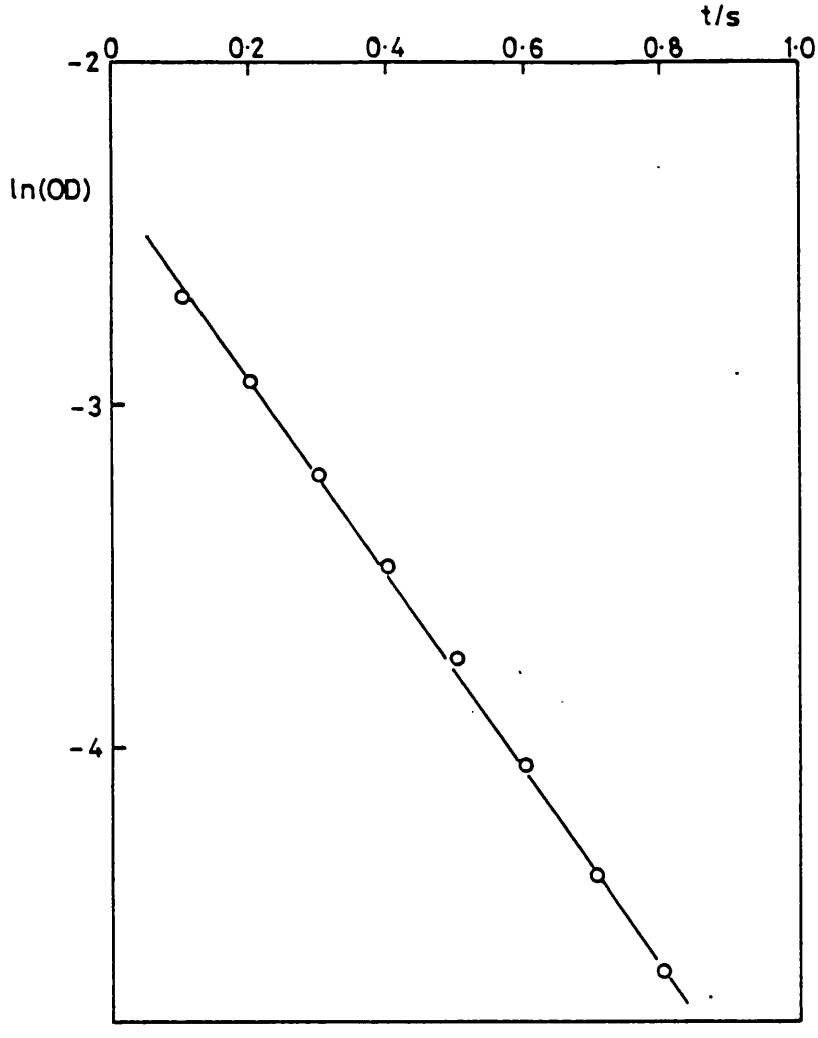

Figure 4.2. Stopped flow data plotted according to equation (4.1).

The ionic strength of solutions was held constant at 0.5 M using Li_2SO_4. Solutions of different acid concentration contained the same concentration of added sulphate, so that the same mixture of ferric complexes was present in each experiment. In this medium[58], Fe(III) exists as a mixture of $[Fe(SO_4)]^+$ and $[Fe(SO_4)_2]^-$ ions. Bisulphate ions are not thought to be involved in the complexation. Literature values[59] for the acid dissociation constant of leucothionine, pK_{a1} = 4.38 and pK_{a2} = 5.3, suggest that the leucothionine species will be in the same, doubly-protonated form throughout the range of acid concentrations studied.

For each pH, measurements were made at temperatures between 25°C and 50°C. A typical Arrhenius plot for the oxidation of leucothionine by Fe(III) is shown in figure (4.3). Values for the activation energy E_A, and the pre-exponential factor, A, at four different values of pH are given in table 4.1.

The data are presented in terms of a frequency factor and activation energy for the reaction rather than in terms of the enthalpy and entropy changes because there is some complexation between leucothionine and ferric and because the reaction can proceed by many paths. The results outline the pH dependence which would be found in an operating photogalvanic cell, the behaviour has not been broken down into the individual reaction routes.

The results are conveniently displayed in figure (4.4) as a contour diagram for k_{-2}. It was difficult to obtain accurate values for the $[H^+]$ in the range studied because of the inaccuracy of glass electrodes in this region and because of the equilibria between H^+ and SO_4^{2-}. However the rate was found to be roughly inversely proportional to $[H^+]$ and the following mechanism may be proposed:

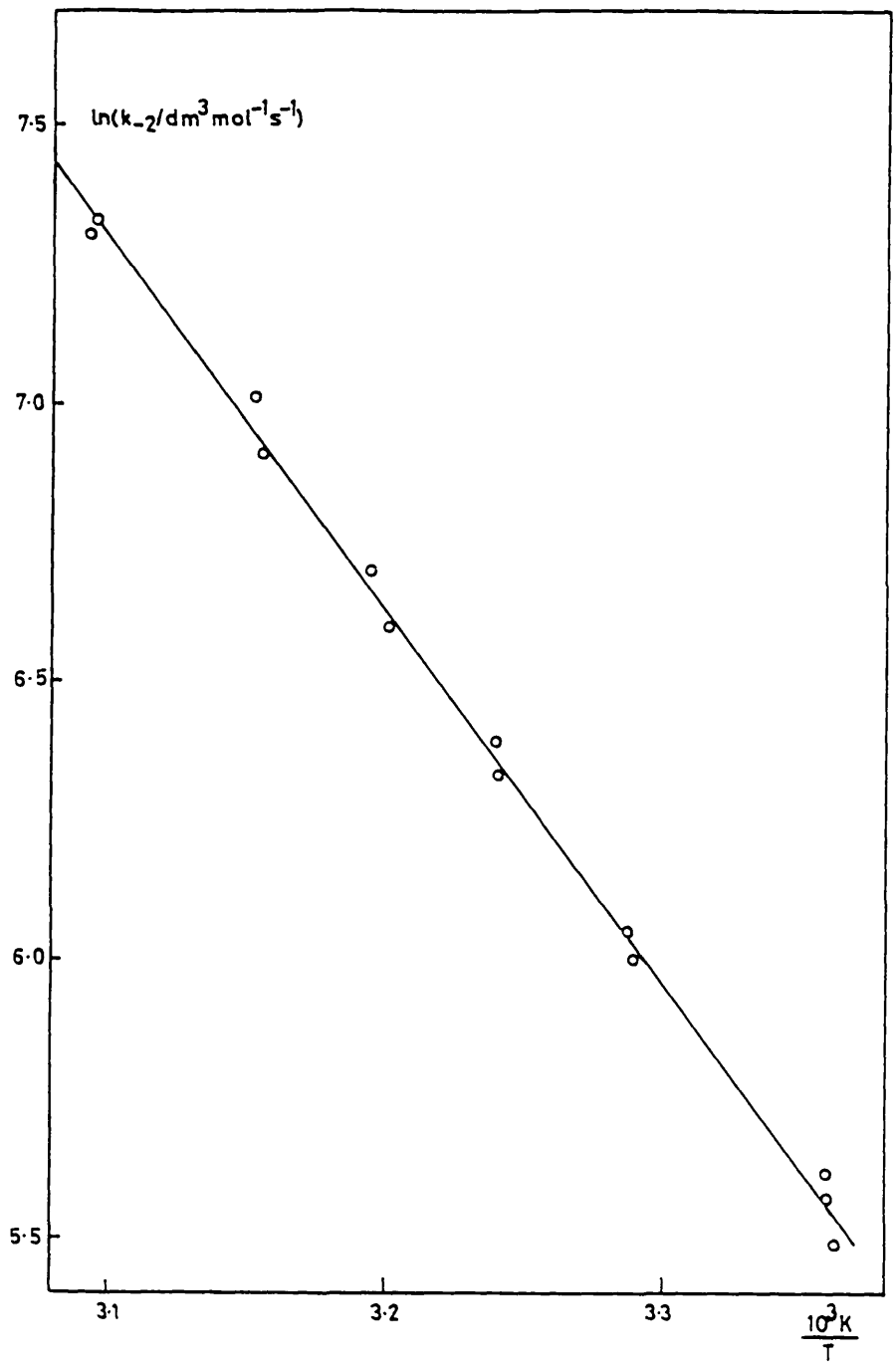

Figure 4.3. Arrhenius plot for the oxidation of leucothionine by ferric.
In this case $[L]_0/M = 9.8 \times 10^{-6}$
$[Fe(III)]/M = 2.4 \times 10^{-3}$
$[H_2SO_4]/M = 0.5$

Table 4.1

Arrhenius parameters for the reaction of leucothionine with Fe(III)

$[H_2SO_4]$/M	E_A/kJ mol^{-1}	10^2A/dm^3 mol^{-1} s^{-1}	$k_{-2}(298)$/dm^3 mol^{-1} s^{-1}
0.01	59(±4)	30	1690
0.02	59(±2)	35	1520
0.05	62(±2)	67	980
0.5	56(±1)	17	270

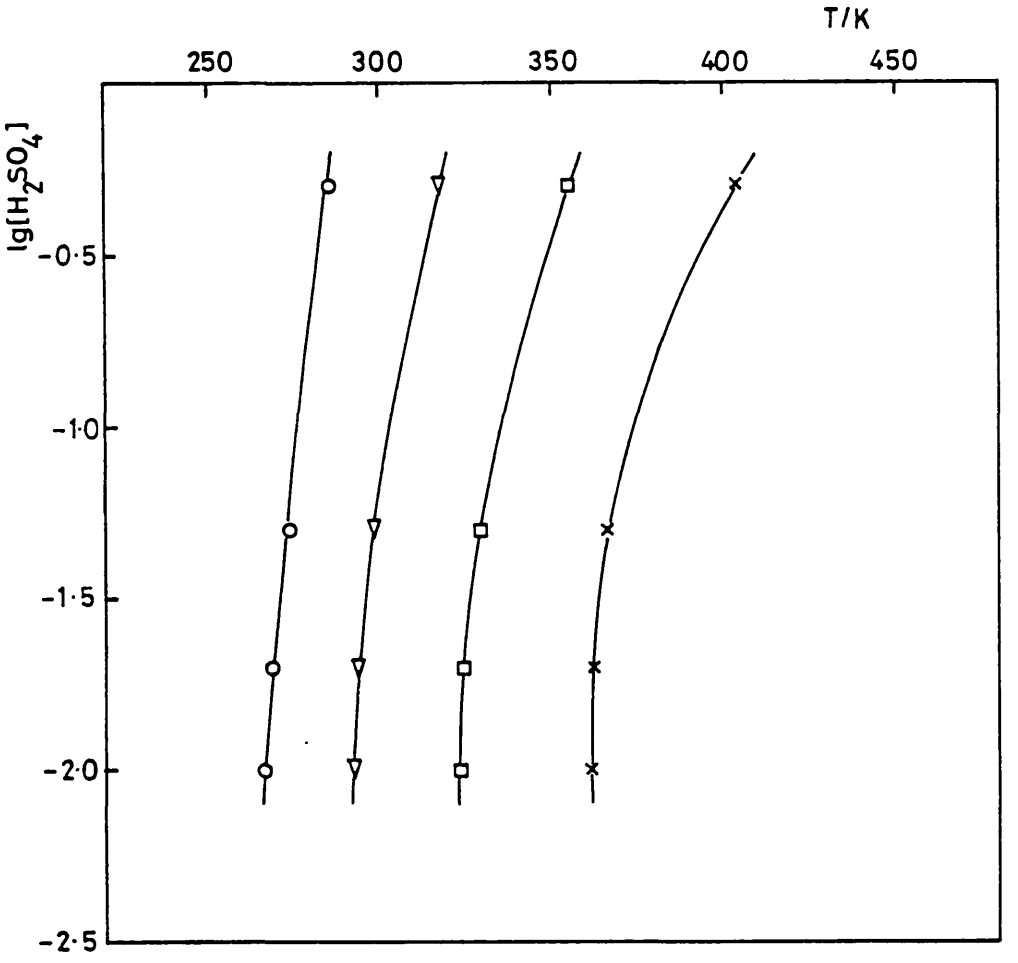

Figure 4.4. Isokinetic plot for the oxidation of leucothionine by ferric. Lines join values of temperature and $\lg[H_2SO_4]$ at which the back reaction rate constant has the same value.

Symbol	$k_{-2}/M^{-1}\ s^{-1}$
o	10^2
▽	10^3
□	10^4
x	10^5

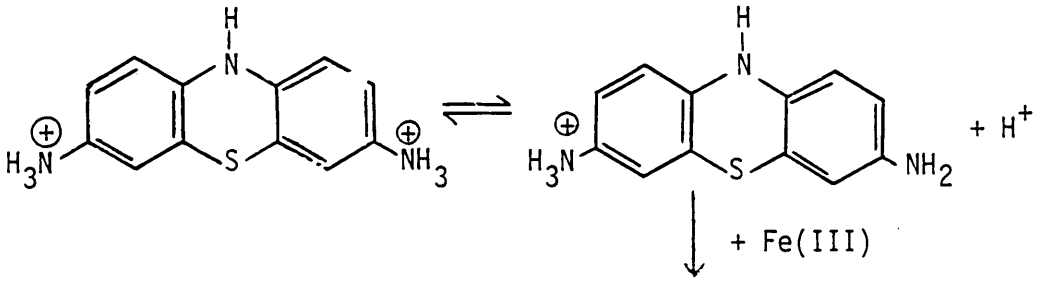

Two ways in which the efficiency of an iron-thionine cell can be improved are to change the redox potential of the dye couple and to increase the solubility of the dye.

The power available from a photogalvanic cell depends on the difference between the standard electrode potentials of the A/B and Y/Z couples. Souto-Bachiller[60] and Wilson[61] have synthesized methoxy-substituted thiazines to make the standard electrode potential of the dye couple more negative and thus increase the potential difference available. Structures of the dyes, dimethoxy thionine (DMeOT) and methoxysulphonated thionine (MeOST) are shown in figure (4.5). DMeOT was found to aggregate strongly to form dimers and higher aggregates. The dark electrochemistry of these dyes is described later.

In chapter 1 we said that in an ideal cell, $X_\varepsilon/cm = 1 \times 10^{-4}$. For a saturated solution of thionine in 50 mM H_2SO_4 (aq) $X_\varepsilon = 0.16$ cm. Thionine is not sufficiently soluble in aqueous solution, so a number of sulphonated thiazines have been synthesised to increased the dye solubility[60,61]. We now describe the properties of dimethyldisulphonated thionine isomer 2 (DMST2) (figure (4.5)) which has a solubility in 0.05 M H_2SO_4 of 1×10^{-3} M to 1×10^{-2} M at 25°C.

4.2. Photochemistry of DMST2

The ground state spectrum of DMST2 is similar to that of thionine and is shown in figure (4.6). Visible spectra of the dye showed no evidence

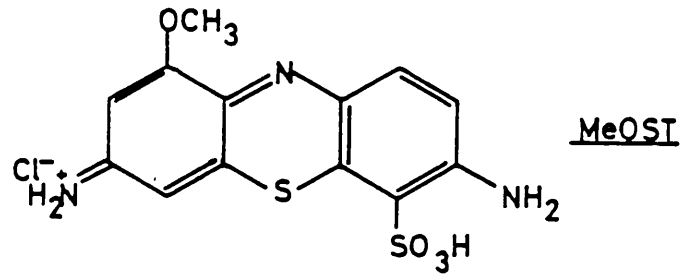

MeOST

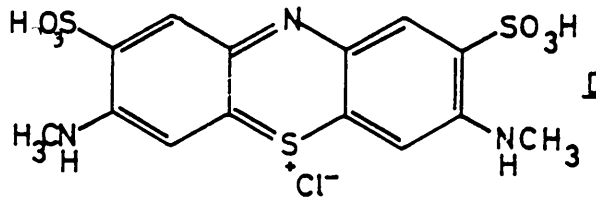

DMST2

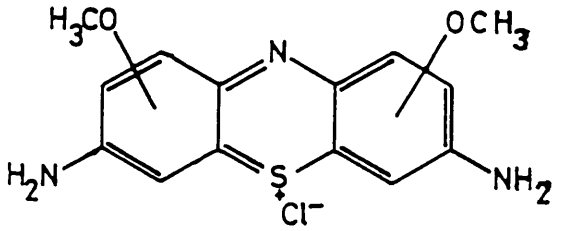

DMeOT

Figure 4.5. Structures of the thiazine dyes.

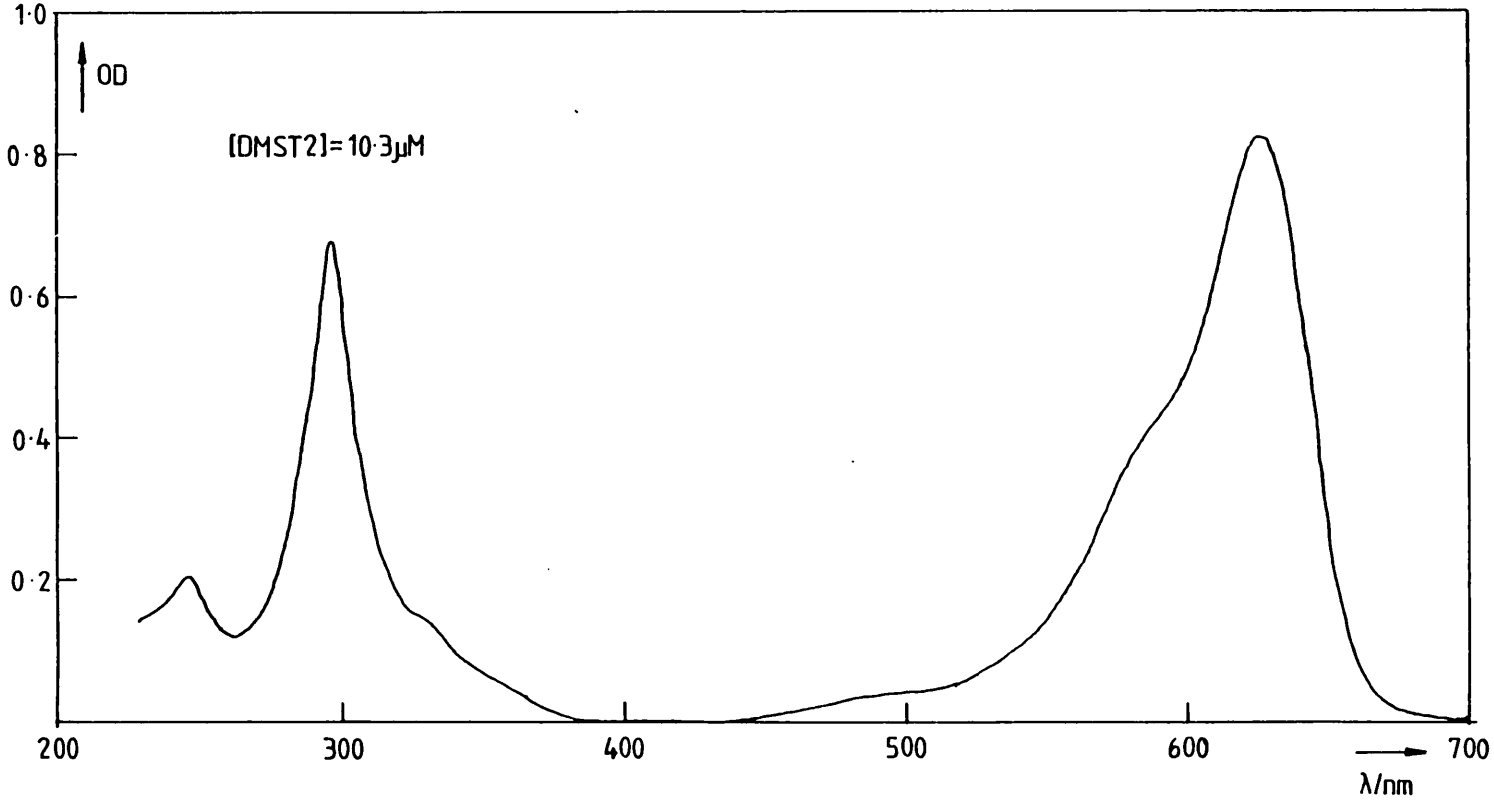

Figure 4.6. Absorption spectrum of DMST2 in 50 mM H_2SO_4.

of dimerisation up to 1 x 10^{-3} M. In this respect, DMST2 and other sulphonated thiazine isomers are considerably more suitable as dyes for a photogalvanic system than, for example, thionine and new methylene blue[62,21], which show dimerisation in aqueous solution at concentrations as low as 1 x 10^{-4} M.

The triplet spectrum of a 1.1 x 10^{-6} M solution of DMST2 was obtained using flash photolysis. Bonnean and Stevens[63] have shown that the triplet absorption spectrum of thionine is pH dependent, as an equilibrium exists between the mono-protonated and di-protonated species:

$$^3TH_2^{2+} \rightleftharpoons {}^3TH^+ + H^+ \qquad (4.2)$$

The triplet spectrum of DMST2 shown in figure (4.7) corresponds to that of the di-protonated thionine species but is shifted to the red by 55 nm.

Kinetic flash photolysis was used to measure the triplet decay by monitoring at 700 nm. A typical decay transient is shown in figure (4.8). The decay obeys first order kinetics and the triplet lifetime may be found by plotting ln(absorbance) against time (figure (4.9)). From an average of several values, the triplet lifetime of DMST2 was estimated as 13(±2)μs.

In the presence of 10 mM Fe(II) in a degassed solution, triplet DMST2 can be efficiently quenched to yield the semithiazine radical. The absorption spectrum of this species was obtained using flash photolysis. Absorbance measurements of semireduced DMST2 in 50 mM H_2SO_4 were recorded 100 μs after a 10 μs photoflash and the resulting spectrum, corresponding to the di-protonated semithiazine species[64,65] is shown in figure (4.10). If we assume that semi-reduced DMST2 does not absorb at 625 nm, a figure for the extinction coefficient at 750 nm can be calculated.

$$\varepsilon_{750}/dm^3\ mol^{-1}\ cm^{-1} = 12{,}8000$$

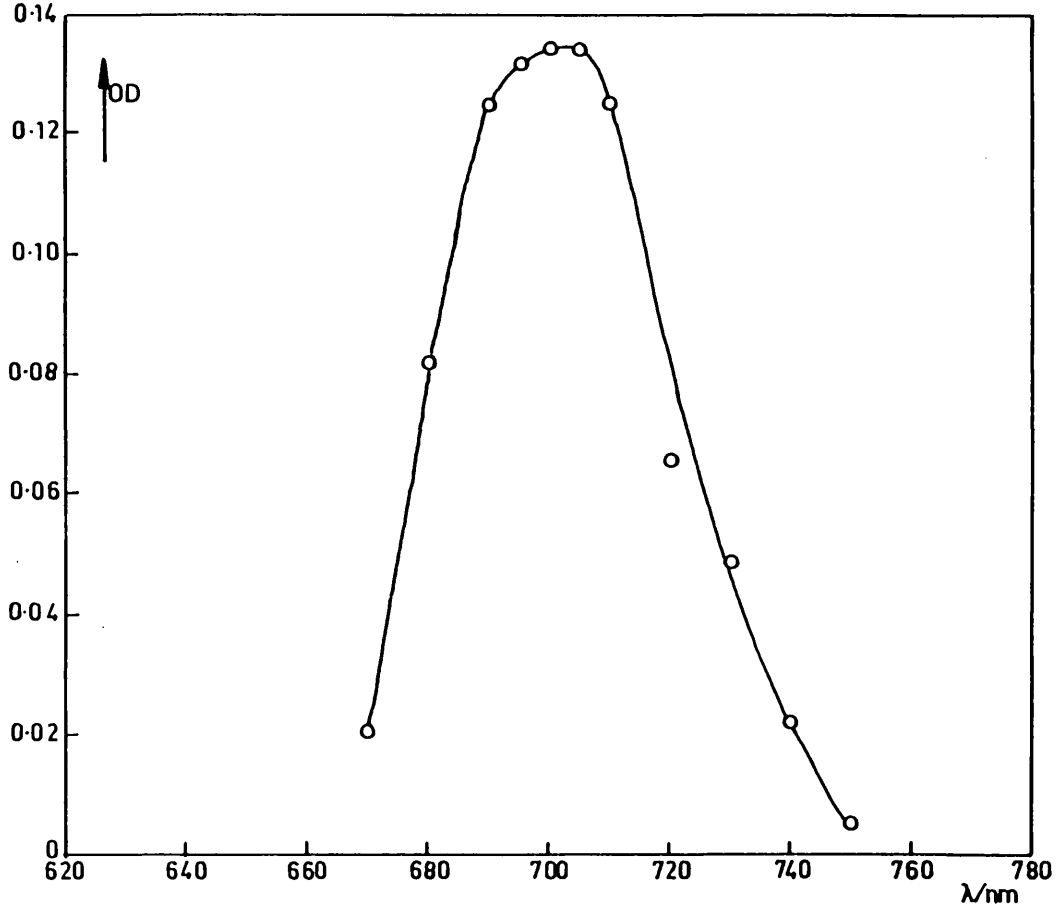

Figure 4.7. Absorption spectrum of diprotonated DMST2 triplet species.

Figure 4.8. Decay of diprotonated triplet DMST2 monitored at 700 nm.

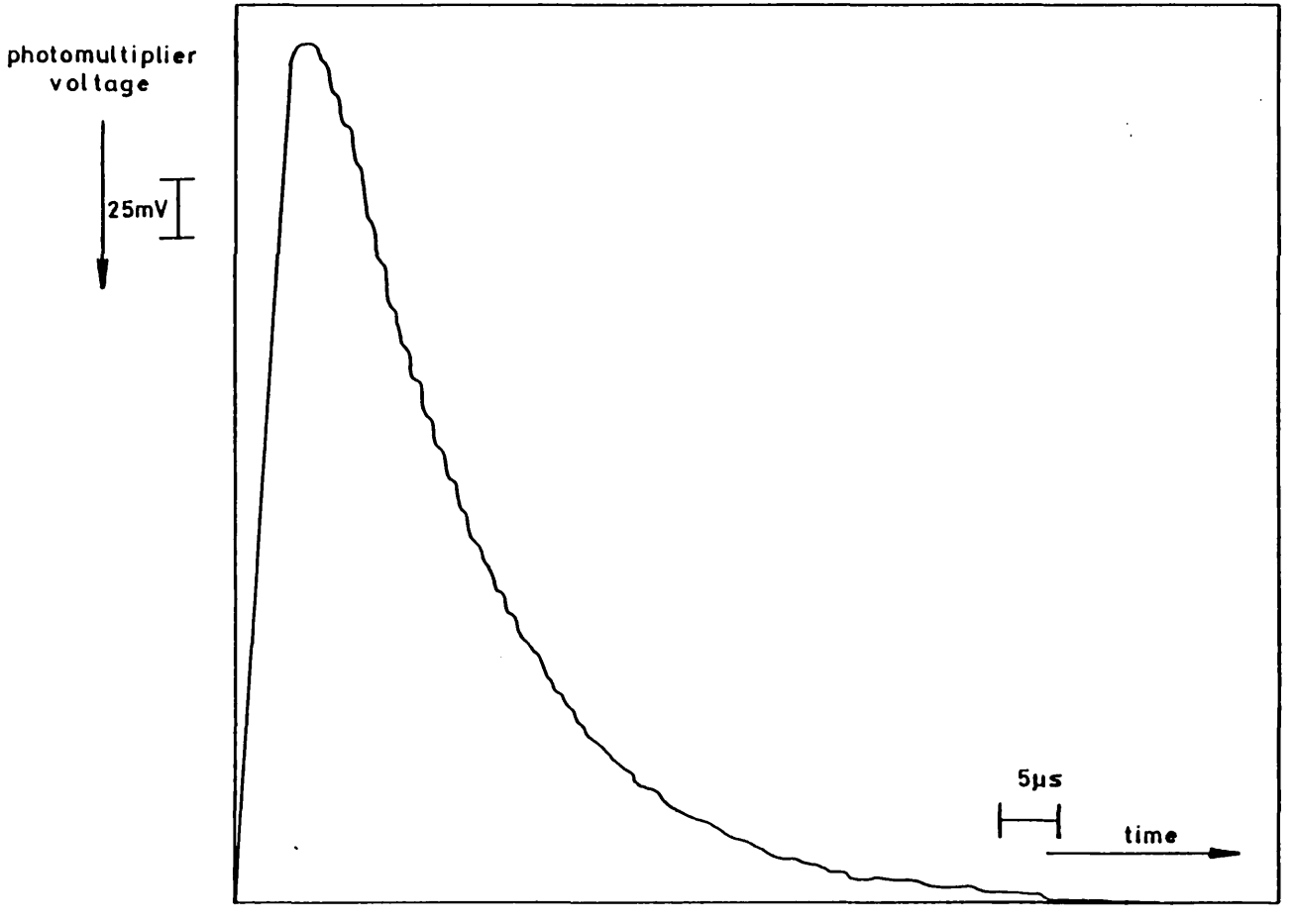

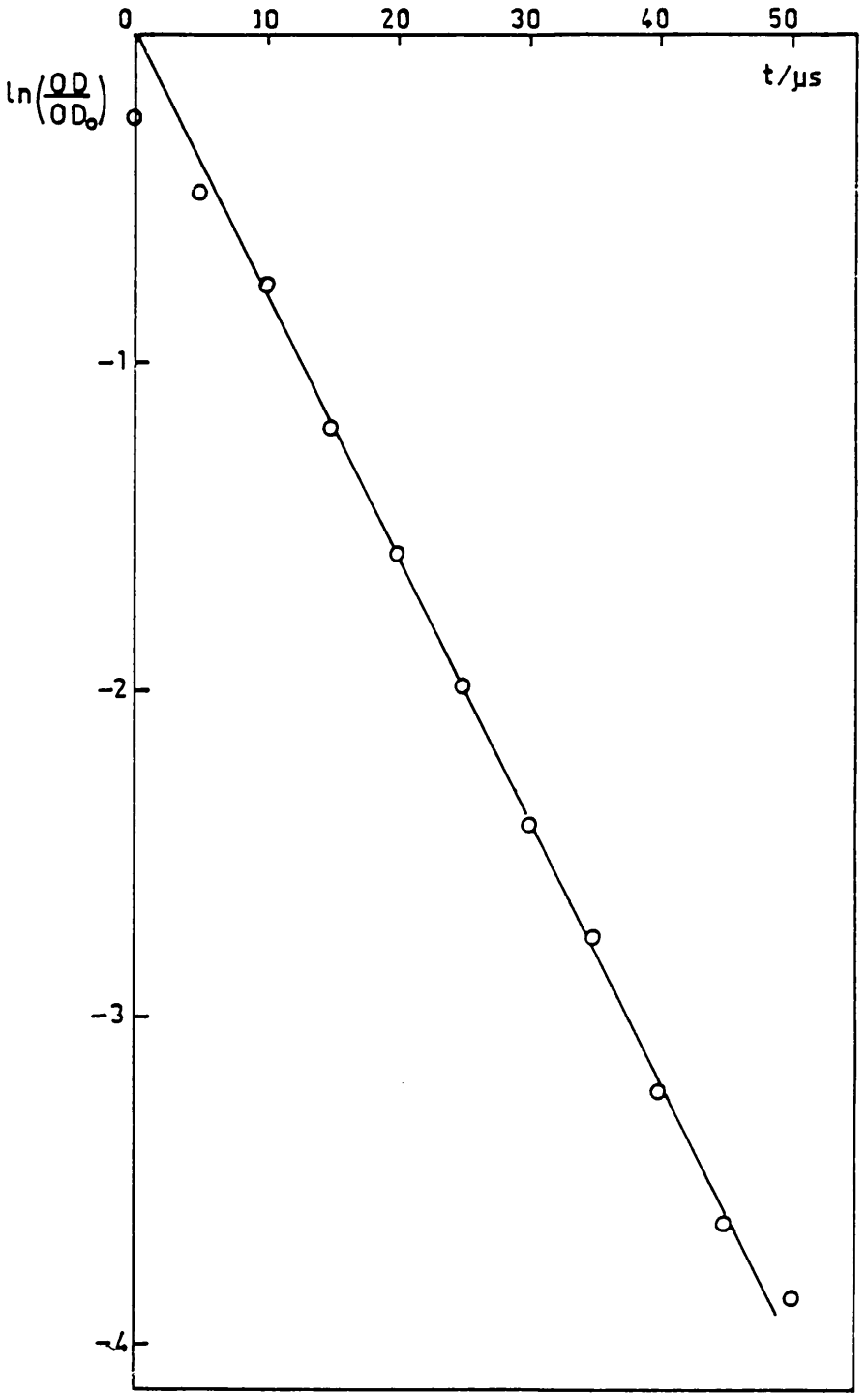

Figure 4.9 Plot of ln(absorbance) against time for triplet DMST2 to find the triplet lifetime.

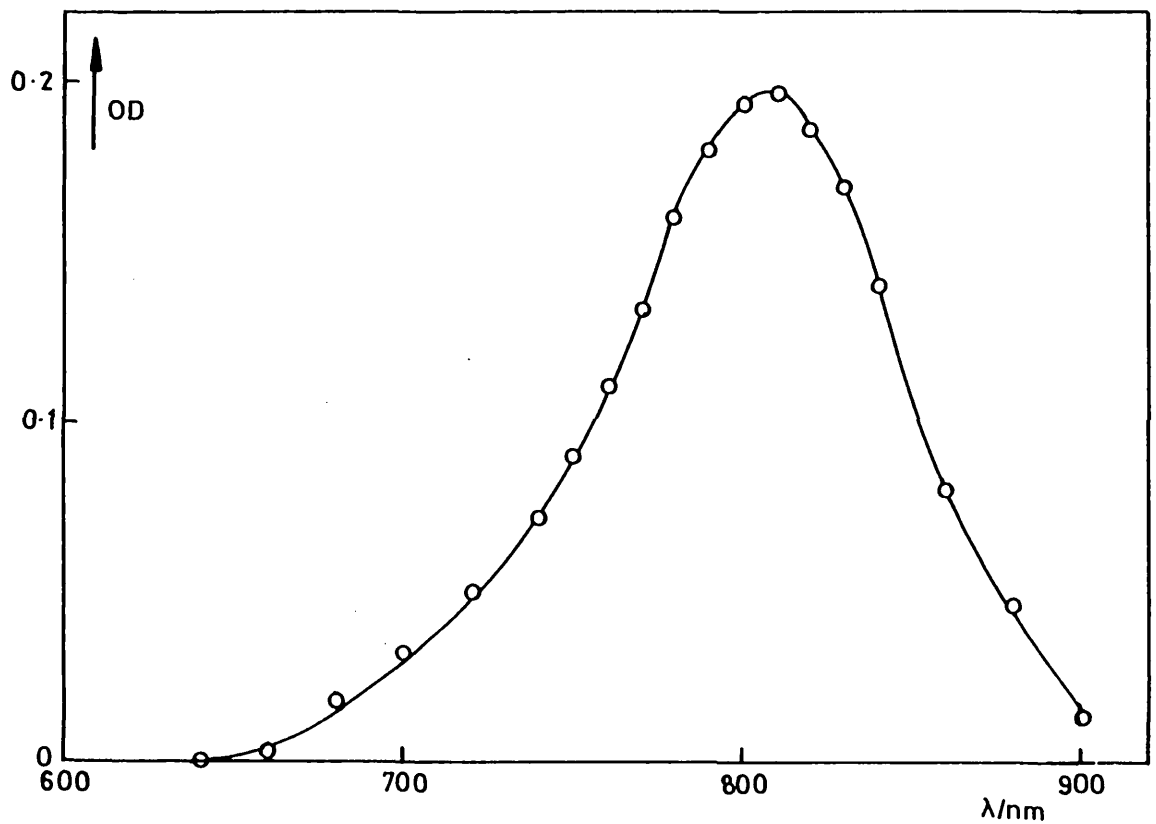

Figure 4.10. Transient absorption spectrum of diprotonated semi-reduced DMST2.

4.3. Thiazine Electrochemistry

DMST2

A current-voltage curve for reduction of DMST2 at a platinum electrode is shown in figure (4.11). Figure (4.12) is a Tafel plot for the wave (eqn. 3.17). The slope of the plot is that expected for a two-electron reversible wave (i.e. $k_o' >> k_D$) and the intercept on the x-axis is at +158 mV vs. SCE which is the formal electrode potential, E'. Figure (4.14) is a Nernst plot for the couple[82]. The slope of this plot confirms a value of n = 2 and the intercept on the y-axis is at +162 mV, which is again a value for the formal electrode potential.

Obtaining solid, crystalline samples of small quantities of the thiazine dyes proved difficult, so the extinction coefficient could not be found by dissolving a known quantity of the solid. The problem can be overcome however, by measuring the concentration of the dye electrochemically. Using the method of Albery and Hitchman[66], the diffusion coefficient of an electroactive species can be determined independent of its concentration or the number of electrons transferred. In this technique a small, known volume of solution is exhaustively electrolysed by a large rotating electrode at the limiting current. Under these conditions the current follows a simple first order decay and a plot of $\ln|i_L|$ against time (figure (4.15)) is linear, with a slope given by:

$$|\text{slope}|_{AH} = \frac{1.554\ AD^{2/3}\ W^{1/2}}{\nu^{1/6}\ V} \qquad (4.3)$$

where V is the volume of solution. A value for D the diffusion coefficient

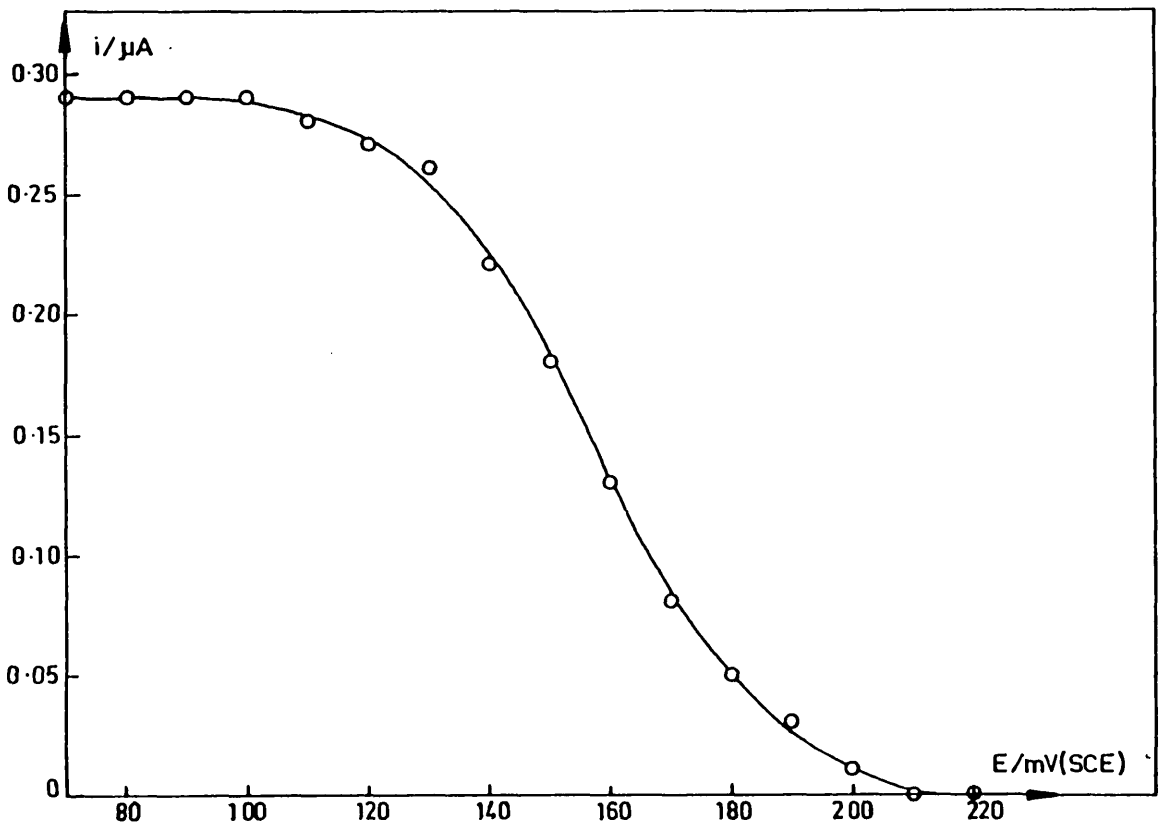

Figure 4.11. Current voltage curve for the reduction of DMST2 at a platinum RDE.

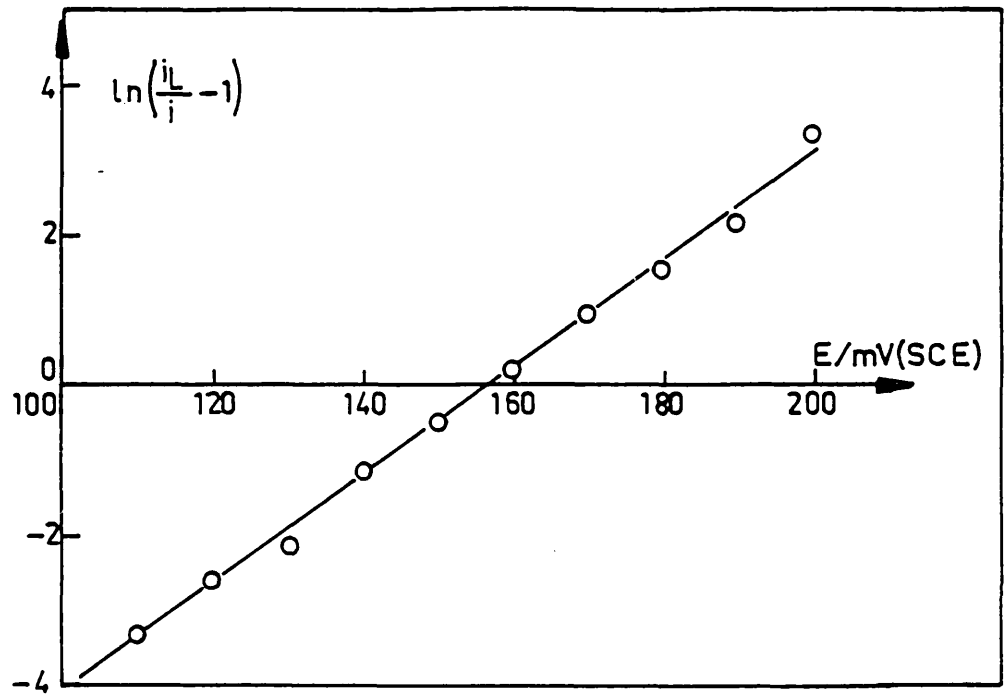

Figure 4.12. Tafel plot for DMST2.

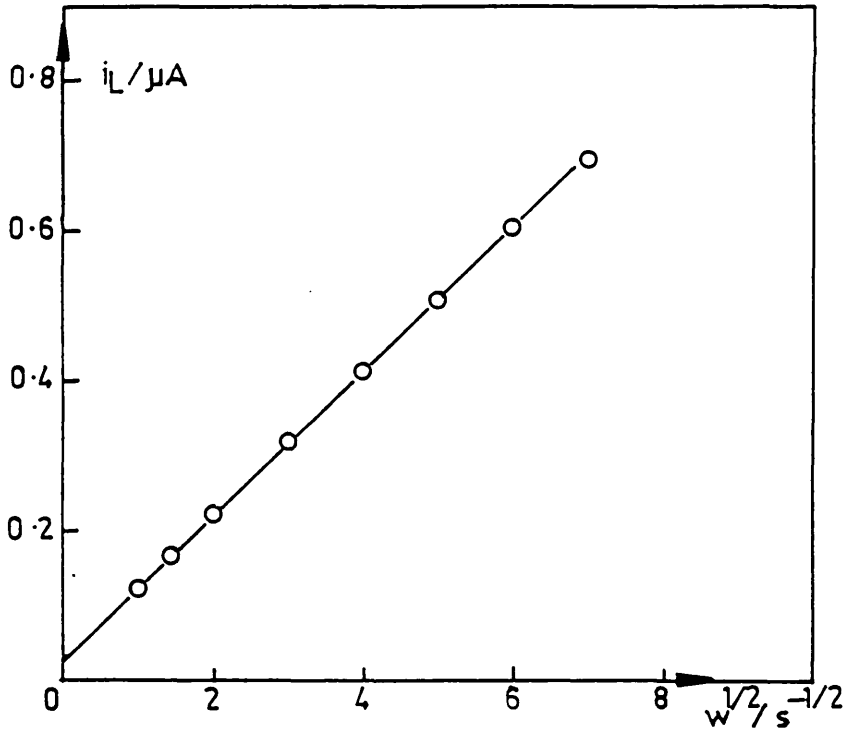

Figure 4.13. Levich plot for DMST2.

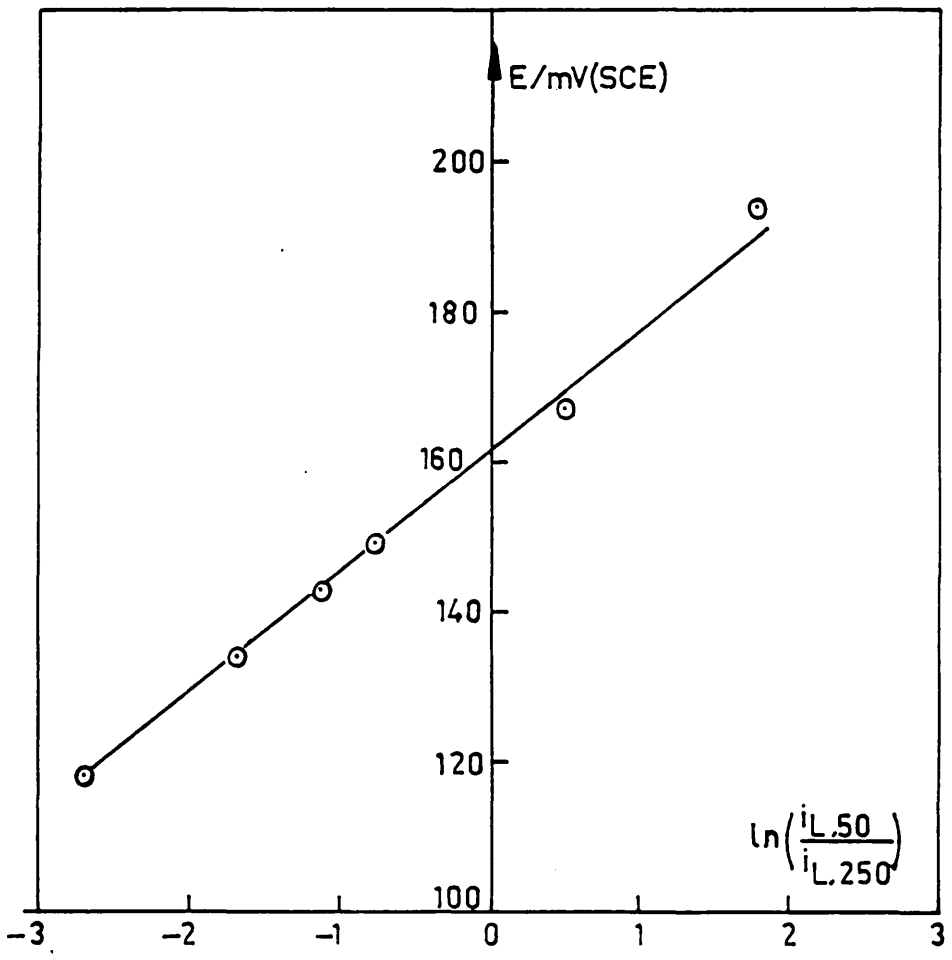

Figure 4.14. Nernst plot for DMST2.

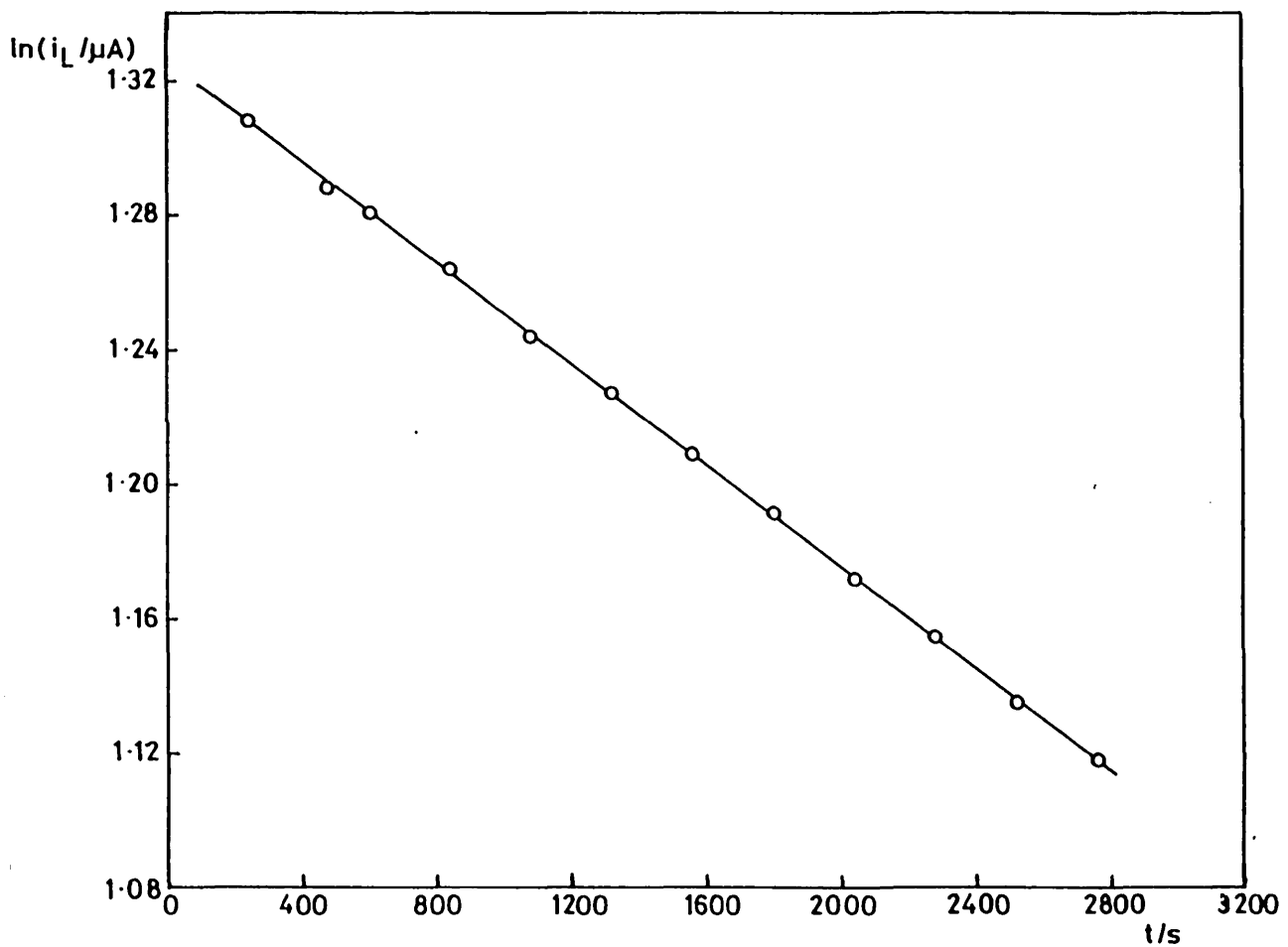

Figure 4.15. Variation of limiting current with time according to equation (4.3) to find the diffusion coefficient of DMST2.

of the dye can be found from equation (4.3). For DMST2

$$D/cm^2\ s^{-1} = 5.1 \times 10^{-6} \qquad (4.4)$$

Since equation (4.3) does not involve the concentration or the number of electrons transferred, the expression may be used to determine the diffusion coefficient. The dye concentration may then be calculated from the variation of limiting current with rotation speed using the Levich equation:

$$i_L = 1.554\ nFAD^{2/3}\ \nu^{-1/6}\ C_\infty\ w^{1/2} \qquad (3.15)$$

Figure (4.13) shows a Levich plot for DMST2 in 50 mM H_2SO_4. Once the concentration of the dye has been found in this manner, the extinction coefficient may be readily determined spectrophotometrically. The value obtained for DMST2 in 50 mM H_2SO_4 was

$$\varepsilon(\text{decadic})/dm^3\ mol^{-1}\ cm^{-1} = 8.0 \times 10^4 \qquad (4.5)$$

Results for DMST2, along with values for DMeOT and MeOST are summarised in table (4.2).

Table 4.2

Properties of thiazine dyes at 25°C in 0.05 M H_2SO_4

	MeOST	DMeOT	DMST2
λ_{max}/nm	590	595	626
$E_{\frac{1}{2}}$/mV (SCE)	+ 99	+117	+158
$E^{\ominus}$/mV (SCE)	+104	+127	+162
$D/10^{-6}$ cm^2 s^{-1}	3.3	2.8	5.1
ε(natural)/10^6 cm^2 mol^{-1}	81	100	180
ε(decadic)/dm^3 mol^{-1} cm^{-1}	35,000	44,000	80,000

Chapter 5

KINETIC STUDIES OF DMST2

One of the sulphonated thiazines, DMST2, was synthesized in sufficient quantity to allow a thorough investigation of the kinetic parameters of the iron-DMST2 system. This chapter describes the use of flash photolysis, stopped flow, flash electrolysis and the ORDE technique to determine quantum efficiencies for the production of semithiazine and leucothiazine and rate constants for the reactions of these species.

Flash Photolysis

In collaboration with Darwent, the fate of the semithiazine radical, both in disproportionation and in reaction with ferric was studied using flash photolysis[67-70].

5.1. Disproportionation Reaction of Semi DMST2

When no ferric has been added to the solution the predominant reaction of $S^{\cdot}$ is disproportionation:

$$H^{+} + 2S^{\cdot} \xrightarrow{k_3} Th + L \qquad (5.1)$$

At constant pH the rate expression for this reaction is given by

$$-d[S^{\cdot}]/dt = 2k_3[S^{\cdot}]^2 \qquad (5.2)$$

By integration, and using the Beer-Lambert Law we obtain

$$\frac{\varepsilon_D \ell}{(OD)} = 2\varepsilon_D \ell k_3 t + \frac{\varepsilon_D \ell}{(OD)_o} \tag{5.3}$$

where

ε_D is the decadic extinction coefficient,

ℓ is the path length, and

$(OD)_o$ is the optical density when t = 0.

The concentration of $S^{\cdot}$ was followed by absorbance measurements at 750 nm. A typical transient is shown in figure (5.1). A plot of 1/(OD) against time according to equation (5.3) is shown in figure (5.2) and from it we can obtain a value for k_3. Measurements were made in 0.05 M H_2SO_4 and 0.50 M H_2SO_4 at 21°C.

$$\text{In 0.05 M } H_2SO_4 \quad k_3/M^{-1}\ s^{-1} = 1.8\ (\pm 0.3) \times 10^9 \tag{5.4}$$

$$\text{In 0.50 M } H_2SO_4 \quad k_3/M^{-1}\ s^{-1} = 1.2\ (\pm 0.3) \times 10^9 \tag{5.5}$$

at 21°C

5.2. Reaction of Semithiazine with Ferric

It is difficult to determine a value for the rate constant of the reaction between $S^{\cdot}$ and Fe(III) by following the disappearance of the semithiazine absorption at 750 nm. This is because the ferric reaction is competing with the very fast (diffusion controlled) disproportion reaction of semithiazine radical. The reaction with ferric was best studied by following the reappearance of DMST2 on a time scale which is short compared to that for the oxidation of leucothiazine by ferric.

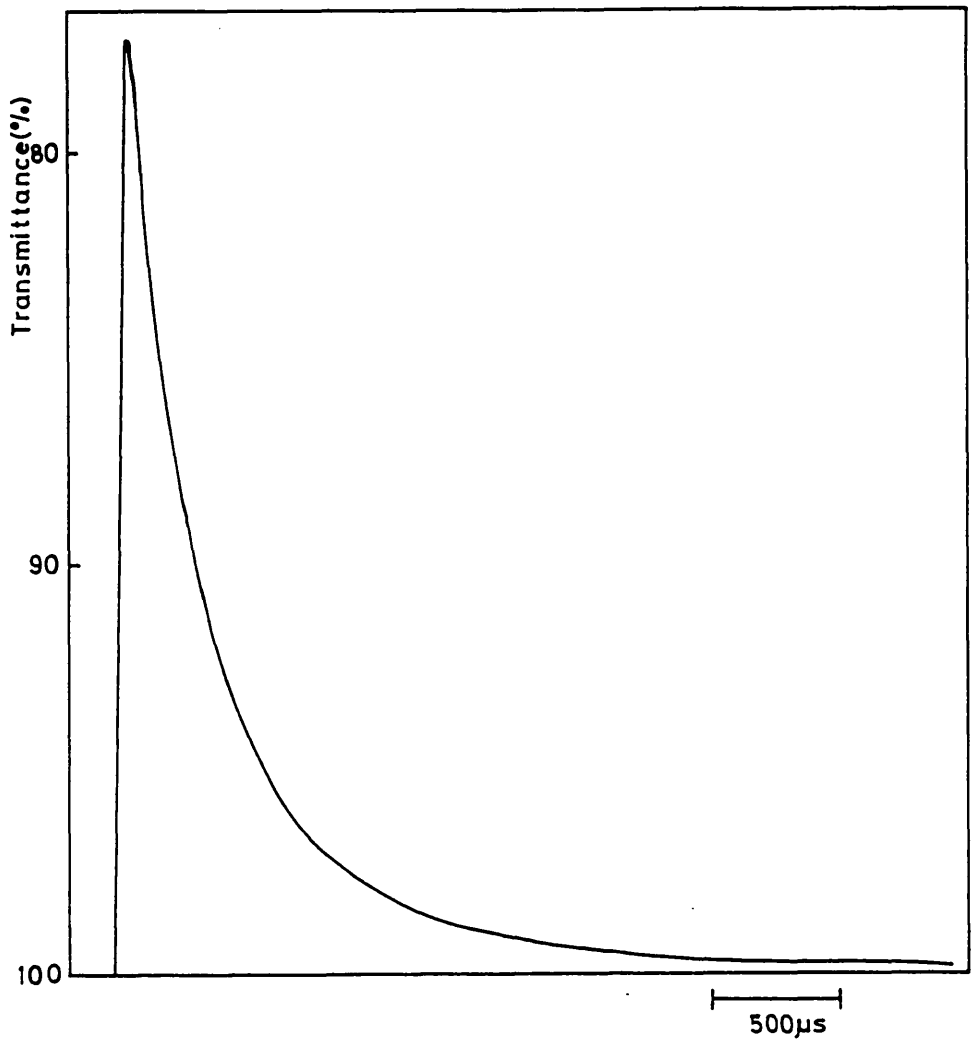

Figure 5.1. Semithiazine decay monitored at 750 nm.

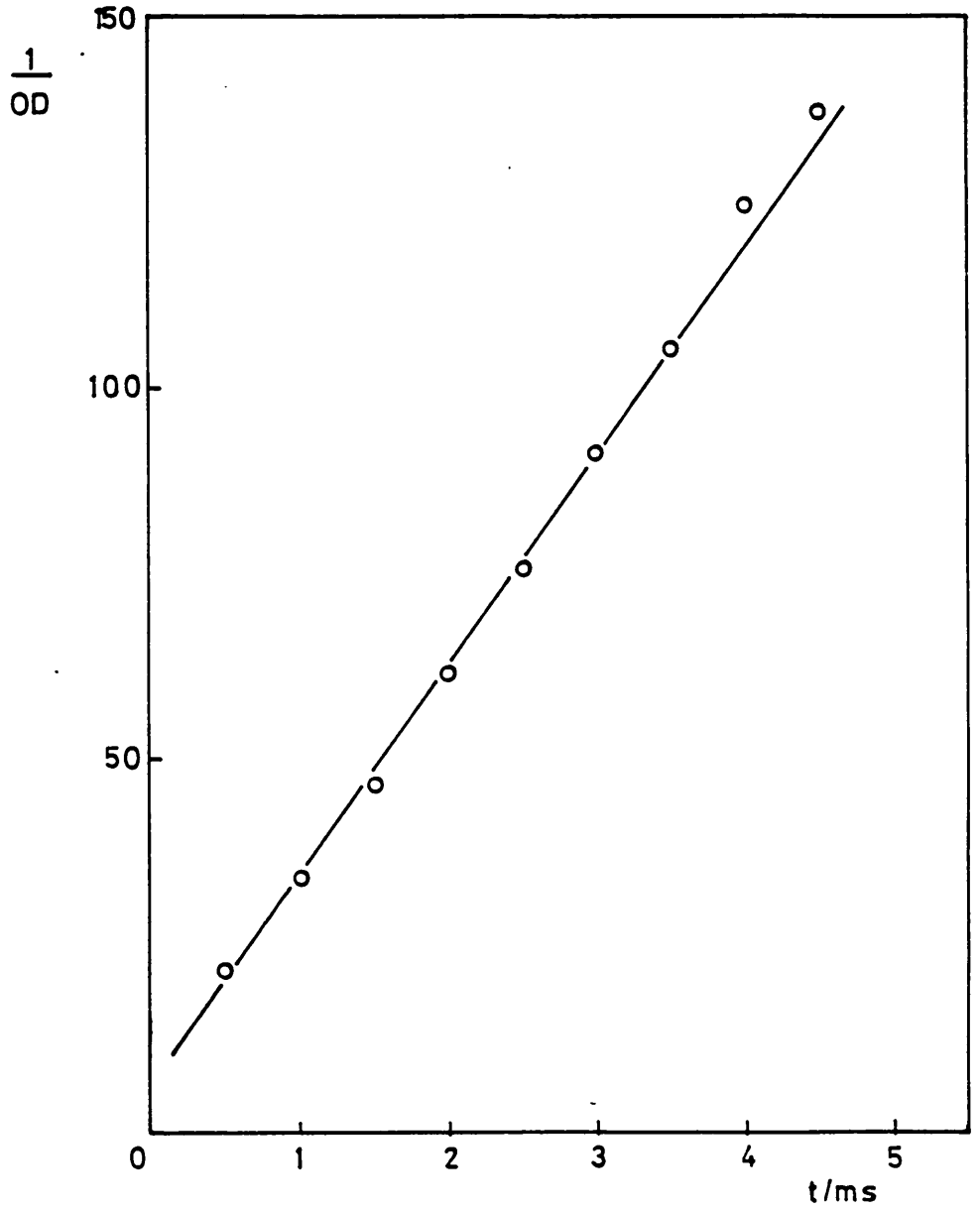

Figure 5.2. Decay of semireduced DMST2 with no added ferric plotted according to equation (5.3).

The two competing reactions are

$$H^+ + S^\cdot + S^\cdot \xrightarrow{k_3} Th + L \tag{5.4}$$

$$Fe(III) + S^\cdot \xrightarrow{k_{-1}} Th + Fe(II) + H^+ \tag{5.5}$$

The rate expressions in terms of the thiazine and semithiazine concentrations are

$$d[Th]/dt = k_3x^2 + k'_{-1}x \tag{5.6}$$

$$dx/dt = -2k_3x^2 - k'_{-1}x \tag{5.7}$$

$$\text{where } x = [S^\cdot] \tag{5.8}$$

$$\text{and } k'_{-1} = k_{-1}[Fe(III)] \tag{5.9}$$

From equations 5.6 and 5.7 we obtain

$$\frac{d[Th]}{dx} = \frac{k_3x + k'_{-1}}{2k_3x + k'_{-1}} \tag{5.10}$$

$$= -\frac{1}{2} - \frac{\frac{1}{2}k'_{-1}}{2k_3x + k'_{-1}} \tag{5.11}$$

$$\int_0^{\infty} d[Th] = -\int_{x_0}^{0} \left(\frac{1}{2} + \frac{\frac{1}{2}k'_{-1}}{2k_3x + k'_{-1}}\right) dx \tag{5.12}$$

$$[Th]_\infty = \left[\frac{1}{2} x + \frac{\frac{1}{2} k'_{-1}}{2k_3} \ln(k'_{-1} + 2k_3 x) \right]_0^{x_0} \tag{5.13}$$

$$= x_0/2 + k'_{-1}/4k_3 \ln(1 + 2x_0 k_3/k_{-1}) \tag{5.14}$$

$$\frac{[Th]_\infty}{x_0} = \frac{1}{2} + \frac{1}{2} (1/\Theta \ln(1 + \Theta)) = R \tag{5.15}$$

where

$$\Theta = 2k_3 x_0/k'_{-1} \tag{5.16}$$

At each concentration of Fe(III), a value of R was obtained from the flash photolysis transient, figure (5.3). In a process of trial and error, values of Θ were inserted into equation (5.15) until Θ corresponding to each experimentally determined value of R was calculated.

From equation (5.7) we have:

$$\frac{dx}{2k_3 x^2 + k'_{-1} x} = -dt \tag{5.17}$$

$$= \frac{dx}{x} \left(\frac{1}{k'_{-1} + 2k_3 x} \right) \tag{5.18}$$

$$= \frac{dx}{k'_{-1}} \left(\frac{1}{x} - \frac{2k_3}{k'_{-1} + 2k_3 x} \right) \tag{5.19}$$

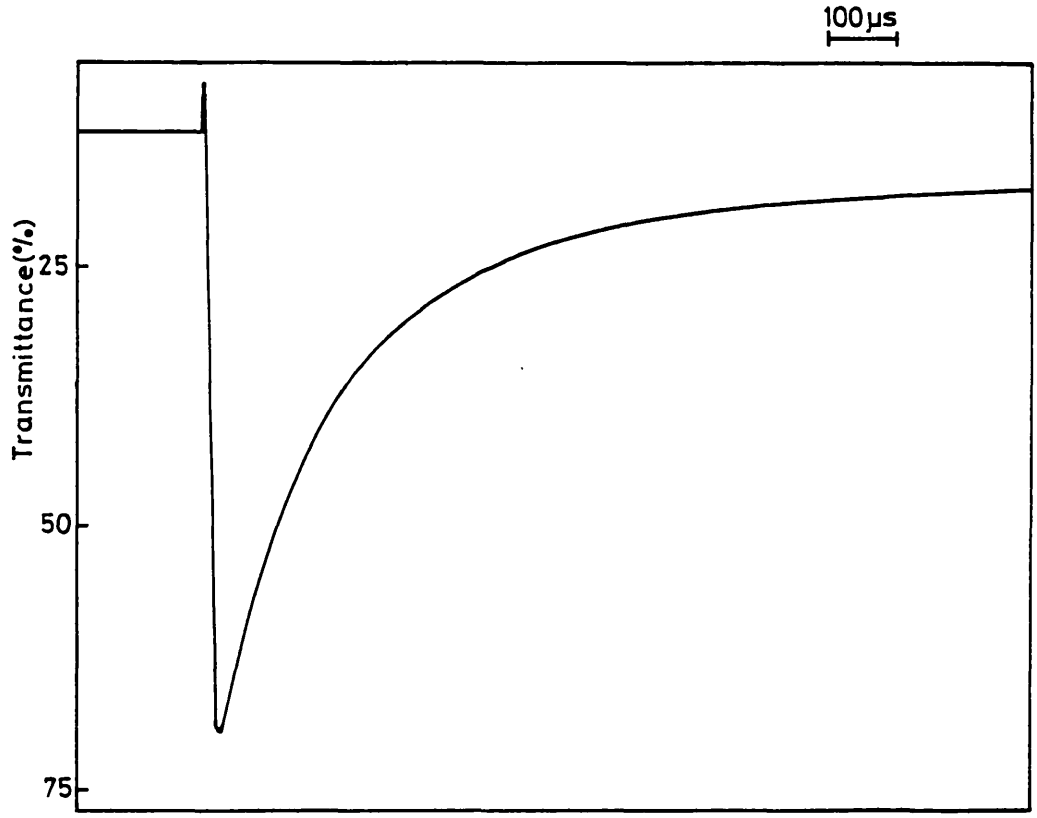

Figure 5.3. Semithiazine decay monitored at 625 nm with [Fe(III)]/mM = 14.9. At this wavelength we follow the re-appearance of DMST2.

$$- k'_{-1}t = \ln x/x_0 - \ln\left(\frac{k'_{-1} + 2k_3x}{k'_{-1} + 2k_3x_0}\right) \tag{5.20}$$

$$\ln\left(\frac{x/x_0}{1 + \theta x/x_0}\right) = - \ln(1 + \theta) - k'_{-1}t \tag{5.21}$$

Integrating equation (5.11) between [Th] = 0 and [Th] = [Th] we obtain

$$\frac{[Th]}{x_0} = \frac{1}{2} + \frac{1}{2\theta} \ln\left(\frac{1 + \theta}{1 + \theta x/x_0}\right) - \frac{x}{2x_0} \tag{5.22}$$

Using equation (5.15) this rearranges to

$$\frac{[Th]_\infty}{x_0} - \frac{[Th]}{x_0} = x/2x_0 + 1/2\theta \ln(1 + \theta x/x_0) \tag{5.23}$$

A series of values of x/x_0 in the range $0 < x/x_0 < 1$ were inserted into equation (5.23) to calculate corresponding values of $([Th]_\infty - [Th])$. Values of time corresponding to $([Th]_\infty - [Th])$ can be read off from the flash photolysis transient (figure (5.3)) and plotted according to equation (5.21), figure (5.4) to find k'_{-1}. Values of k'_{-1} were determined over a range of ferric concentrations and the variation of k'_{-1} with Fe(III) is shown in figure (5.5). This plot yields a figure for the second order rate constant in 0.05 M H_2SO_4 at 21°C:

$$k_{-1}/dm^3\ mol^{-1}\ s^{-1} = 8.4 \times 10^4 \tag{5.25}$$

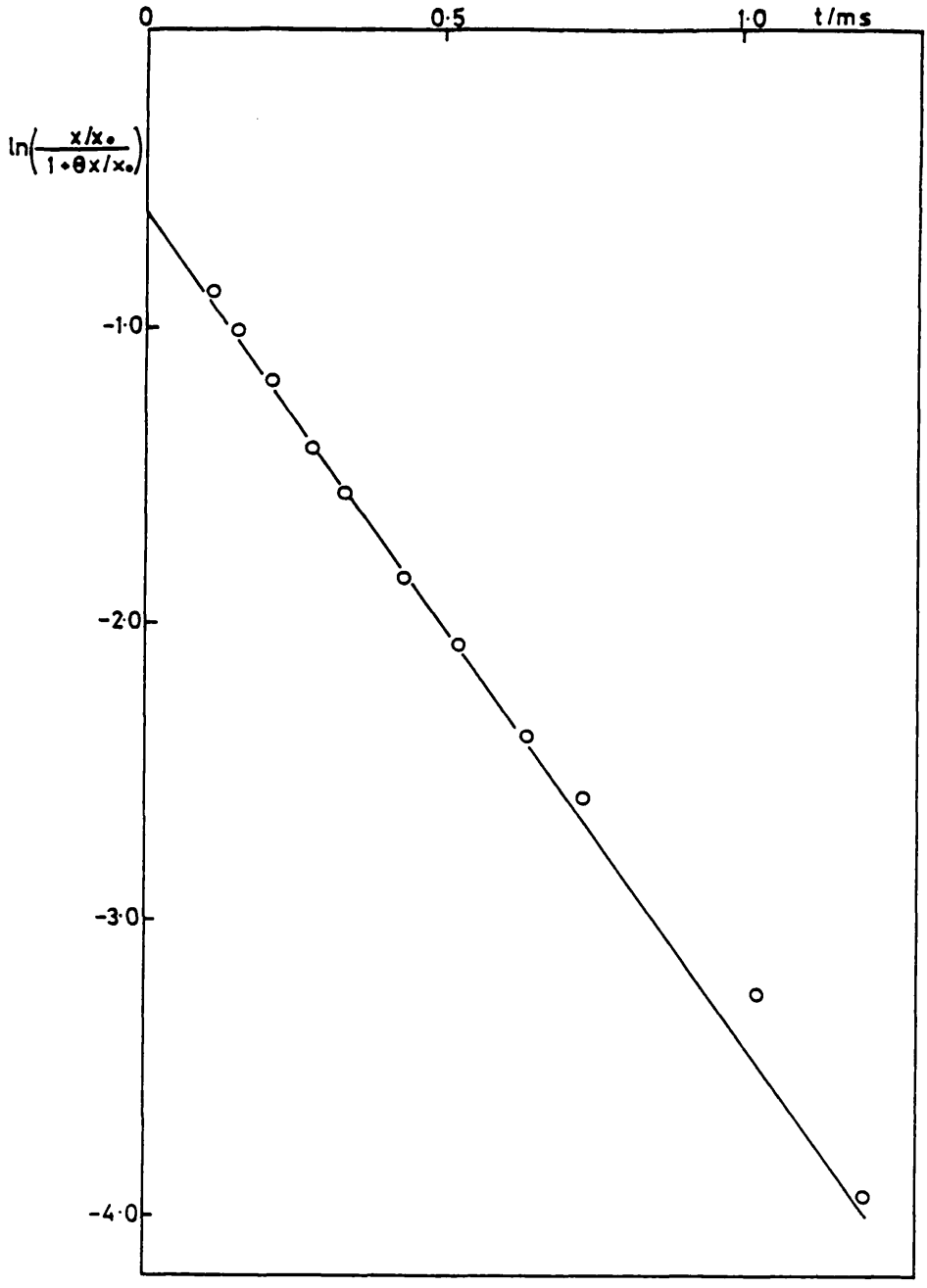

Figure 5.4. Plot of $\ln\left\{\frac{x/x_0}{1 + \theta x/x_0}\right\}$ against t according to equation (5.21). For this data [Fe(III)]/mM = 14.9.

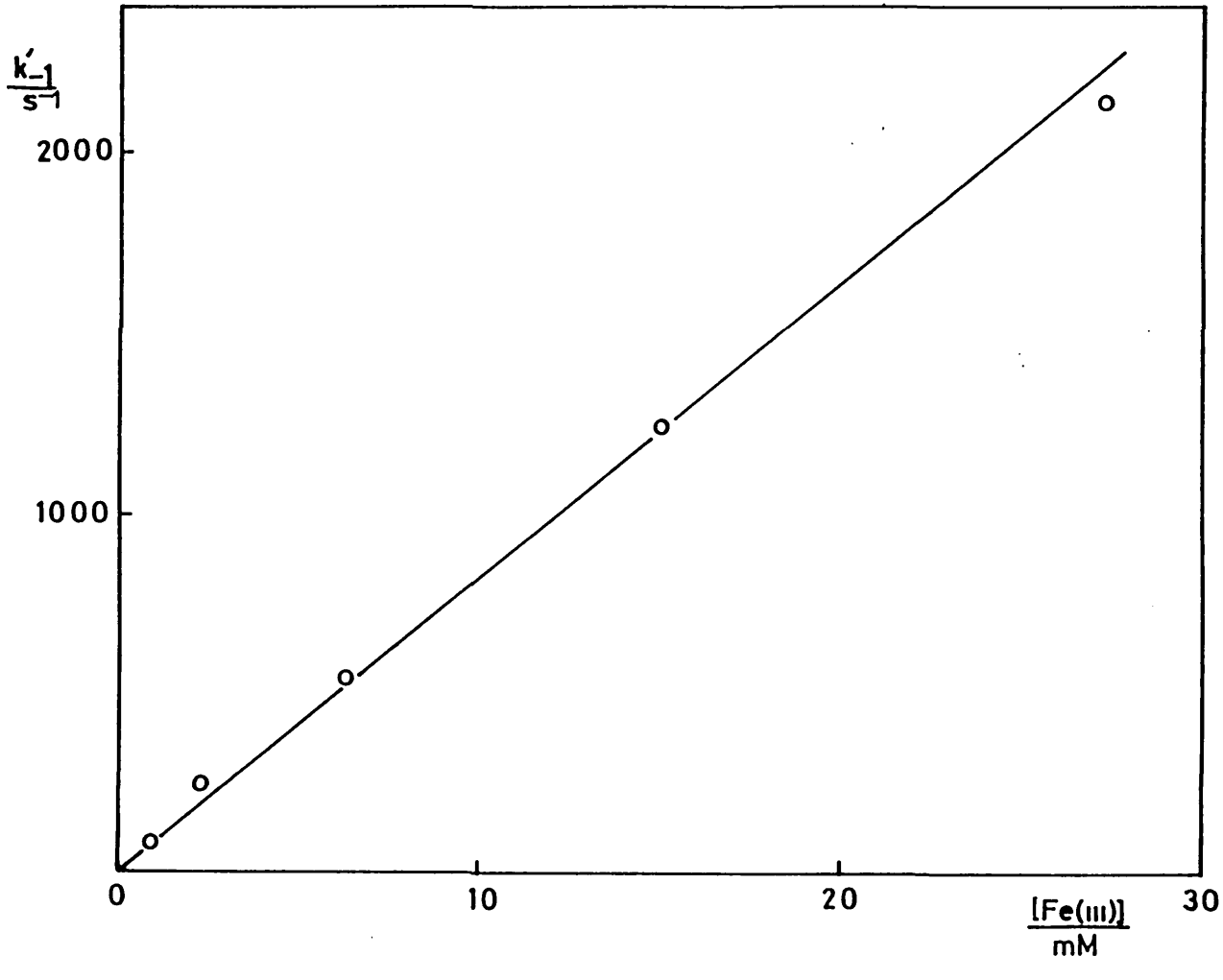

Figure 5.5. Plot of the pseudo first order rate constant for oxidation of $S^{\cdot}$ by ferric against [Fe(III)].

The plot of k'_{-1} vs [Fe(III)] (figure (5.5)) suggests that complexation between $S^{\cdot}$ and Fe(III) is not significant for DMST2 in the range of Fe(III) concentrations studied. The formation of a complex between Fe(III) and $S^{\cdot}$ has been suggested for thionine in 50 v/v% aqueous acetonitrile. Lichtin and co-workers[28] found that, for thionine, the value of k'_{-1}/k_3 decreased with increasing [Fe(III)]. However the decrease was too small and the experimental uncertainty too large to permit evaluation of an association constant. The method which we have used to investigate the possibility of complexation is more sensitive than that used by Lichtin because we obtain an individual rate constant k'_{-1} from the analysis, rather than the ratio of constants k'_{-1}/k_3 found previously.

5.3. Flash Photolysis Determination of k_{-2} for DMST2

Reaction of leucothiazine with ferric produces semithiazine which rapidly disproportionates to form thiazine. The disproportionation of semi DMST2 is diffusion-controlled, so the oxidation of leuco DMST2 by ferric can be studied by following the concentration of DMST2 at 625 nm.

A series of flash photolysis transients were obtained with:

DMST2/M = 1.5×10^{-6}

[Fe(II)]/mM = 10

[Fe(III)]/mM = 1.04

A typical transient is shown in figure (5.6). In figure (5.7) the data are plotted as ln[L] against time and this yields a rate constant for the back reaction:

$$k_{-2}/M^{-1}\ s^{-1} = 2.4(\pm\ 0.2) \times 10^3 \text{ (at } 21^{o}C) \qquad (5.26)$$

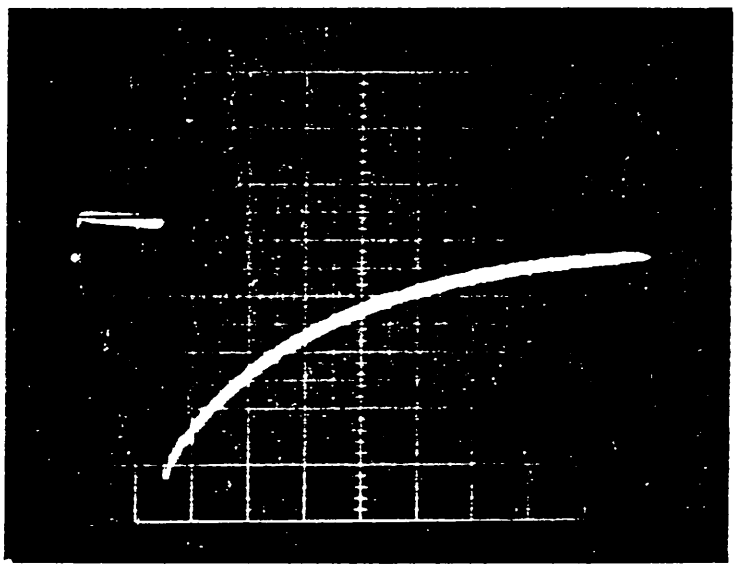

Figure 5.6. A typical flash photolysis transient used to determine k_{-2} for DMST2. In this case [Fe(III)]/M = 1.04×10^{-3}.
Timescale: 0.1 s/division.

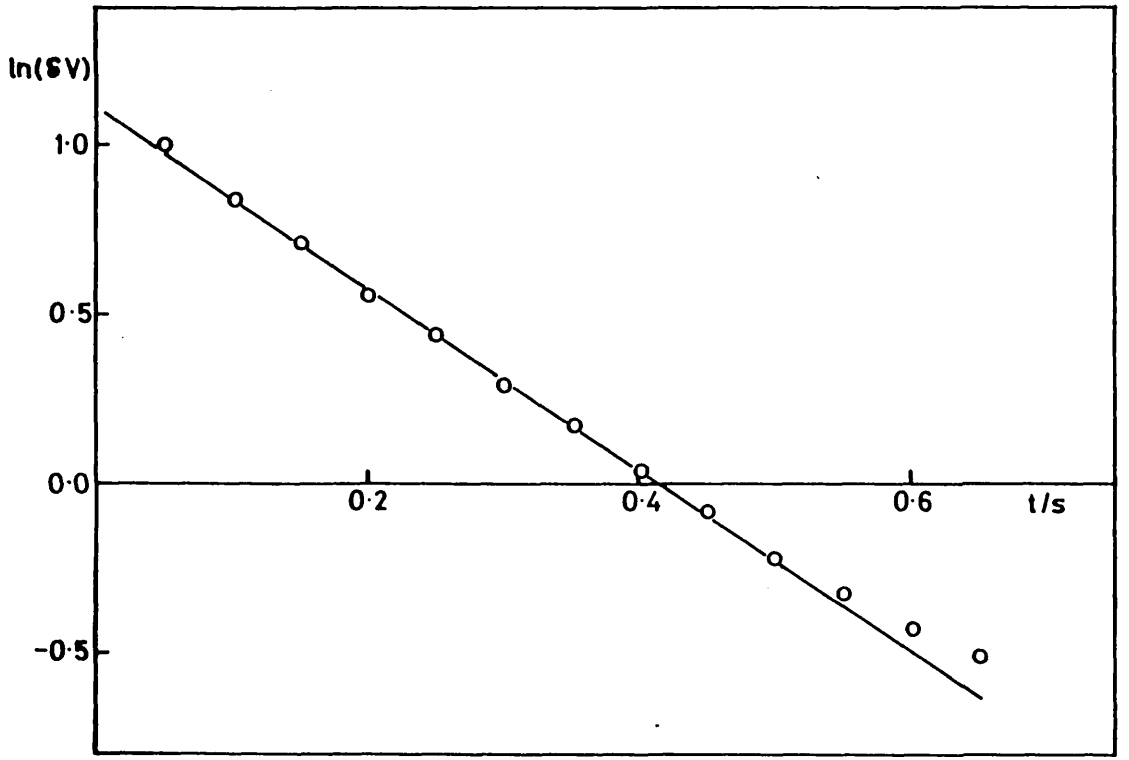

Figure 5.7. First order plot for the reaction of leuco-DMST2 with ferric. For this data [Fe(III)]/mM = 1.04.

5.4. Stopped Flow Determination of k_{-2} for DMST2

The reaction between ferric and leuco DMST2 in 50 mM H_2SO_4 was studied using the stopped flow technique. Kinetics were measured under pseudo-first order conditions over a range of concentrations of both reactants.

From the reaction scheme for the iron-thiazine system given in equation (3.27)

$$\text{If } k_3[S^{\cdot}] >> k_{-1}[Fe(III)] \tag{5.27}$$

$$\text{then } \partial[L]/\partial t = -\frac{1}{2} k_{-2}[Fe(III)][L] \tag{5.28}$$

since half of the leucothiazine lost returns to the leuco form by disproportionation.

$$\text{If } k_3[S^{\cdot}] << k_{-1}[Fe(III)] \tag{5.29}$$

$$\text{then } \partial[L]/\partial t = -k_{-2}[Fe(III)][L] \tag{5.30}$$

since no leuco dye is regenerated by disproportionation. The factor of two arises from the fate of semithiazine which can react with either $S^{\cdot}$ or Fe(III).

Using the steady-state assumption for $[S^{\cdot}]$ and writing

$$[L] = c \tag{5.31}$$

$$[S^{\cdot}] = x \tag{5.32}$$

$$k'_{-1} = k_{-1}[Fe(III)] \tag{5.33}$$

$$k'_{-2} = k_{-2}[Fe(III)] \tag{5.34}$$

we have:

$$k'_{-2}\ c = k'_{-1}x + 2k_3x^2 \tag{5.35}$$

and considering the consumption of Fe(III):

$$\frac{dc}{dt} = -\frac{1}{2}(k'_{-2}c + k'_{-1}x) \tag{5.36}$$

From equation (3.53),

$$2k_3x^2 + k'_{-1}x - k'_{-2}c = 0 \tag{5.37}$$

and solving this quadratic expression for x we obtain

$$\frac{\partial c}{\partial t} = -\frac{1}{2}k'_{-2}c\left\{1 + \frac{(k'_{-1})^2}{4k_3\ k'_{-2}\ c}\left[\left(1 + \frac{8k_3\ k'_{-2}\ c}{(k'_{-1})^2}\right)^{\frac{1}{2}} - 1\right]\right\} \tag{5.38}$$

The vital switch parameter between the two cases is γ where

$$\gamma = 4k_3k'_{-2}c/(k'_{-1})^2 \tag{5.39}$$

So

$$\frac{\partial c}{\partial t} = -\frac{1}{2}k'_{-2}c\ \{1 + ((1 + 2\gamma)^{\frac{1}{2}} - 1)/\gamma)\} \tag{5.40}$$

$$\simeq \frac{1}{2}k'_{-2}c \qquad \text{when } \gamma >> 1 \tag{5.41}$$

$$\simeq k'_{-2}c \qquad \text{when } \gamma << 1 \tag{5.42}$$

Now γ is proportional to c, and writing

$$\tau = k_{-2}[Fe(III)]t \tag{5.43}$$

we have

$$\frac{\partial\gamma}{\partial\tau} = -\frac{1}{2}(\gamma + (1 + 2\gamma)^{\frac{1}{2}} - 1) \tag{5.44}$$

By integration we obtain

$$\tau = \text{constant} - \ln\left[\frac{\gamma(3 + (1 + 2\gamma)^{\frac{1}{2}})^3}{1 + (1 + 2\gamma)^{\frac{1}{2}}}\right] \tag{5.45}$$

It is helpful to define τ_1, the value of τ for which $\gamma = 1$, the balance point between the two regimes.

From eqn. (3.45) we now obtain

$$\tau - \tau_1 = -\ln\left[\frac{\gamma(3 + (1 + 2\gamma)^{\frac{1}{2}})^3}{(1 + (1 + 2\gamma)^{\frac{1}{2}}\ 6(3 + 2\sqrt{3})}\right] \tag{5.46}$$

$[L] = [L]_0$ when $t = 0$

A plot of $\ln([L]/[L]_0)$ against $[Fe(III)]t$ is shown in figure (5.8) along with a plot of $\ln\gamma$ against $(\tau - \tau_1)/k_{-2}$ obtained from equation (5.46).

Figure 5.8. Comparison of theory (solid line) and experiment (circles) for back reaction data obtained by stopped flow. A value of $k_{-2}/M^{-1}s^{-1} = 3.7 \times 10^3$ was used for the theory curve.

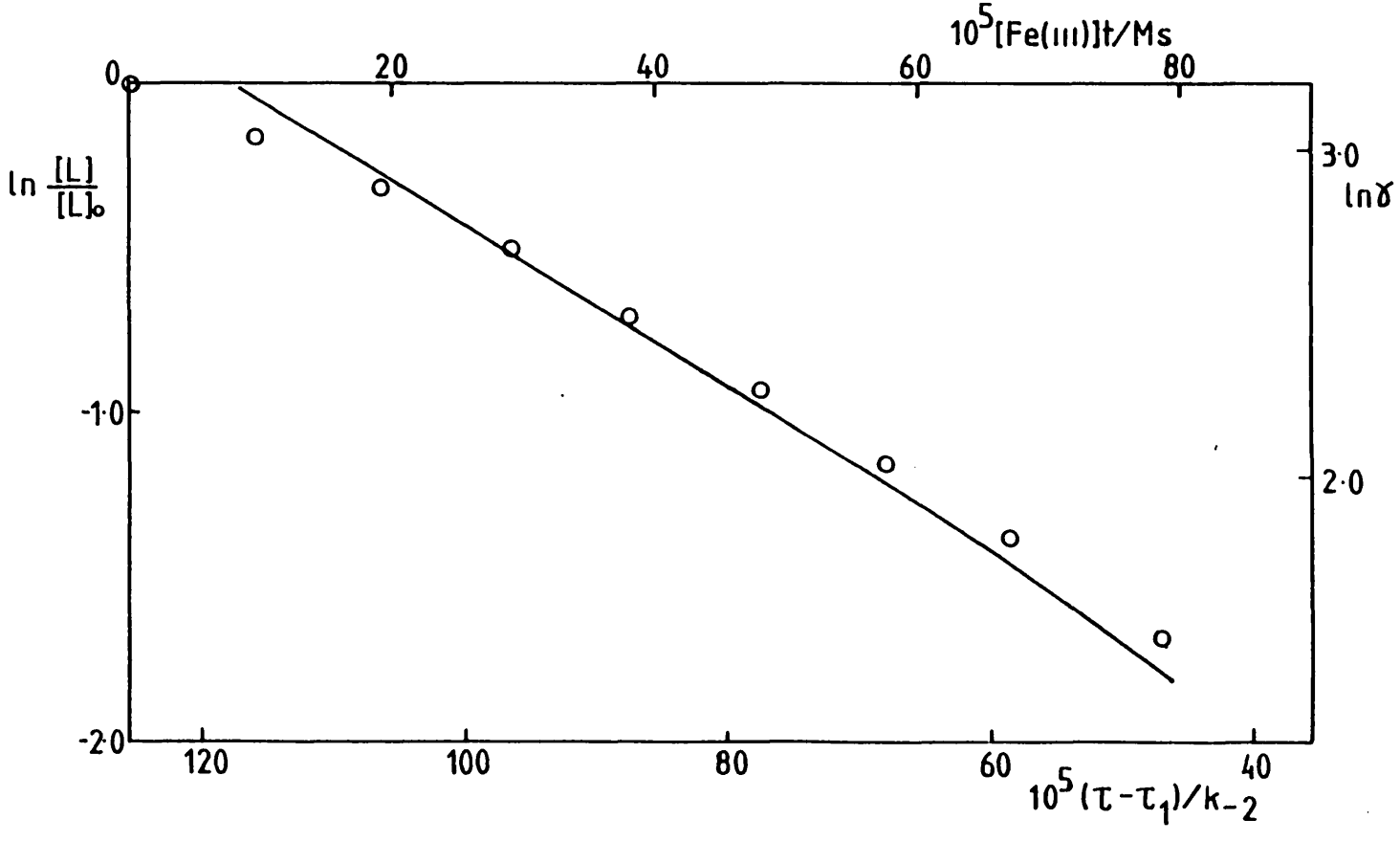

In these stopped flow results for DMST2 $\gamma \simeq 1$ and the experimental data clearly shows a switch from the initial gradient, where

$$\partial \ln[L]/\partial t = 1.7 \times 10^3 \ M^{-1} \ s^{-1} = k_{-2}/2 \qquad (5.47)$$

to the final gradient, where

$$\partial \ln[L]/\partial t = 3.7 \times 10^3 \ M^{-1} \ s^{-1} = k_{-2} \qquad (5.48)$$

A value of $k_{-2}/M^{-1} \ s^{-1} = 3.7 \times 10^3$ (at 25^oC) was used in the theoretical plot shown with the data in figure (5.8).

From the experimental and theoretical curves in figure (5.8) and comparing equations (5.38), (5.39), (5.43) and (5.46) we obtain

$$\ln([L]/[L]_o) - \ln\gamma = \ln(k_{-1}^2[Fe(III)]/4k_3k_{-2}[L]_o) \qquad (5.49)$$

$$= -3.2 \qquad (5.50)$$

From the previous analysis, equation (5.48)

$$k_{-2}/M^{-1} \ s^{-1} = 3.7 \times 10^3 \qquad (5.48)$$

and for this transient

$$[L]_o/M = 7.6 \times 10^{-6}$$

$$[Fe(III)]/M = 3.8 \times 10^{-3}$$

Hence we obtain a value for k_3/k_{-1}^2

$$k_3/k_{-1}^2 = 0.83 \text{ (at } 25^oC) \tag{5.51}$$

Using flash photolysis we found

$$k_3/k_{-1}^2 = \frac{1.8 \times 10^9}{(8.4 \times 10^4)^2} = 0.26 \text{ (at } 21^oC) \tag{5.52}$$

There is reasonably good agreement between the rate constants obtained using flash photolysis and those obtained using stopped flow considering that the experiments were conducted at different temperatures.

Re-writing equation (5.40) as

$$\frac{\partial \ln\gamma}{\partial \tau} = \tfrac{1}{2}\{1 + [(1 + 2\gamma)^{\frac{1}{2}} - 1]/\gamma\} \tag{5.53}$$

and by differentiation, we find that the point of maximum curvature in a plot of $\ln\gamma$ against $(\tau - \tau_1)/k_{-2}$ (figure (5.8)) occurs when $\gamma \simeq 1.7$.

Kinetic parameters for DMST2 and thionine are compared in table (5.1).

For stopped flow experiments using $[L]_0 = 7.6 \times 10^{-6}$ M and $[Fe(III)] = 3.8 \times 10^{-3}$ M, initial values of γ are:

γ_0 (thionine) = 0.014

γ_0 (DMST2) = 7.6

Table 5.1

Kinetic Parameters for Thionine and DMST2

	Thionine†	DMST2
$k_{-1}/M^{-1}s^{-1}$	5.8 (± 2.1) x 10^5	8.4 x 10^4
$k_{-2}/M^{-1}s^{-1}$	2.4 (± 0.4) x 10^2	3.7 x 10^3
$k_3/M^{-1}s^{-1}$	2.4 x 10^9	1.8 x 10^9

†Results of Brokken-Zijp and de Groot[19] at 22°C

0 < pH < 2.5.

In an experiment using thionine, $\gamma < 1$ throughout the transient, $-\partial \ln[L]/\partial t = k_{-2}$ and a plot of $\ln([L]/[L]_0)$ against $[Fe(III)]t$ is linear with slope = $-k_{-2}$. Using DMST2, at the beginning of the transient $\gamma > 1$ and $-\partial \ln[L]/\partial t = \frac{1}{2} k_{-2}$. At the end of the transient when almost all of the leuco dye has been consumed, $\gamma < 1$ and $-\partial \ln[L]/\partial t = k_{-2}$. Hence a plot of $\ln([L]/[L]_0)$ against $[Fe(III)]t$ for DMST2 shows curvature with a factor of 2 between the initial and final slopes.

An Arrhenius plot, describing the temperature variation of the reaction between leuco DMST2 and ferric is shown in figure (5.9). The kinetics were measured under pseudo-first order conditions with $[DMST2] = 9.1 \times 10^{-6}$ M and $[Fe(III)] = 5.2 \times 10^{-4}$ M. From figure (5.9) we obtain a value for the activation energy of the back-reaction

$$E_{act}/kJ\ mol^{-1} = 60\ (\pm\ 2) \qquad (5.54)$$

and a value for the rate constant at 25°C

$$k_{-2}/M^{-1}\ s^{-1} = 3.6\ (\pm\ 0.3) \times 10^{3} \qquad (5.55)$$

5.5. Flash Electrolysis Measurements on DMST2

The rate of the back-reaction between Fe(III) and leucothiazine can be determined by flash electrolysis. Figure (5.10) shows a typical current transient with $[DMST2] = 35 \times 10^{-6}$ M and $[Fe(III)] = 4.0 \times 10^{-3}$ M. The electrode was held at +401 mV (SCE), the potential of zero dark current.

Figure (5.11) shows the data from a flash electrolysis transient plotted according to equation (3.66). In this case $[Fe(III)]/M = 2.2 \times 10^{-3}$ and the observed rate constant is $k'_{-2}/s^{-1} = 9.8$. A series of transients

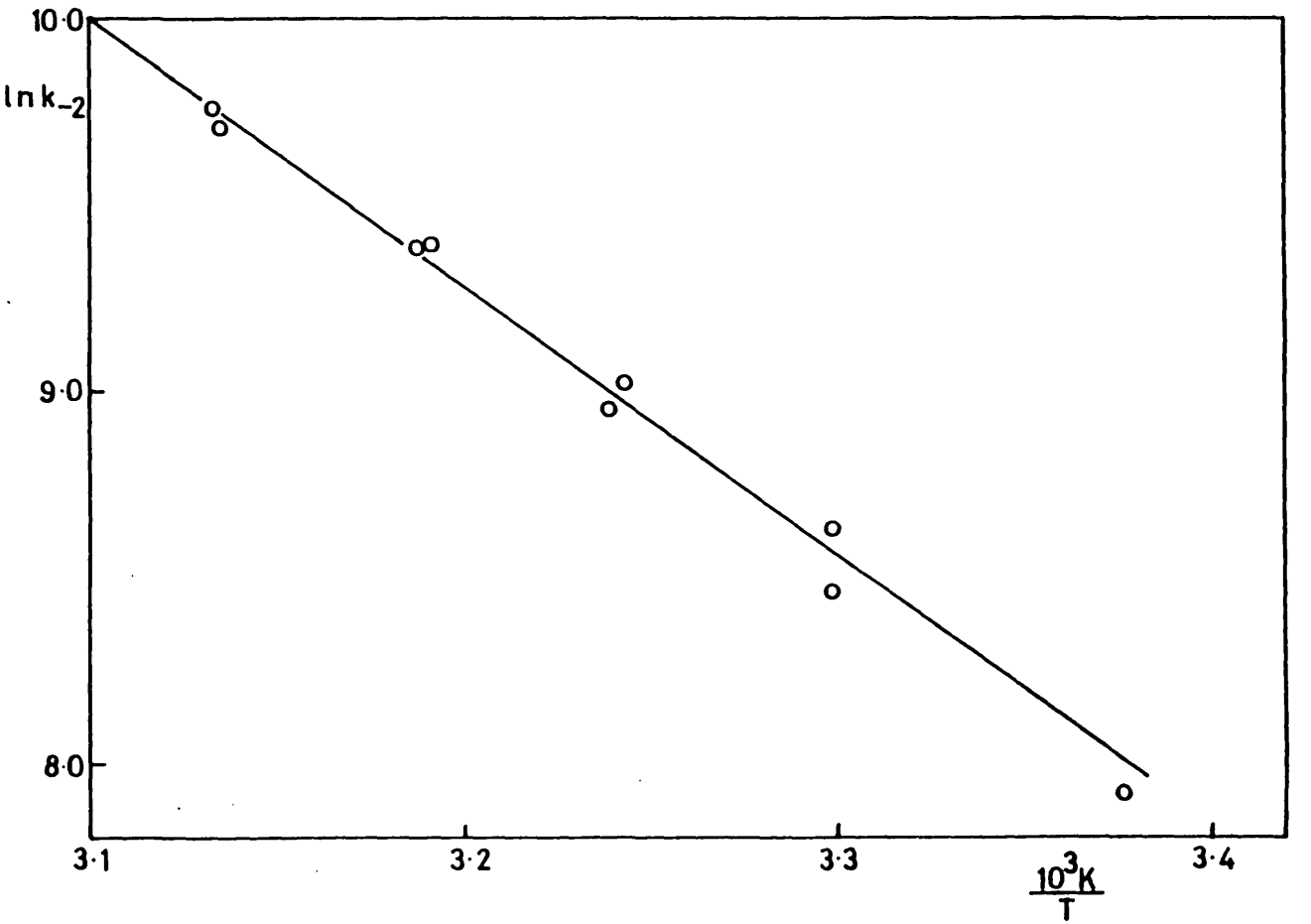

Figure 5.9. Arrhenius plot for the reaction between leuco-DMST2 and ferric in 0.05 M H_2SO_4.

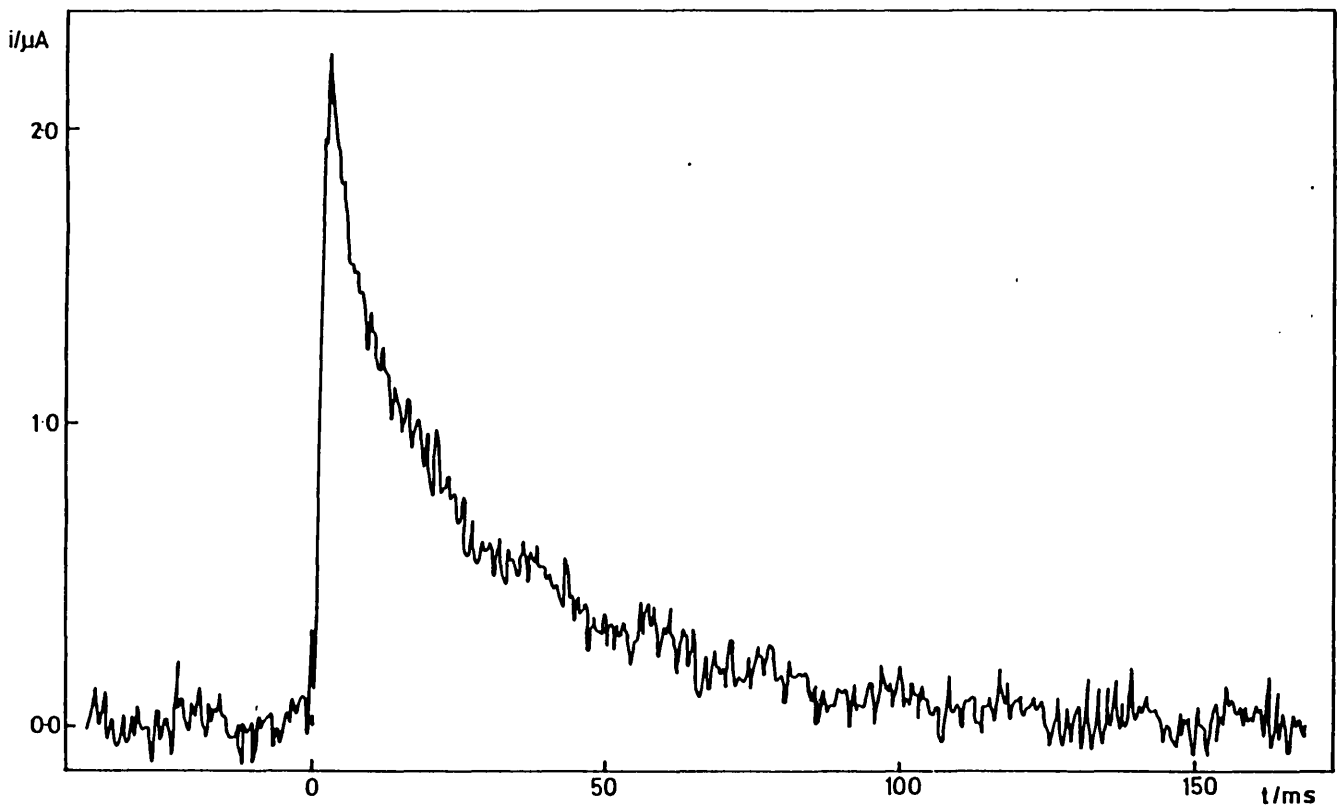

Figure 5.10. Typical flash electrolysis transient. In this case [Fe(III)]/mM = 4.02.

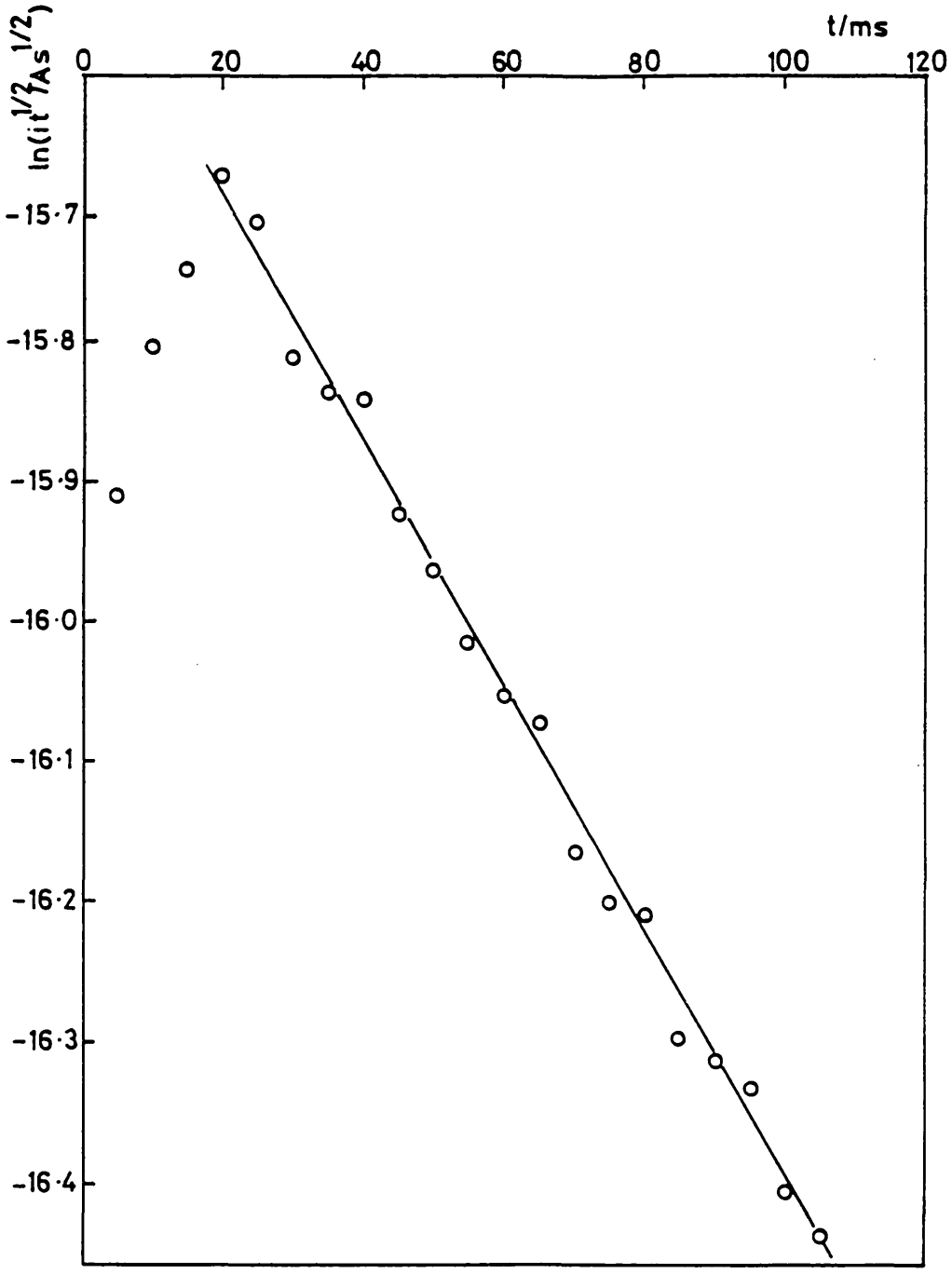

Figure 5.11. Flash electrolysis transient analysed according to equation (3.66). In this case [Fe(III)] = 2.2 mM.

were obtained in a range of ferric concentrations and the variation of observed rate constant with ferric concentration is plotted in figure (5.12). In the [Fe(III)] range studied, [Fe(III)] >> [DMST2] and

$$k'_{-2} = [Fe(III)]\, k_{-2} \qquad (5.56)$$

The back-reaction rate constant k_{-2} can thus be determined.

$$k_{-2}/M^{-1}\, s^{-1} = 4.5\ (\pm\ 0.6) \times 10^{3}\ (\text{at } 25^{o}C) \qquad (5.57)$$

5.6. ORDE Experiments on DMST2

All of the ORDE experiments were carried out at $25^{o}C$ in 0.05 M H_2SO_4 with 10^{-2} M Fe(II) and irradiating at 626 nm unless otherwise stated.

Figure (5.13) shows current voltage curves for the photogalvanic solution at an ORDE in both the light and the dark. In the potential range +0.25 V to 0.55 V vs SCE the major electrochemical reaction is the oxidation of photogenerated leuco-DMST2.

(a) ORDE Experiments Without Added Ferric

Experimental results for the DMST2/Fe system are shown in figure (5.14). The results are for a 'clean' ORDE which has not been coated with thionine and so is not perfectly selective between leuco dye and ferric.

Reduction of photogenerated Fe(III) thus makes a contribution to the photocurrent. When $X_G < X_D$, L has only to diffuse across the short distance X_G to reach the electrode but the escape of photogenerated Fe(III) across the diffusion layer is a slower process and so Fe(III) builds up within the diffusion layer. Photocurrents are measured at the potential of zero dark current which means that the only current contribution from the

Figure 5.12. Variation of observed rate constants with ferric concentration for flash electrolysis experiments on DMST2.

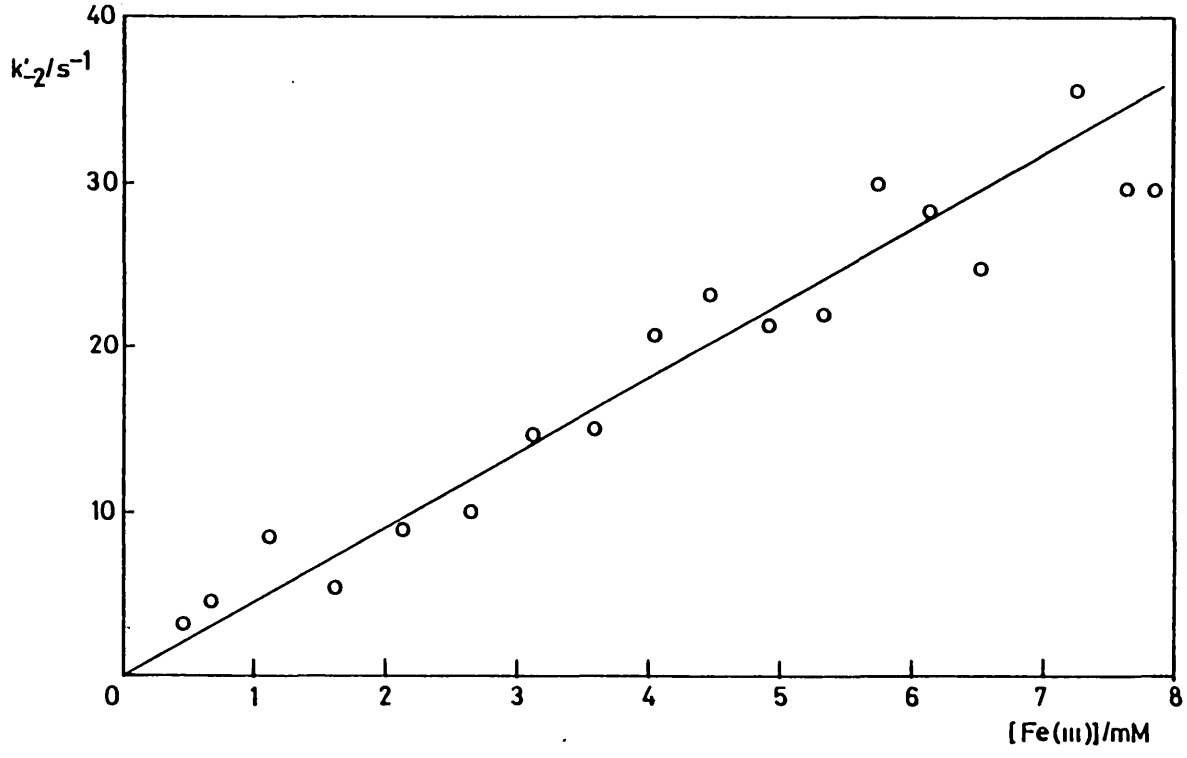

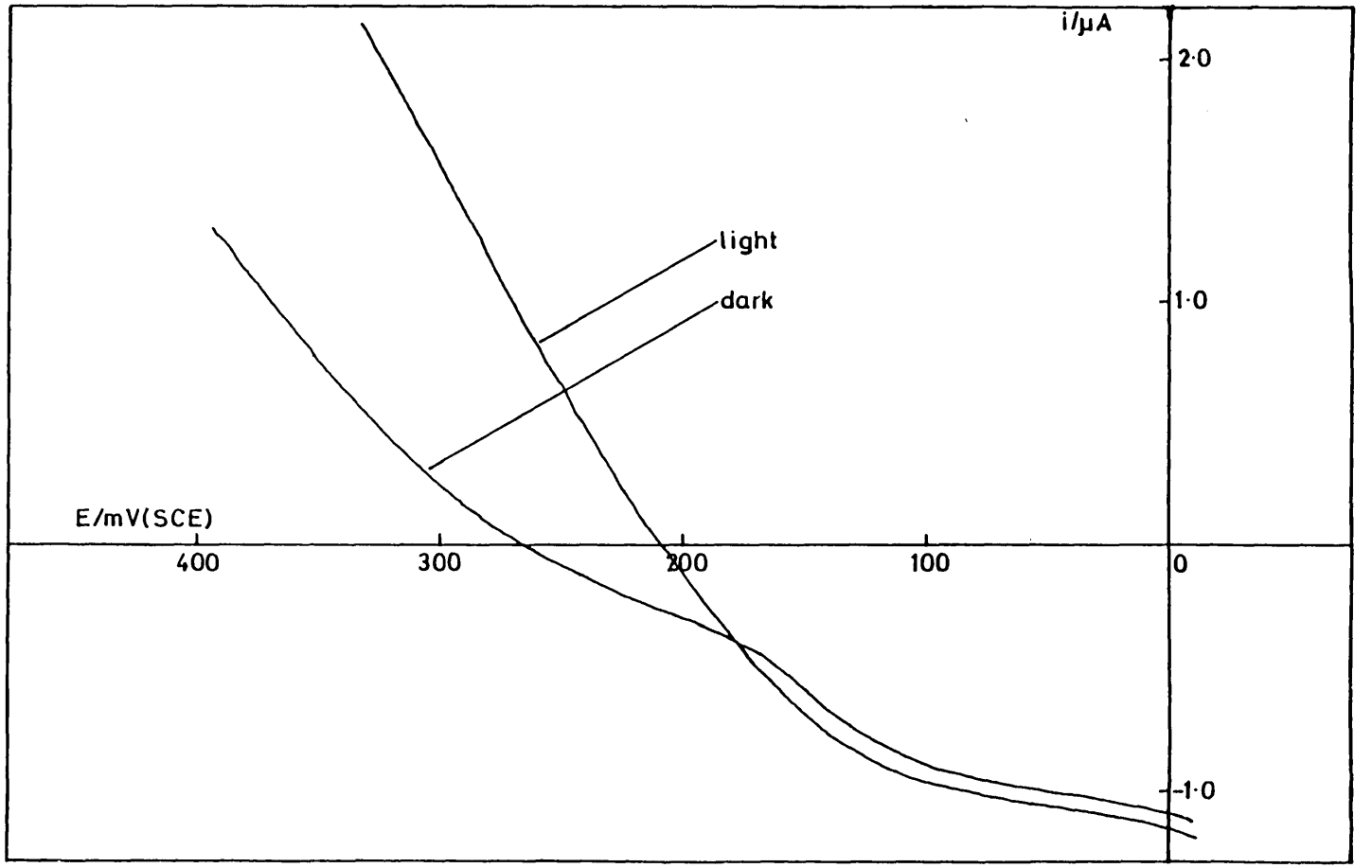

Figure 5.13. Current-voltage curves at an ORDE in the light and in the dark for a solution containing $[H_2SO_4]$/M = 0.05, [DMST2]/μM = 20 and [Fe(III)]/M = 0.010.

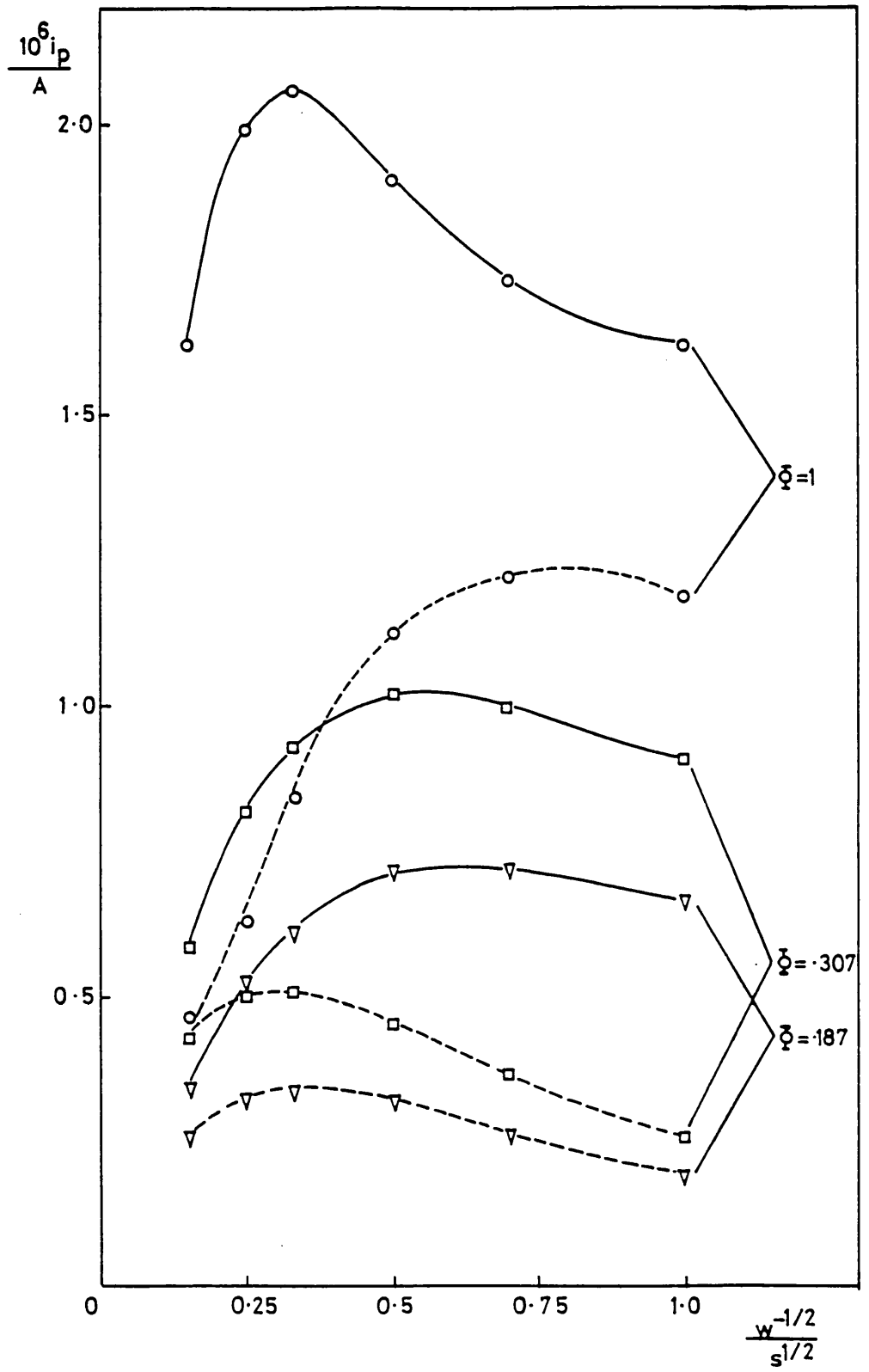

Figure 5.14. (see overleaf).

Figure 5.14. Typical photocurrent-rotation speed curves for solutions with no added Fe(III). Each curve is labelled with the fractional transmittance of the neutral density filter used, Φ. The photocurrents were measured at the potential of zero dark current. Broken lines connect the observed data; the solid lines connect points for the data after correction for the reaction of photogenerated Fe(III) at the electrode, according to equation (5.89).

Fe(II)/Fe(III) couple arises from photogeneration. A correction for the current caused by photogenerated Fe(III) may be calculated using equation (5.89) in Appendix (5.1).

$$i_L = i_{obs}\left(1 + \frac{k'X_D}{D}\left[1 + \frac{[Fe(III)]_D}{[Fe(II)]_D}\right]\right) \qquad (5.89)$$

where $i_{obs} = i_L - i_{Fe}$, the concentrations of Fe(II) and Fe(III) are their values in the dark and k' is the electrochemical rate constant for reduction of Fe(III) on the electrode at the potential of zero dark current. Values of k' were estimated from a Tafel plot for the reduction of Fe(III) on the electrode at the time of the experiment. The effect of the correction is shown in figure (5.14) by the full line. The residual maxima are more marked in experiments on DMST2 than those of thionine[50], and probably arise from losses due to the back reaction of leuco dye with Fe(III) which has built up in the concentration close to the electrode. This hypothesis is supported by the fact that the effect is greatest under conditions of high light intensity and low rotation speed.

The following scheme describes the generation of semi-reduced DMST2 ($S^{\cdot}$).

$$\begin{array}{l} Th \xrightarrow{h\nu} {}^1Th \xrightarrow{\phi_S} {}^3Th \xrightarrow[\phi_{SV}]{k_{SV}\ Fe(II)} (S^{\cdot}, Fe(III)) \nearrow S^{\cdot} + Fe(III) \\ \qquad\qquad\qquad\qquad\qquad\qquad\qquad\qquad\qquad\qquad\qquad\qquad\qquad\qquad\quad \searrow Th + Fe(II) \\ \qquad\quad \downarrow \qquad\qquad\quad \downarrow k_T \\ \qquad\quad Th \qquad\qquad\quad Th \end{array} \qquad (5.58)$$

where

ϕ_S is the efficiency of intersystem crossing

ϕ_{SV} is the efficiency of Stern-Volmer quenching

ϕ_C is the efficiency of escape from the solvent cage

k_T is the rate constant for thermal deactivation of the triplet thiazine.

The quantum efficiency for production of $S^{\cdot}$ is then given by

$$\phi_1 = \phi_S \phi_C \left(\frac{k_{SV}[Fe(II)]}{k_{SV}[Fe(II)] + k_T} \right) \tag{5.59}$$

Hence

$$\frac{1}{\phi_1} = \frac{1}{(\phi_S \phi_C)_\infty} \left\{ 1 + \frac{K_Q}{[Fe(II)]} \right\} \tag{5.60}$$

where K_Q is the Stern-Volmer quenching constant and

$$K_Q = \frac{k_T}{k_{SV}} \tag{5.61}$$

Combining equations (3.39) and (5.60) we obtain

$$\frac{\Phi}{iW^{\frac{1}{2}}} \simeq \frac{(\text{constant})}{(\phi_S \phi_C)_\infty} \left[1 + \frac{K_Q}{[Fe(II)]} \right] \tag{5.62}$$

A plot of $\Phi/iW^{\frac{1}{2}}$ against $1/[Fe(II)]$ for DMST2 is shown in figure (5.15). The slope yields a value of

$$K_Q/\text{mol dm}^{-3} = 1.1 \times 10^{-3} \tag{5.63}$$

The current at the ORDE with no added ferric is described by equation (3.39). This equation may be re-written as

$$i/\Phi = \phi_1 a_1 W^{-\frac{1}{2}} + \phi_1 b_1 \tag{5.64}$$

where a_1 and b_1 are known constants. ϕ_1 can thus be found from a plot of i/Φ against $W^{-\frac{1}{2}}$ as in figure (5.16).

Using the experimentally determined values of

$$i_{h\nu}/A = 440 \times 10^{-6} \tag{5.65}$$

$$X_{D,1}/\text{cm} = 5.0 \times 10^{-3} \tag{5.66}$$

and

$$X_\varepsilon/\text{cm} = 0.14 \tag{5.67}$$

we find

$$\phi_1 = 0.44 \tag{5.68}$$

By keeping the photon flux, $I_{\Phi = 1}$ constant and varying the irradiation wavelength, an action spectrum for the dye may be determined. Figure (5.17) shows the action spectrum obtained using this technique to closely follow the absorption spectrum of the dye.

Figure 5.15. Variation of photocurrent with [Fe(II)] plotted according to equation (5.62).

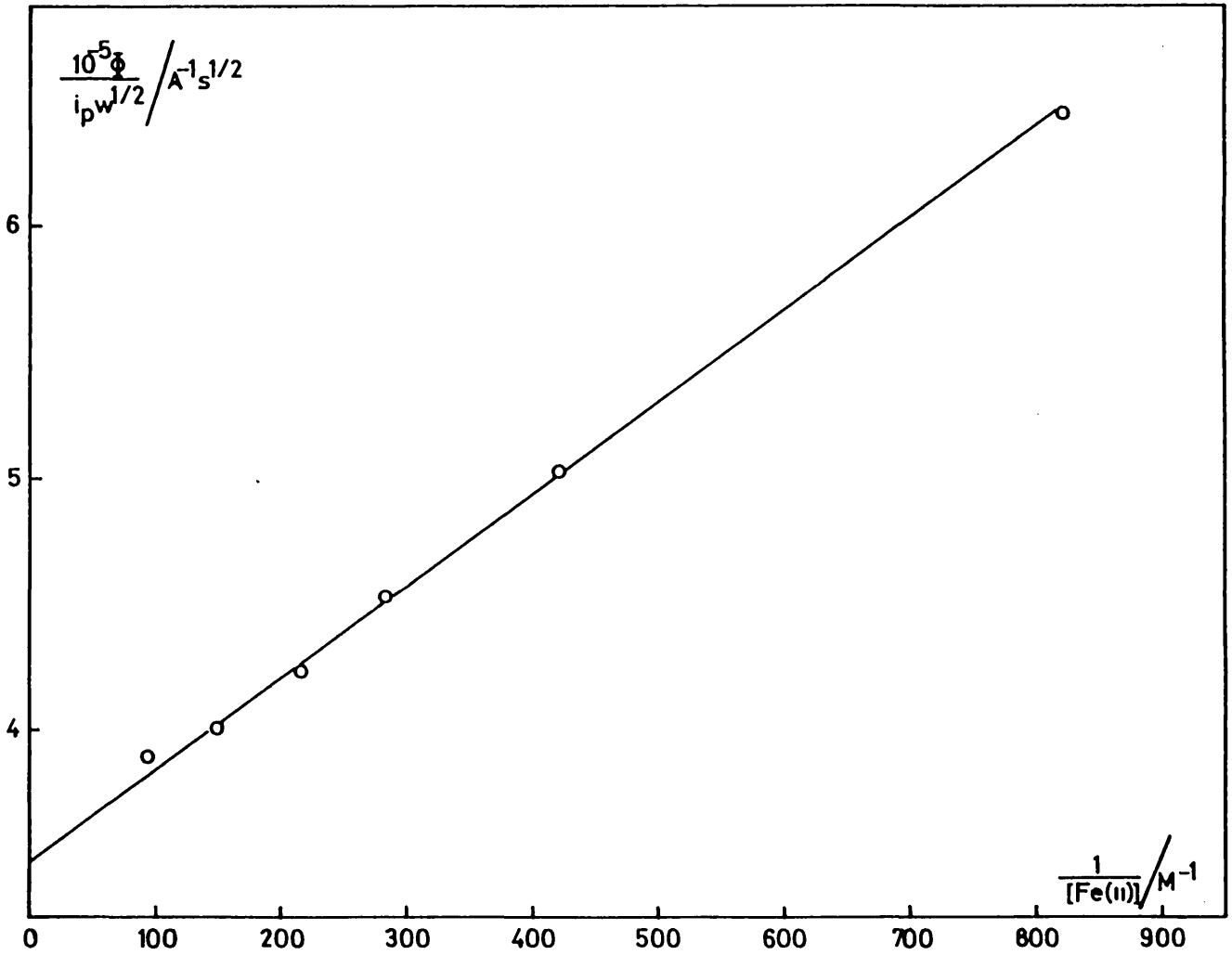

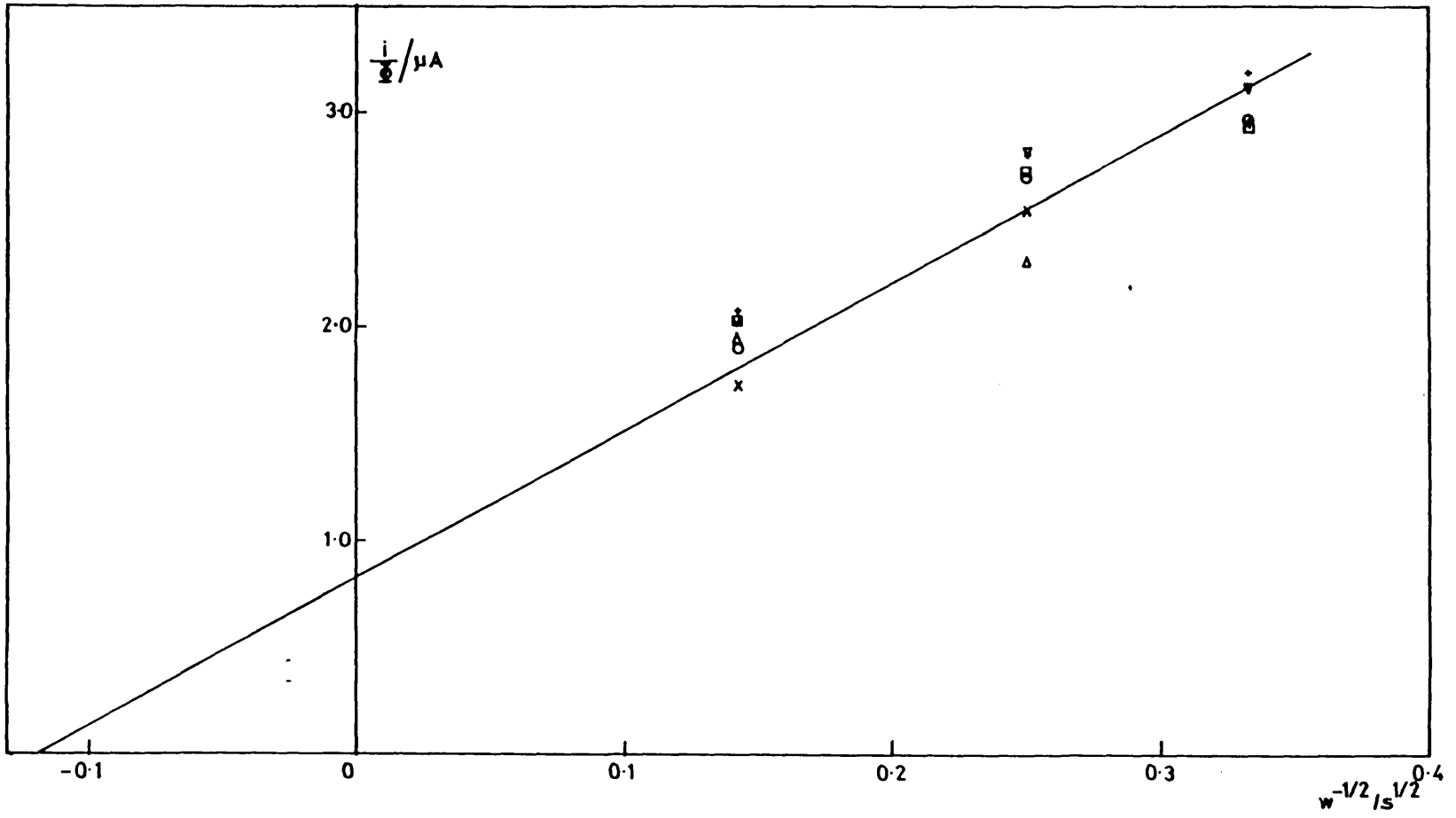

Figure 5.16. (see overleaf).

Φ	Symbol
1·0	Δ
0·49	□
0·31	∇
0·19	+
0·097	×
0·073	o

Figure 5.16. Variation of (i/Φ) with rotation speed which enables us to find ϕ_1 for DMST2.

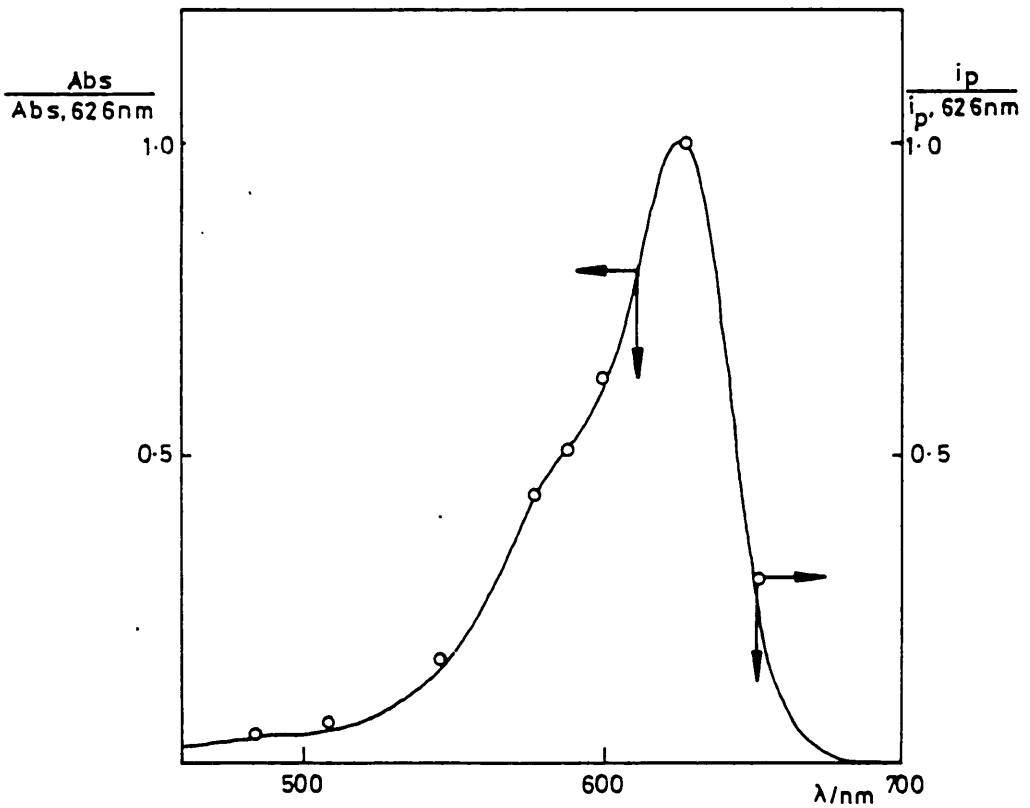

Figure 5.17. Action spectrum (circles) and absorption spectrum (solid line) of DMST2 normalised to their values at 626 nm.

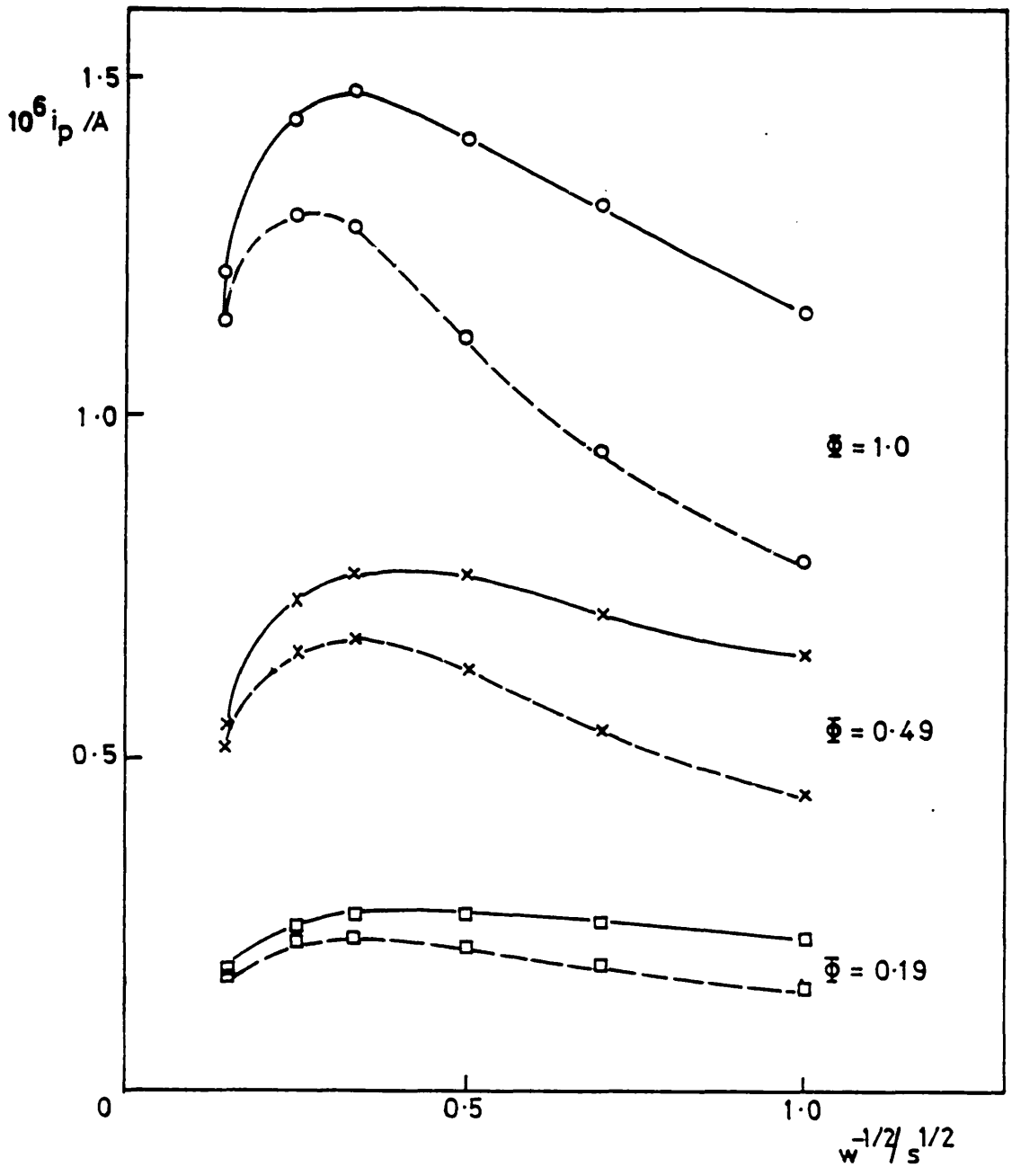

Figure 5.18. Typical photocurrent-rotation speed curves for a solution with [Fe(III)]/mM = 0.27. The notation is the same as that for figure 5.14. The electrode was set at a potential of +330 mV (SCE).

(b) ORDE Experiments with Added Ferric

Figure (5.18) shows photocurrent-rotation speed results at the potential of zero dark current (+ 330 mV (SCE)) for a solution containing 39 x 10^{-6} M DMST2 and 2.7 x 10^{-4} M Fe(III).

Equation (3.44) relates $N_{h\nu}$, the photoelectrochemical collection efficiency, to N_{lim}, the limiting value at low rotation speed where

$$N_{h\nu} = N_{lim} = \phi_1\phi_2 \frac{X_{G,k}}{X_\varepsilon} \qquad (3.42)$$

Using equations (3.42) and (3.44) we are able to calculate values for $N_{h\nu}$ and for the photocurrent (i_{calc}) which we would expect to flow at an optical rotating disc electrode.

$$i_{calc} = \Phi N_{h\nu} i_{h\nu} \qquad (5.69)$$

The concentration of ferric at the electrode surface $[Fe(III)]_0$ is greater than that in the bulk $[Fe(III)]_\infty$ because photogenerated ferric builds up in the diffusion layer. A value for $[Fe(III)]_0$ can be calculated using equation (5.70).

$$[Fe(III)]_0 = [Fe(III)]_\infty + 2i_F X_D/nAFD \qquad (5.70)$$

where i_F is the current which flows at the electrode with $[Fe(III)]_\infty$ = 1.0 M and a rotation speed of 1 Hz.

In a typical experiment:

$$i_F = 9.5 \times 10^{-3} \text{ A}$$
$$\phi_1 = 0.44 \qquad (5.68)$$

$i_{h\nu}$ = 436μA

A = 0.12 cm^2

X_ε = 0.138 cm

[DMST2] = 39 μM

From the exhaustive electrolysis determination,

$$D = 5.1 \times 10^{-6}\ cm^2\ s^{-1} \qquad (4.4)$$

so $X_{D,1} = 5.0 \times 10^{-3}$ cm

From stopped flow and flash electrolysis experiments,

$$k_{-2} = 5 \times 10^3\ M^{-1}\ s^{-1}$$

and from flash photolysis

$$k_{-1} = 8.1 \times 10^4\ M^{-1}\ s^{-1} \qquad (5.25)$$

$$k_3 = 2 \times 10^9\ M^{-1}\ s^{-1} \qquad (5.4)$$

In figure (5.19) we compare the observed photocurrent from a DMST2 ORDE experiment with that calculated from theory. Agreement between the two values is quite good over two orders of magnitude, confirming the ORDE theory given in section (3.3).

As further evidence for the agreement between theory and experiment we can compare values of ϕ_2 calculated using eqn. (3.52) with values calculated by another method.

By combining equations (3.46), (3.47) and (3.48) obtained using the steady-state assumption, we find an expression for the concentration of leucothiazine in the photostationary state.

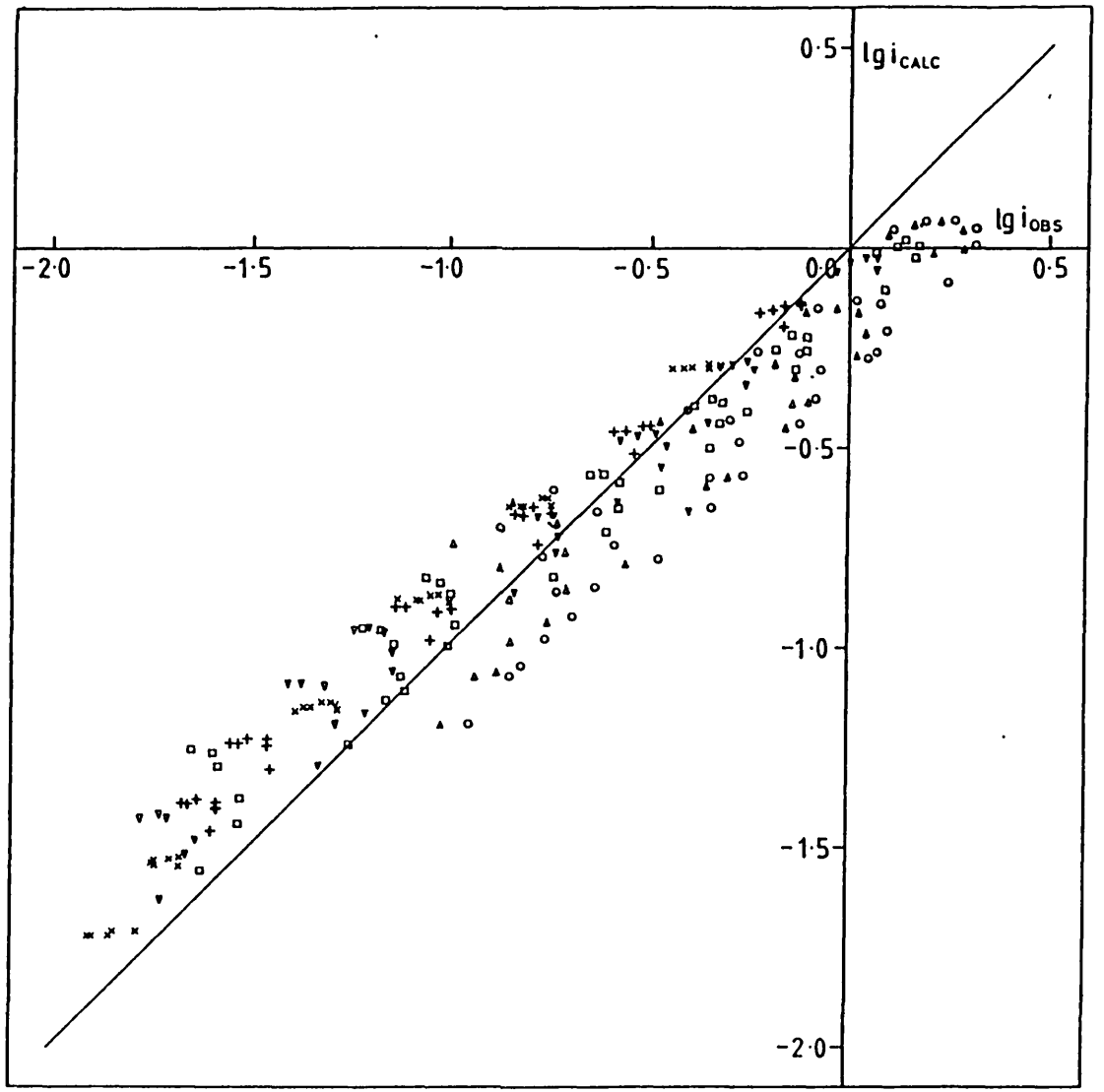

Figure 5.19.

[Fe(III)]/mM	Symbol
0·040	o
0·077	Δ
0·27	□
0·49	∇
1·02	+
1·87	X

Figure 5.19. Comparison of observed and theoretical values of photocurrent for the DMST2 ORDE with added ferric.

$$[L]_{pss} = \frac{f\phi_2}{(1 - \phi_2)\, k_{-2}\, [Fe(III)]} \tag{5.71}$$

By analogy with equation (3.13), the flux of leucothiazine to the electrode in the photostationary state is given by

$$j_L = \frac{D[L]_{pss}}{X_k} \tag{5.72}$$

and from the definitions of the characteristic lengths

$$X_k = (D/(1 - \phi_2)\, k_{-2}\, [Fe(III)])^{\frac{1}{2}} \tag{3.29}$$

Combining these three equations we obtain the expression

$$j_L = \phi_2 f_1 \Phi (D/(1 - \phi_2)\, k_{-2}\, [Fe(III)])^{\frac{1}{2}} \tag{5.73}$$

or from equation (3.14)

$$i_L = nAF\phi_2 f_1 \Phi (D/(1 - \phi_2)\, k_{-2}\, [Fe(III)])^{\frac{1}{2}} \tag{5.74}$$

Thus

$$i[Fe(III)]^{\frac{1}{2}}/\Phi = nAF\phi_2 f_1 [D/(1 - \phi_2)\, k_{-2}]^{\frac{1}{2}} = y \tag{5.75}$$

where

$$f = \Phi f_1. \tag{5.76}$$

In figure (5.20) we plot $i[Fe(III)]^{\frac{1}{2}}/\Phi$ against $([Fe(III)]/W)^{\frac{1}{2}}$. At low rotation speed y is constant for a particular light intensity and ferric concentration and is determined by the value of ϕ_2.

From the definition of ϕ_2, the limiting value is $\phi_2 = \frac{1}{2}$ so the limiting value of y in this low rotation speed region is given by

$$y_{lim} = nAFf_1 (D/2k_{-2})^{\frac{1}{2}} \tag{5.77}$$

and thus

$$\frac{y}{y_{lim}} = \phi_2[2/(1 - \phi_2)]^{\frac{1}{2}} = r \tag{5.78}$$

Solving this quadratic equation we obtain values of ϕ_2.

$$\phi_2 = r^2[(1 + 8/r^2)^{\frac{1}{2}} - 1]/4 \tag{5.79}$$

In figure (5.21) values of $(\phi_2)_{obs}$, obtained in this way (using $y_{lim} = 0.7\ \mu A\ mM^{\frac{1}{2}}$) are compared with values found using equation (3.52), $(\phi_2)_{calc}$. Good agreement holds between the two methods.

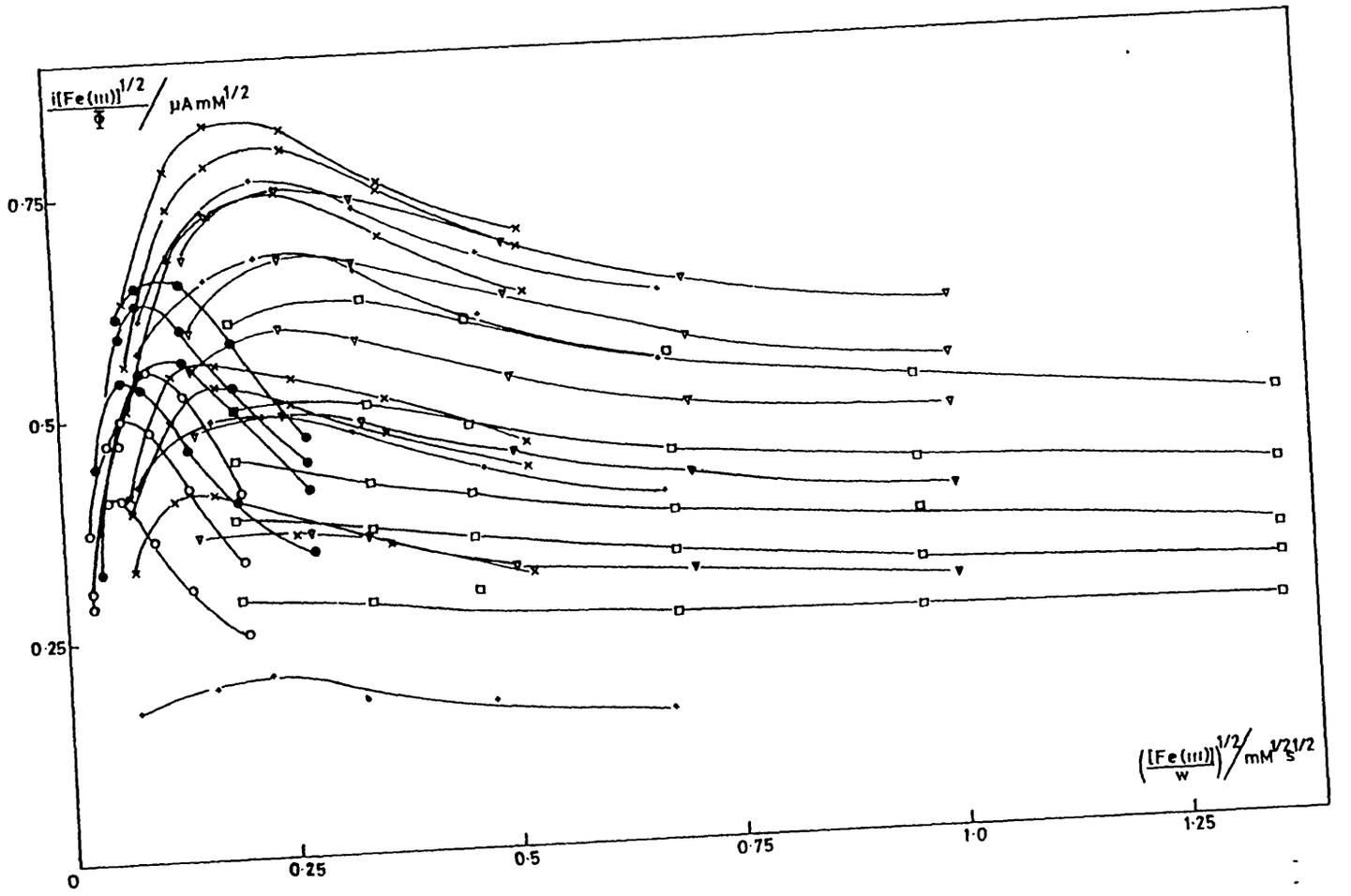

Figure 5.20. (see overleaf).

[Fe(III)] / mM	Symbol
0·040	o
0·077	●
0·27	x
0·46	•
1·02	▽
1·87	□

Figure 5.20. Plot of $i[Fe(III)]^{\frac{1}{2}}/\Phi$ against $([Fe(III)]/w)^{\frac{1}{2}}$ for the DMST2 ORDE.

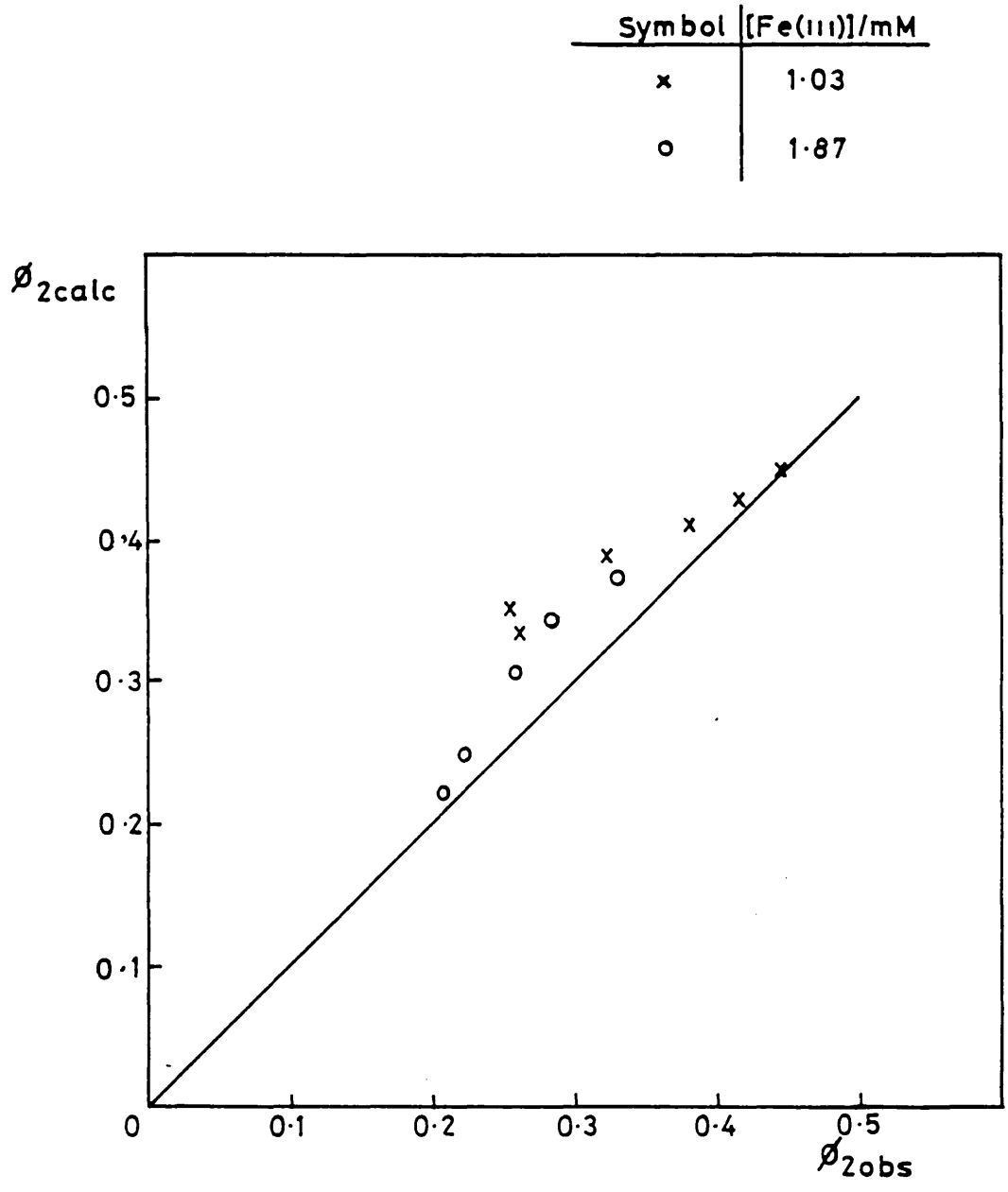

Figure 5.21. Comparison of observed and theoretical values of ϕ_2 for the DMST2 ORDE.

APPENDIX 5.1

ORDE Correction for Photogenerated Ferric

If the electrode is not perfectly selective, there will be a contribution to the photocurrent from Fe(III) generated by the photoredox reactions:

$$i_{obs} = i_L - i_{Fe} \tag{5.80}$$

where

i_{obs} is the observed photocurrent

i_L is the photocurrent due to leucothiazine and

i_{Fe} is the photocurrent due to the Fe(II)/Fe(III) couple.

In the dark, when the electrode is held at the potential of zero current

$$\vec{k}'[Fe(III)]_D = \overleftarrow{k}'[Fe(II)]_D = 0 \tag{5.81}$$

where $\overleftarrow{k}'$ and $\vec{k}'$ are the heterogeneous rate constants for the reactions of Fe(II) and Fe(III) at the electrode at this potential.

If we assume that the currents are small enough to avoid concentration polarisation, and that on illumination there is a small displacement in their concentration ($C_{h\nu}$), then we can write

$$\frac{i_{Fe}}{AF} = \vec{k}'([Fe(III)]_D + C_{h\nu}) - \overleftarrow{k}'([Fe(II)]_D - C_{h\nu}) \tag{5.82}$$

and hence from equation (5.81)

$$\frac{i_{Fe}}{AF} = \vec{k}'(C_{h\nu})_o \left(1 + \frac{[Fe(III)]_D}{[Fe(II)]_D} \right) \tag{5.83}$$

An estimate of $\vec{k}'$ can be obtained from the analysis of a polarogram of Fe(III) at the electrode used.

We must also estimate the value of $C_{h\nu}$ at the electrode surface. This term is made up of contributions from the diffusion layer and from the bulk. Two cases are considered:

(i) $X_D >> X_{G,k}$

Under these conditions the major contribution to i_{Fe} is from Fe(III) generated close to the electrode.

In order to maintain steady state conditions, the photogenerated Fe(III) must diffuse across the diffusion layer to balance the flux of leucothiazine removed by the electrode. Thus

$$(C_{h\nu})_o \simeq \frac{2j_L X_D}{D} \tag{5.84}$$

where j_L is the flux of leucothiazine removed by the electrode and the factor of two arises from the stoichiometry.

(ii) $X_D << X_{G,k}$

These conditions correspond to zone C of the ORDE analysis. The flux of leucothiazine to the electrode is made up of approximately equal contributions from the diffusion layer and the bulk (figure (5.22)).

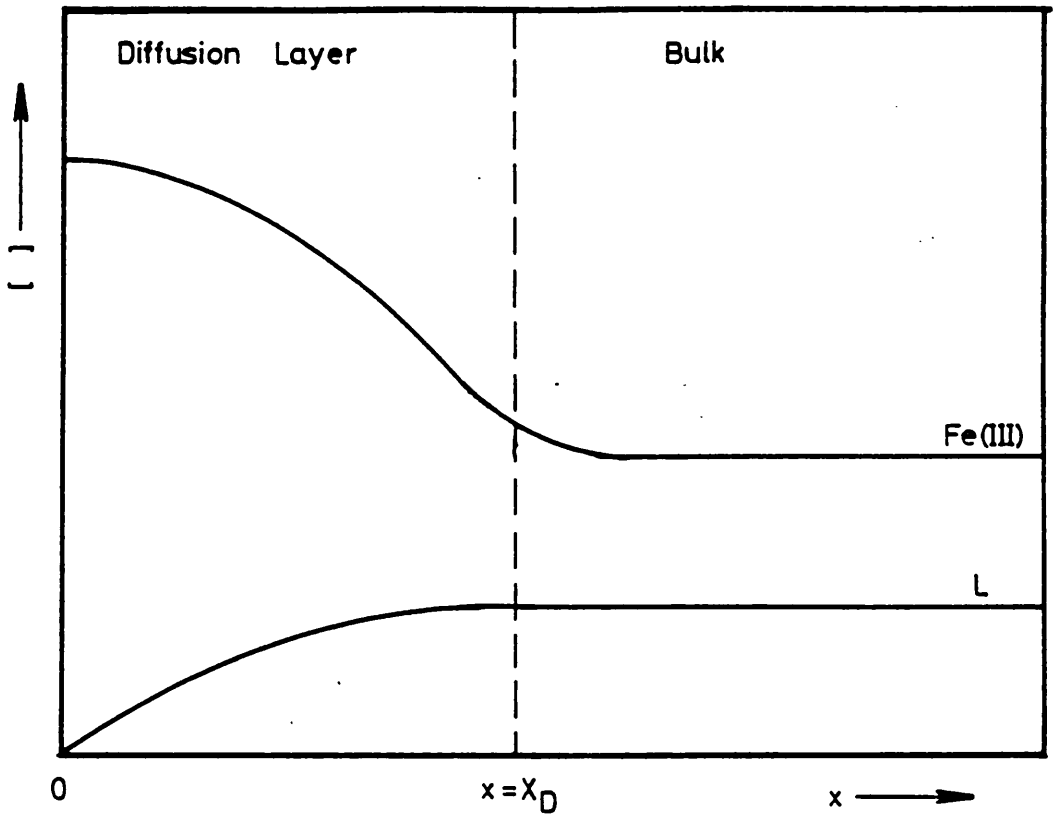

Figure 5.22. Schematic concentration profiles for Fe(III) and L.

Thus

$$(C_{h\nu})_o \simeq \frac{j_L X_D}{D} + (C_{h\nu})_{x = X_D} \tag{5.85}$$

where $(C_{h\nu})_{x = X_D}$, the concentration at the diffusion layer boundary is given by

$$(C_{h\nu})_{x = X_D} \simeq \frac{j_L X_D}{D} \tag{5.86}$$

and so

$$(C_{h\nu})_o \simeq \frac{2 j_L X_D}{D} \tag{5.87}$$

Thus for different reasons we obtain the same result from the two limiting cases. Substituting in equations (5.86) and (5.83) gives the approximate correction required:

$$i_L \simeq i_{obs} \left(1 + \frac{k' X_D}{D} \left[1 + \frac{[Fe(III)]_D}{[Fe(II)]_D} \right] \right) \tag{5.89}$$

This correction for the current due to photogenerated Fe(III) has been tested experimentally[37] by using 0.1 M HCl as background electrolyte, in which the Fe(II)/Fe(III) electrode kinetics are less reversible[11]. Under these conditions the calculated correction is very small (< 2%) and the observed photocurrents fit the theory without correction.

Chapter 6

IMPLICATIONS FOR IRON-THIAZINE PHOTOGALVANIC CELLS

In an ideal photogalvanic cell (see chapter 1) the absorption length, X_ε, should be about 1×10^{-4} cm. Thiazine dyes have natural extinction coefficients of about 1×10^{-8} cm^2 mol^{-1} and this means that the dye concentration must be about 0.1 M. With this dye concentration the rate of the back reaction, k_{-2} must be less than 6×10^3 M^{-1} s^{-1} but in 0.05 M H_2SO_4 at 25°C the maximum solubility of DMST2 is about 1×10^{-2} M. In an efficient cell using this dye concentration the rate of the back reaction should be less than 6×10^2 M^{-1} s^{-1} but the experimentally determined value for DMST2 is about 4×10^3 M^{-1} s^{-1}. Even with the introduction of two sulphonate groups into the thiazine nucleus, the dye is not sufficiently soluble in acid solution for a cell to be efficient.

Results for thionine and DMST2 are given in table (6.1).

The photoelectrochemical collection efficiency of a photogalvanic cell is given by[55]

$$N_{h\nu} = 1/[1 + (\phi_1 I_o X_\ell X_\varepsilon^2 k_{-2}/D^2)^{1/3}] \qquad (6.1)$$

Using the figures in table (6.1) and with

$$I_o = 4 \times 10^{-8} \text{ mol cm}^{-2} \text{ s}^{-1} \qquad (6.2)$$

and $X_\ell = 1 \times 10^{-2}$ cm we have

$$\text{for thionine} \quad N_{h\nu} = 3.1 \times 10^{-2} \qquad (6.3)$$

$$\text{and for DMST2} \quad N_{h\nu} = 0.34 \qquad (6.4)$$

Table 6.1

Collected Data for Thionine and DMST2

	Thionine	DMST2
$k_{-1}/M^{-1}s^{-1}$	$5.8 \times 10^{5\dagger}$	8.4×10^{4}
$k_{-2}/M^{-1}s^{-1}$	$2.4 \times 10^{2\dagger}$	3.7×10^{3}
$k_{-3}/M^{-1}s^{-1}$	$2.4 \times 10^{9\dagger}$	1.8×10^{9}
$[Th]_{sat}/M$	5×10^{-5}	1×10^{-2}
ϕ_1	0.5	0.44
ε(decadic)$/M^{-1}cm^{-1}$	5.6×10^{4}	8×10^{4}
D/cm^2s^{-1}	6×10^{-6}	5.1×10^{-6}

†Results of Brokken-Zijp and de Groot[19]

$0 < pH < 2.5$.

Although the back reaction for DMST2 is faster than that for thionine, the collection efficiency is strongly dependent on the absorption length and X_ε is much shorter for the sulphonated dye.

For a photostationary state where leuco dye is being destroyed on an electrode instead of reacting with ferric the quantum efficiency for production of leucothiazine is given by[18]

$$\phi_2 = 1/(2 + k_{-1}[Fe(III)]/k_3[S^\cdot]) \tag{6.5}$$

If $k_{-1}[Fe(III)] >> k_3[S^\cdot]$ then most of the photogenerated semithiazine returns to thiazine by reaction with ferric, ϕ_2 is very small and the cell is inefficient. However, if $k_3[S^\cdot] >> k_{-1}[Fe(III)]$ the semithiazine is destroyed by disproportionation and half of the photogenerated semithiazine becomes leuco dye. In this case ϕ_2 reaches its optimum value of $\frac{1}{2}$. Hence we require

$$\frac{2k_3[S^\cdot]}{k_{-1}[Fe(III)]} > \frac{2k_3 g}{k_{-1}^2[Fe(III)]} > 1 \tag{6.6}$$

or from the definition of g, (eqn. 1.2)

$$[Fe(III)] < (2\phi_1 I_0 k_3 \varepsilon [Th]/k_{-1}^2)^{\frac{1}{2}} \tag{6.7}$$

Using the results in table (6.1) and taking $I_0 = 4 \times 10^{-8}$ mol cm^{-2} s^{-1} we obtain

for thionine $[Fe(III)] < 1.4 \times 10^{-3}$ M (6.8)

and for DMST2 $[Fe(III)] < 0.13$ M (6.9)

For the cell to be efficient, ferric must be added to the photogalvanic electrolyte to carry current across the cell without causing concentration polarisation at the dark electrode. In a working cell the ferric concentration should be about 1×10^{-2} M, and this is above the ferric concentration limit for a thionine cell. However the calculation above shows that the quantum efficiency for production of leuco DMST2 is not reduced by this concentration of ferric. Although the addition of ferric to carry current reduces the collection efficiency of a thionine cell, the problem is not encountered in a cell using DMST2 because of the much slower reaction between ferric and the semi-reduced dye.

The standard electrode potential for reduction of DMST2 is 50 mV more negative than that for reduction of thionine. This means that the voltage available from a cell containing DMST2 will be about 50 mV greater than that for a thionine cell and that the power generated will be correspondingly greater.

Measurement of the standard electrode potentials of methoxy-substituted thiazines has shown that the voltage between the two electrodes of an iron-thiazine cell can be increased still further by introduction of these electron-releasing substituents. However, Albery *et al*[55] have shown that an increase in the voltage difference between the Th/L and Fe(II)/Fe(III) couples is accompanied by an increase in the rate of the back reaction, k_{-2}. The efficiency of a cell based on DMST2 would not be increased by introduction of methoxy groups to the thiazine nucleus because k_{-2} is already too large for this dye.

Ideal values of ΔE^{Θ} and $N_{h\nu}$ are 1.1 V and 1 respectively. With these values and a cell that absorbed all of the solar radiation above 1.8 eV the efficiency of a photogalvanic cell would be about 20%[8]. In using

I_0/mol cm^{-2} s^{-1} = 4 x 10^{-8} in our calculations we have assumed that the dye absorbs 1/8 of the required photons. Factors which determine the efficiency of an iron-thiazine cell are summarised in table (6.2).

The value of about 0.07 for $\Delta EN_{h\nu}$ at X_ε/cm = 1 x 10^{-4} means that a further factor of 14 is lost in the cell operation. Consequently we arrive at a predicted efficiency for an iron-DMST2 cell of only about 0.4%. Kinetic studies of the iron-thionine system in section (4.1) suggest that the rate of the back reaction can be reduced by changing the pH. In this way the power available from a cell could be approximately doubled by using an optimised pH value.

The work on DMST2 shows that the efficiency of an iron-thiazine cell can be improved by increasing the dye solubility. However, even when the solubility of the dye is increased to 1 x 10^{-2} M the efficiency is still very poor. The efficiency of a photogalvanic cell could be improved if the solubility, extinction coefficient and breadth of spectral absorption of the dye could be increased still further. Water-soluble porphyrins and metalloporphyrins show broad spectral absorptions and high extinction coefficients and the remainder of this thesis describes work done to characterise a metalloporphyrin photogalvanic system.

Table 6.2

Factors determining the efficiency of the iron-thiazine cell with $X_\varepsilon/cm = 1 \times 10^{-4}$

	DMST2 Cell	Best Possible
Absorption of radiation[a]	0.12	0.5[b]
Quantum efficiency, ϕ_1	0.44	0.5[c]
Collection efficiency, $N_{h\nu}$	0.34	0.5
Voltage factor	0.2	0.3[d]
	0.4%	4%

[a]A single dye only absorbs about 1/8 of the total insolation.

[b]An ideal mixture of dyes should absorb about one-half of the total insolation.

[c]The ideal value should be unity but results for thionine show $\phi_1 \approx 0.5$.

[d]The ideal cell should produce 1.5 V but trying to achieve larger voltages leads to lower collection efficiencies and it is unrealistic to expect more than about 0.3 V.

Chapter 7

PORPHYRINS AND METALLOPORPHYRINS

7.1. Introduction

The porphyrins and metalloporphyrins show many of the characteristics required of a good photosensitiser. Metalloporphyrins are characterised by strong absorbances across the visible region of the spectrum and a zinc porphyrin can collect about 30% of the incident solar energy. The metalloporphyrins generally have a high triplet yield, readily undergo photoredox reactions and compared to the thiazine dyes for example, many of them have a high solubility in water.

Some of the problems encountered in using porphyrins as photosensitisers are discussed below.

(i) Aggregation

The porphyrins H_2TMPyP, H_2TPPS and H_2TPPC and most of their metal derivatives are soluble over a wide range of pH and concentration. However, their usefulness for solar energy conversion is limited by the extent to which aggregation occurs. Dimerisation broadens and decreases the extinction coefficient of the B-band in the UV-visible spectrum and causes a non-linear Beer's law plot. Dimerisation also increases the rate of internal conversion from the first excited singlet state[71] and so there is a lower fraction of excited state porphyrin species available to the photoredox reaction.

The metalloporphyrin tetrasulphonates tend to dimerise in aqueous solution even at modest concentrations, in the order

$$PdTPPS^{4-} > ZnTPPS^{4-} > SnTPPS^{4-}$$

The dimerisation constant for $ZnTPPS^{4-}$ has been measured by nmr methods[72] as

$$K_{DIM}/M^{-1} \simeq 10^4 \qquad (7.1)$$

Aggregation is also found for H_2TPPC and its derivatives[73], even though the carboxyl groups are ionised below pH 5.

The N-methylpyridinium salts are much less prone to aggregation. The dimerisation constant for $ZnTMPyP^{4+}$ in aqueous solution of ionic strength 0.1 M has been measured[72] as

$$K_{DIM}/M^{-1} = 8 \qquad (7.2)$$

Dimerisation of Fe(III) complexes of H_2TMPyP and H_2TPPS has been shown to be pH dependent[74,75].

(ii) Demetallation

An equilibrium exists between a metalloporphyrin and the metal and free base porphyrin,

$$M^{2+} + PH_2 \underset{}{\overset{K_e}{\rightleftharpoons}} MP + 2H^+ \qquad (7.3)$$

The equilibrium constant K_e is given by

$$K_e = \frac{k_i}{k_d} \quad , \qquad (7.4)$$

the ratio between the rates of incorporation (k_i) and displacement (k_d) of the central metal atom from the free base porphyrin.

For $ZnTMPyP^{4+}$, the rate of incorporation is given by[76]

$$R_i = k_i[PH_2][Zn^{2+}] \tag{7.5}$$

and the rate of displacement is given by

$$R_d = k_d[ZnP][H^+]^2 \tag{7.6}$$

At 25.5°C and ionic strength 1 M

$$k_i/M^{-1}\ s^{-1} = 3.7 \times 10^{-2} \tag{7.7}$$

$$k_d/M^{-2}\ s^{-1} = 8.5 \times 10^{-3} \tag{7.8}$$

and

$$K_e/M = \frac{k_i}{k_d} = 4.4 \tag{7.9}$$

The displacement reaction is catalysed by chloride ions and in the presence of chloride the rate equation is found to be[77]

$$R_d = k_d[ZnP][H^+]^2[Cl^-]^2 \tag{7.10}$$

At 27°C the rate constant k_d is

$$k_d/M^{-4}\ s^{-1} = 6.8 \times 10^{-2} \tag{7.11}$$

7.2. Photochemistry

The most intense band in the absorption spectrum of the metalloporphyrins is the B band at about 420 nm which is the origin of the second excited singlet state. The weaker Q bands in the region 500-650 nm are caused by excitation to the first excited singlet state and to a vibrational overtone. Spectral data for many water soluble metalloporphyrins has been obtained by Kalyanasundaram and Neumann-Spallart[78]. The spectrum of a typical water soluble metalloporphyrin $ZnTMPyPCl_4$ is shown in figure (7.1).

Information about the excited singlet and triplet states has been obtained using flash photolysis[78,79]. Data for some of the water soluble metalloporphyrins is collected in table (7.1).

Fluorescence lifetimes of the metalloporphyrins are too short for the excited singlet state to be useful in intermolecular photoredox processes. The triplet lifetimes are much longer than those of the excited singlet states and the yield of triplets is high, so there is much more chance of intermolecular photoredox processes occurring via the triplet state.

7.3. Redox Reactions of the Metalloporphyrins

Redox reactions may involve either the central metal ion or the porphyrin periphery. Where the porphyrin ligand is involved, π-radical anions or cations are created (figure (7.2)).

No direct evidence can be obtained from electrochemistry as to the exact nature of the redox process. However, it is often possible[80] to assign a redox reaction to either the central metal ion or the porphyrin ligand from UV-visible spectra or from the difference between the standard electrode potentials of oxidation and reduction. Additional information can be obtained from esr and from bulk susceptibility measurements.

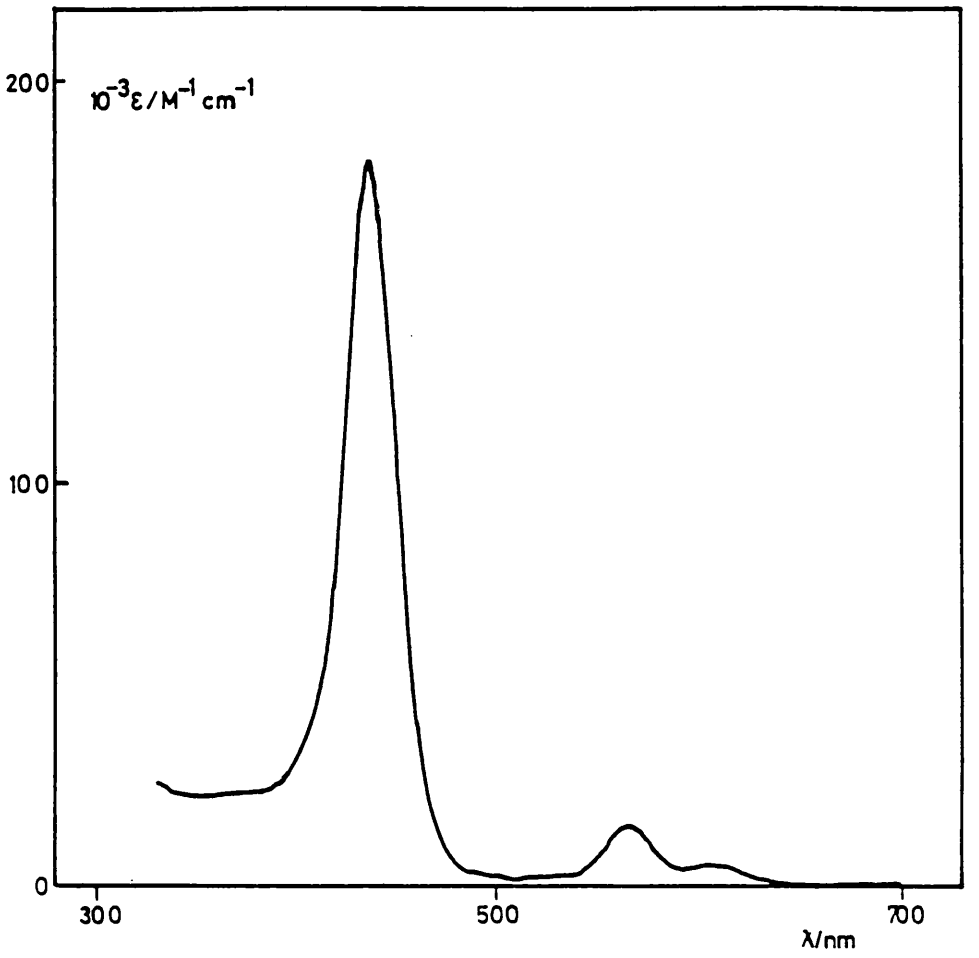

Figure 7.1. Visible spectrum of $ZnTMPyPCl_4$ in water.

Table 7.1

Photophysical Properties of Some Metalloporphyrins in Outgassed Aqueous Solution[78,79]

Metalloporphyrin	τ_S/ns	ϕ_T	τ_T/μs
ZnTMPyP	1.5	0.90	1220
PdTMPyP	< 0.5	1.00	170
SnTMPyP	-	0.95	900
H_2TPPS	10.4	0.78	420
ZnTPPS	1.7	0.84	1400
PdTPPS	< 0.5	1.00	380
SnTPPS	-	0.95	1000

τ_S excited singlet-state lifetime.

τ_T triplet-state lifetime.

ϕ_T quantum yield for formation of triplet state.

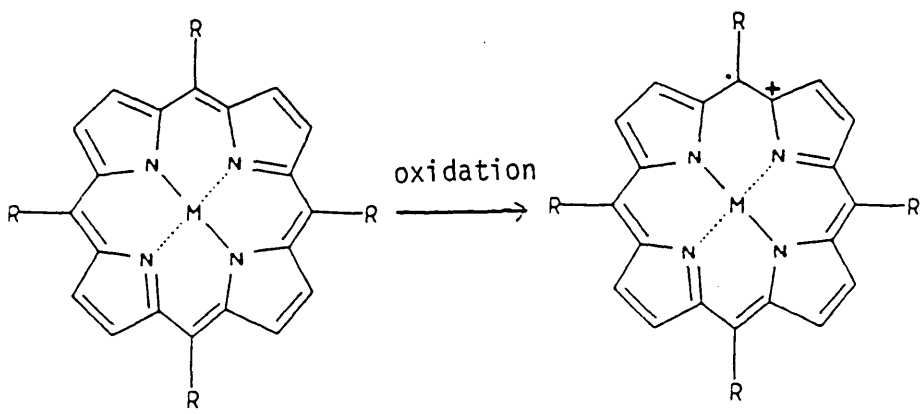

metalloporphyrin π-radical cation

Figure 7.2. Oxidation of a metalloporphyrin to form a π-radical cation.

7.4. Photoredox Reactions of the Metalloporphyrins

The triplet excited states of the metalloporphyrins are mild reductants[79] and are oxidised by a wide range of electron acceptors to the π-radical cation

$$P^* + Q \rightarrow P^{+\cdot} + Q^{-\cdot} \qquad (7.12)$$

Values of the electron transfer rate constants for some water-soluble metalloporphyrins and quenchers have been measured by flash photolysis[79] and are given in table (7.2).

From classical kinetic theory, the rate of a reaction between charged species is dependent on the ionic strength (μ) and this behaviour may be described by equation (7.13).

$$\lg k = \lg k_o + 1.02\ Z_A Z_B \sqrt{\mu} \qquad (7.13)$$

where k_o is the rate of the reaction when $\mu = 0$. For reactions between highly charged species like $ZnTMPyP^{4+}$ and MV^{2+} (where $Z_A Z_B = 8$) the rate of the reaction is strongly affected by the ionic strength of the medium.

Once quenching of the triplet state metalloporphyrin has occurred, the products of the quenching reaction must escape from the solvent cage before the separated ion products can react at the electrode. The quantum efficiency for the formation of redox products (ϕ_{ions}) is given by

$$\phi_{ions} = \phi_T \times \phi_Q \times \phi_S \qquad (7.14)$$

where ϕ_S is the fraction of products of the electron transfer quenching reaction leaving the solvent cage as separated ions. Escape from the cage

Table 7.2

Rate Constants for Quenching of the Metalloporphyrin Excited State (from ref. 79)

Metalloporphyrin	Quencher	$k_Q/M^{-1}\ s^{-1}$
$ZnTPPS^{4-}$	MV^{2+}	1.4×10^{10}
	$S_2O_8^{2-}$	6.9×10^{6}
$PdTPPS^{4-}$	MV^{2+}	*ca.* 10^{10}
	$S_2O_8^{2-}$	-
$SnTPPS^{4-}$	MV^{2+}	$< 10^{4}$
	$S_2O_8^{2-}$	*ca.* 10^{5}
$ZnTMPyP^{4+}$	MV^{2+}	1.8×10^{7}
	$S_2O_8^{2-}$	9.0×10^{8}
	$[Co(NH_3)_5Cl]^{2+}$	1.5×10^{8}
	Fe^{3+}	1.9×10^{8}
$PdTMPyP^{4+}$	MV^{2+}	3.5×10^{4}
	$S_2O_8^{2-}$	1.9×10^{4}
	$[Co(NH_3)_5Cl]^{2+}$	1.4×10^{8}
	Fe^{3+}	6.9×10^{7}
$SnTMPyP^{4+}$	MV^{2+}	$< 10^{4}$
	$S_2O_8^{2-}$	1.0×10^{7}
	Fe^{3+}	*ca.* 10^{6}

depends on the electrostatic forces between the excited species and quencher, and these forces are particularly important for water-soluble porphyrins because of their high charges. This has been demonstrated by Harriman *et al*[81] who found a high yield of separated ion products in the reaction between $ZnTMPyP^{4+}$ and MV^{2+} (ϕ_S = 0.8) but a very low yield of ion products from the reaction between $ZnTPPS^{4-}$ and MV^{2+} (ϕ_S < 0.01) under the same conditions.

Experimental Results for the Metalloporphyrin System

The metalloporphyrin species studied in this work are shown in figure (7.3).

7.5. Dark Electrochemistry of $ZnTMPyPCl_4$

Figure (7.4) shows a steady-state polarogram, corrected for solvent decomposition for the oxidation of $ZnTMPyPCl_4$ at pH 2.5. The wave corresponds to the oxidation of the porphyrin ring to the π-radical cation. Tafel analysis, (Figure (7.5)) shows that the wave is quasi-reversible[82] with half-wave potential, $E_{\frac{1}{2}}$ = +962 mV (SCE). The standard electrode potential is calculated as E^{Θ} = +940 (± 10) mV (SCE).

In contrast with the observations made by Neumann-Spallart and Kalyanasundaram[83] using cyclic voltammetry, no second oxidation of the metalloporphyrin to the dication species was observed. Controlled potential electrolysis studies suggest that the π-monocation slowly reverts back to the porphyrin species. This observation is in agreement with the work of Neumann-Spallart and Kalyanasundaram[83]. Attempts to study the fate of the π-monocation at a ring-disc electrode were frustrated by the large currents caused by solvent decomposition. The 'solvent window' can be extended to more positive potentials by making the medium

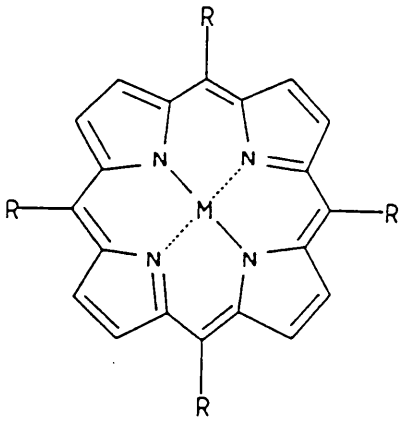

$ZnTMPyPCl_4$: M=Zn , R= 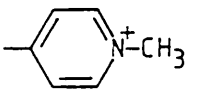

$ZnTHPyPCl_4$: M=Zn , R= 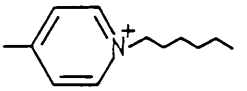

$ZnTPSPyP$: M=Zn , R= 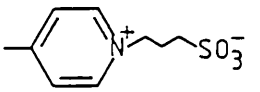

$ZnTPPSNa_4$: M=Zn , R= 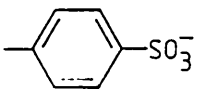

$Co(III)TPPSNa_3$: M=Co(III) , R= 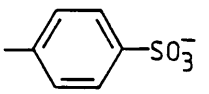

$Fe(III)TPPSNa_3$: M=Fe(III) , R= 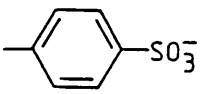

Figure 7.3. Structures of the water soluble metalloporphyrins studied.

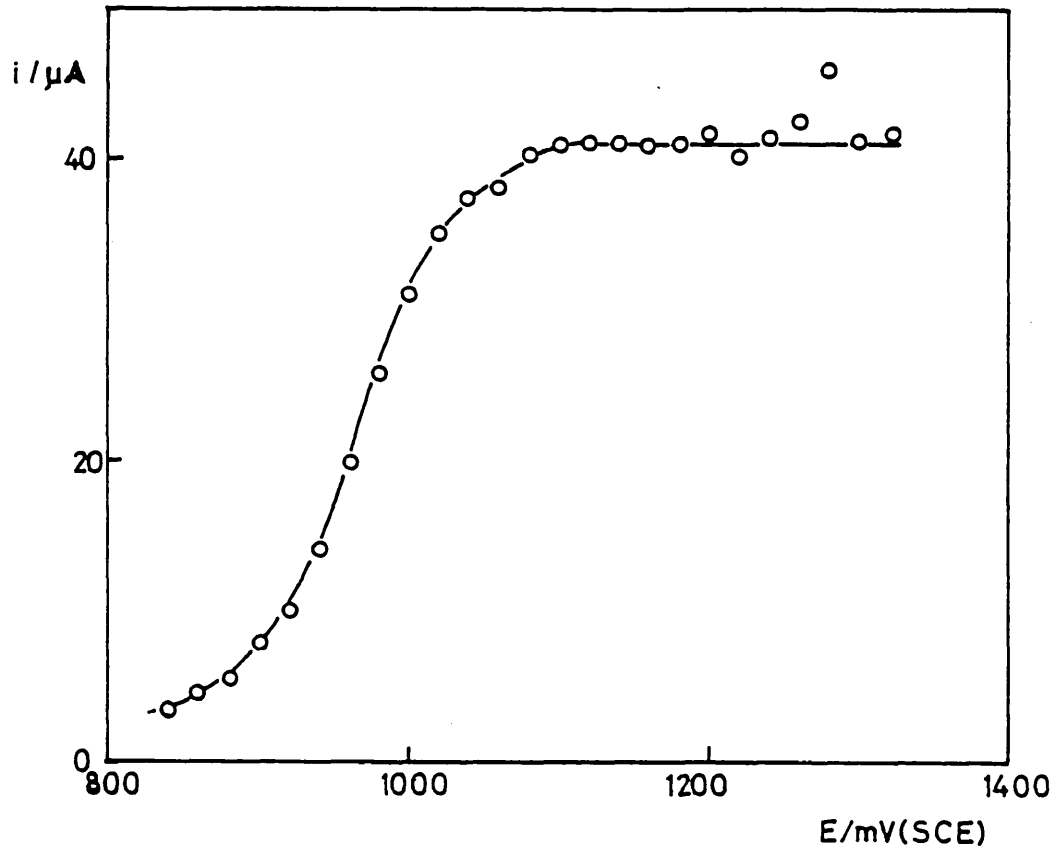

Figure 7.4. Steady-state polarogram for the oxidation of $ZnTMPyPCl_4$ at pH 2.5.

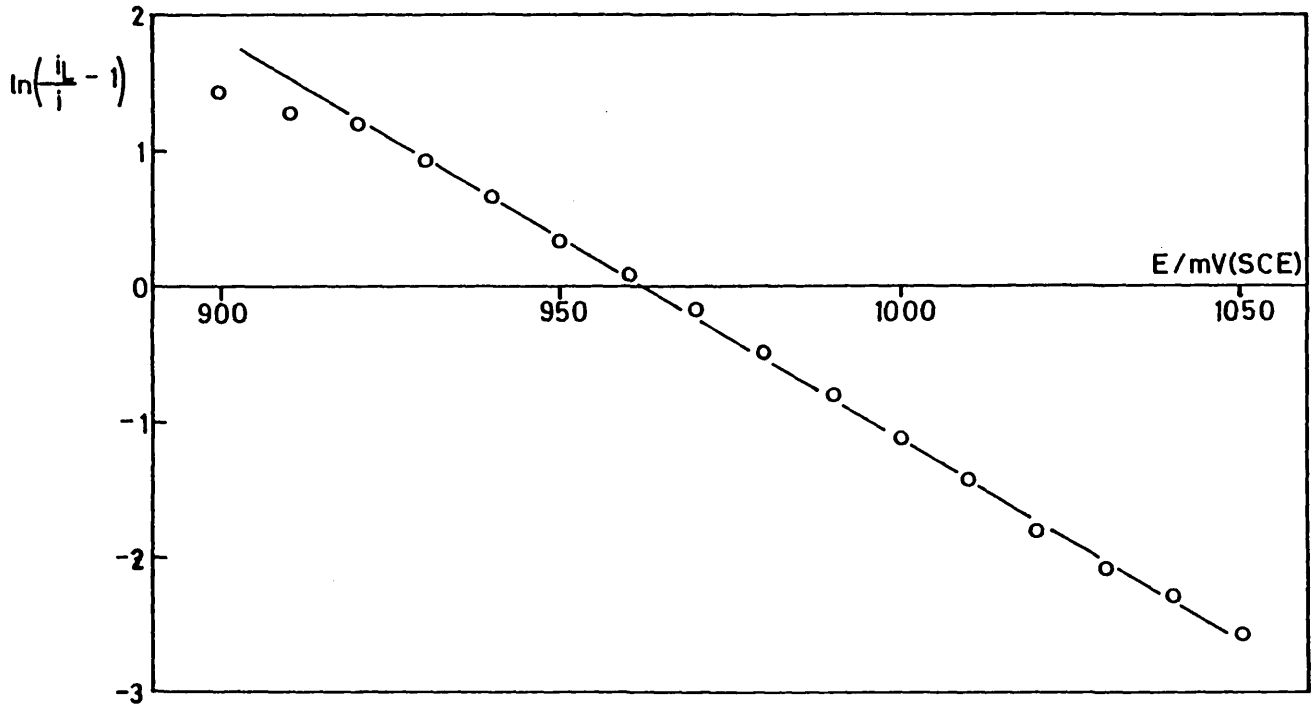

Figure 7.5. Tafel plot for the oxidation of $ZnTMPyPCl_4$.

more acidic but this would increase the rate of acid-catalysed demetallation of the porphyrin.

A Levich plot for $ZnTMPyP^{4+}$ at +1150 mV (SCE) is shown in figure (7.6). The background electrolyte used for this experiment was 50 mM Na_2SO_4 brought to pH 2.5 with H_2SO_4. This plot has been corrected for currents caused by the background electrolyte.

The diffusion coefficient of $ZnTMPyP^{4+}$ in a 0.58 mM porphyrin solution was measured using the rotation-speed step technique of Albery *et al*[84] in the pH 2.5 medium. Rotation speed was stepped from 3 Hz to 9 Hz. A typical current transient is shown in figure (7.7) and a plot of $W_\infty t_f$ τ_S is shown in figure (7.8).

A value for the diffusion coefficient was obtained using the mean of 8 determinations.

$$\text{For } ZnTMPyP^{4+},\ D/cm^2\ s^{-1} = 3.1 \times 10^{-6} \qquad (7.15)$$

7.6. Dark Electrochemistry of $ZnTHPyPCl_4$

The electrochemistry of $ZnTHPyPCl_4$ was studied at a glassy carbon RDE. As with $ZnTMPyPCl_4$ at pH 2.5, a single one-electron wave was obtained corresponding to the generation of the π-radical cation. This oxidation is quasi-reversible and has a half-wave potential of +974 mV (SCE). The standard electrode potential was calculated as $E^\ominus$ = +960 mV (SCE). No second wave was observed although currents were measured at values of potential as high as +1240 mV (SCE).

Attempts to follow the fate of the π-radical cation using a rotating ring-disc electrode (RRDE) apparatus were frustrated by high currents caused by solvent decomposition at the potential needed to reduce this species. An example of work using the RRDE apparatus is given by the study of $Fe(III)TPPSNa_3$.

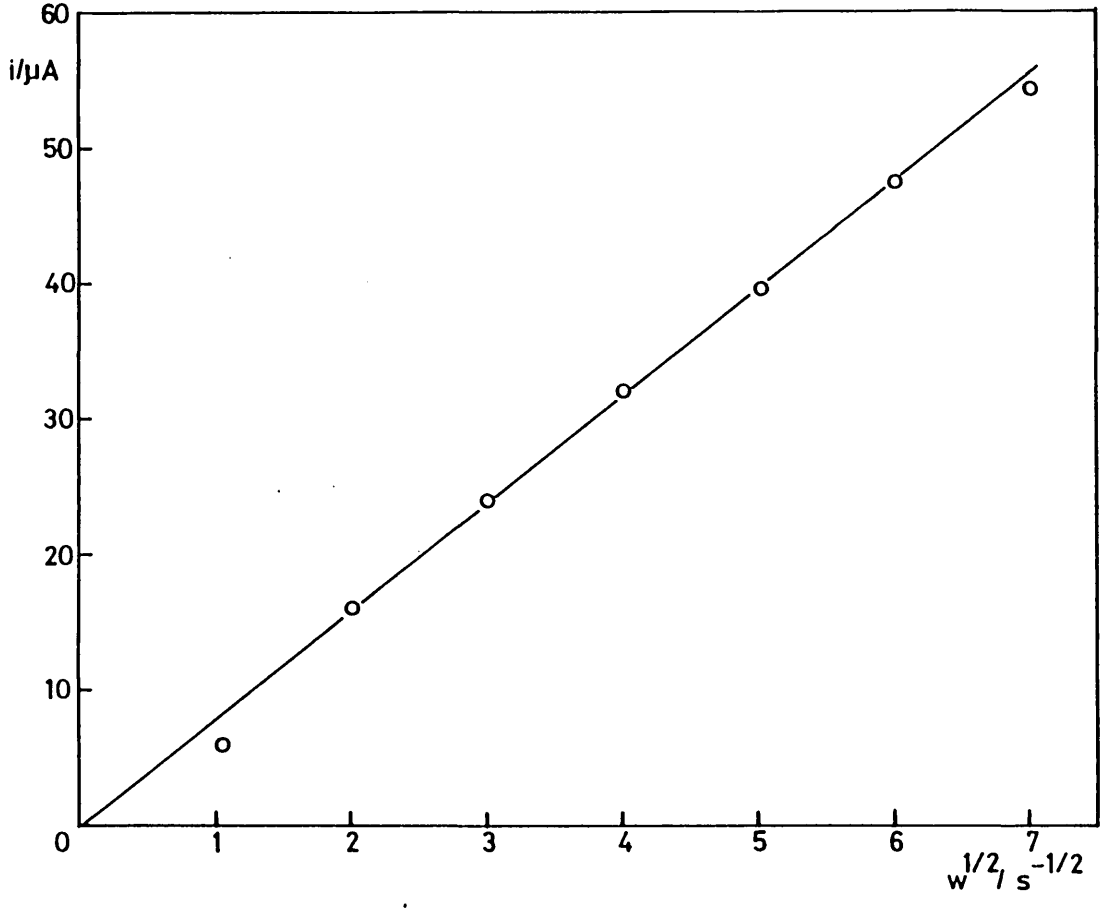

Figure 7.6. Levich plot at +1150 mV for $ZnTMPyPCl_4$ at pH 2.5.

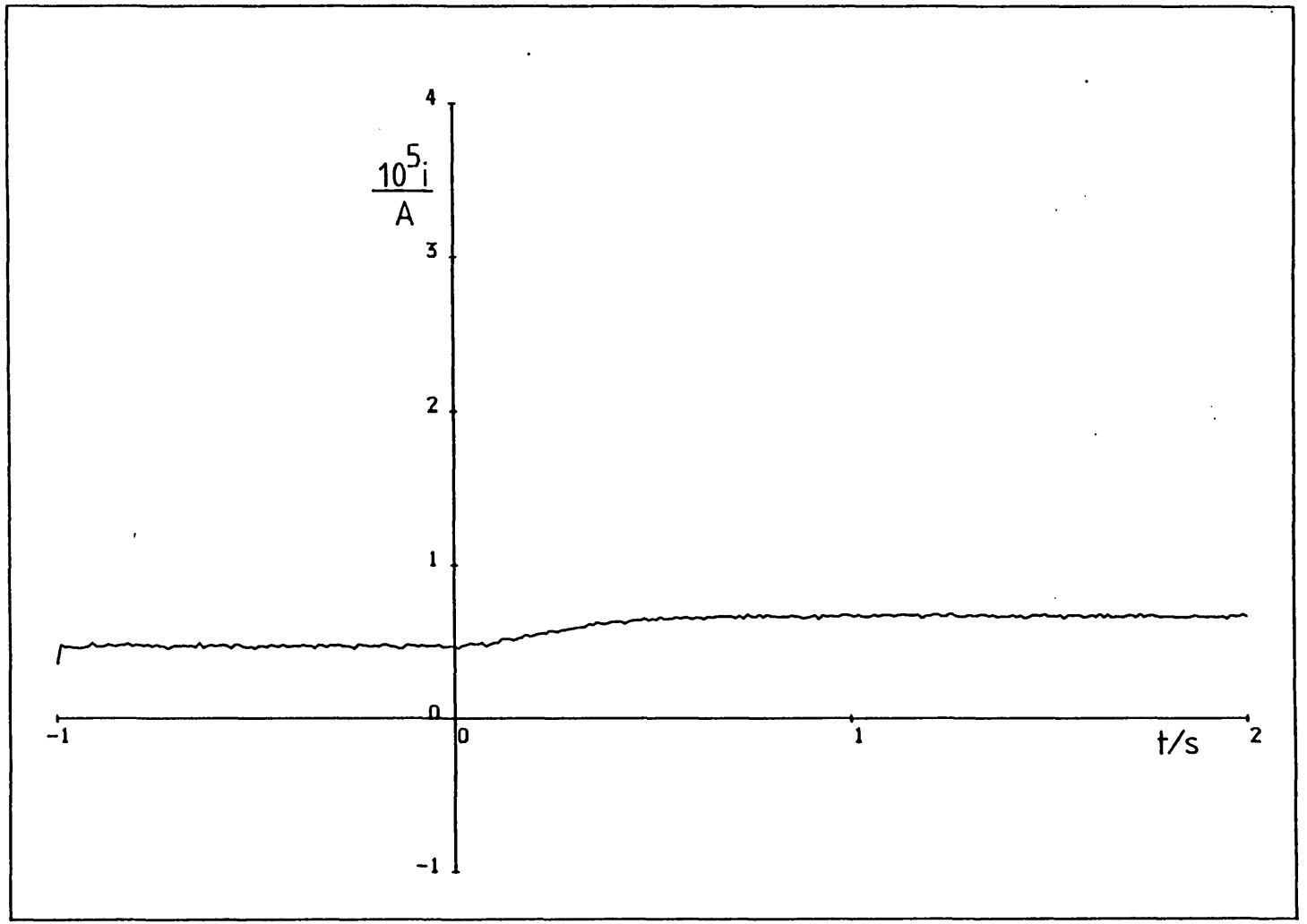

Figure 7.7. Rotation speed step transient for $ZnTMPyPCl_4$.

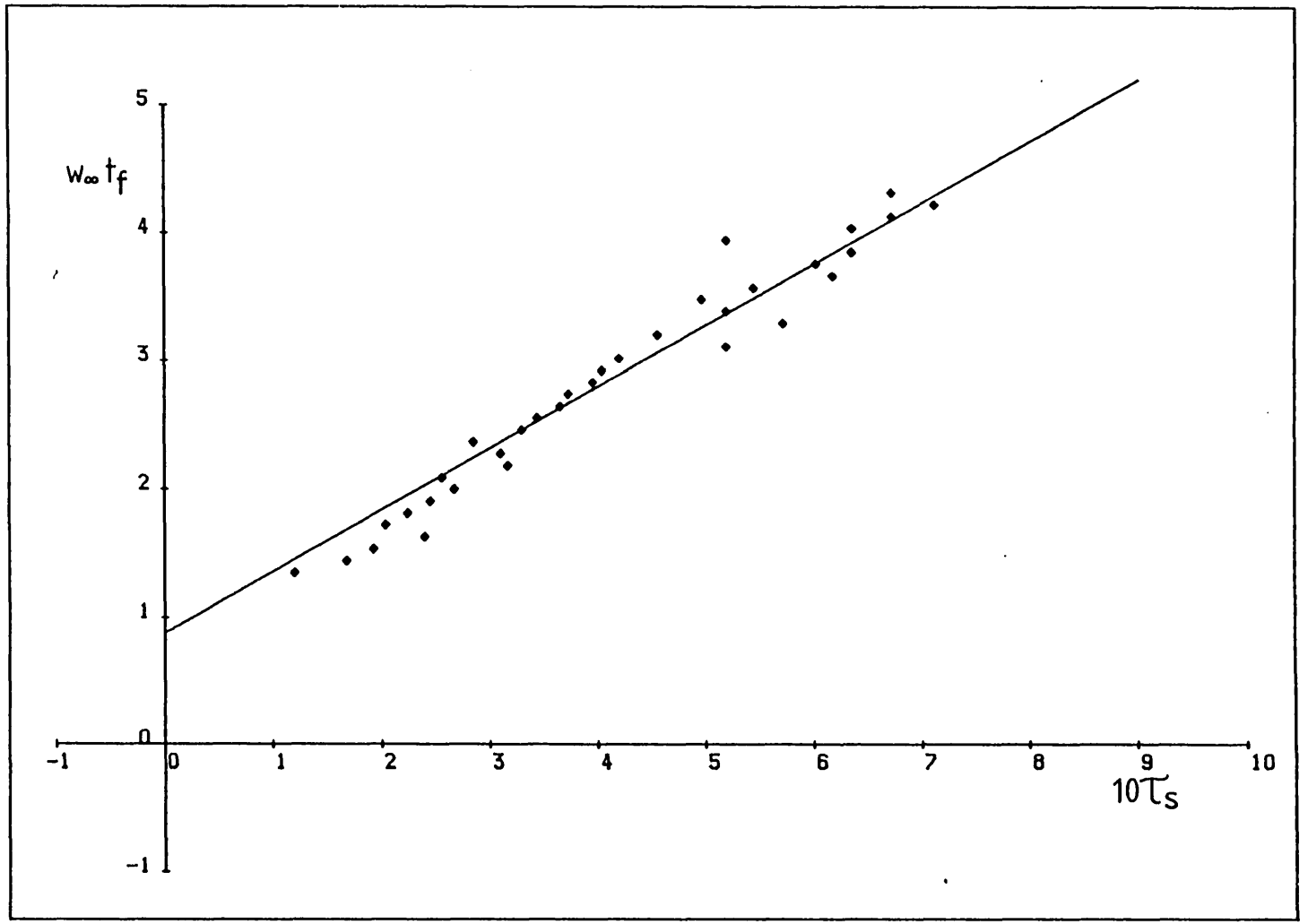

Figure 7.8. Rotation speed step transient for $ZnTMPyPCl_4$ analysed by the method of Albery *et al*[84].

7.7. Ring-Disc Experiments on $Fe(III)TPPSNa_3$

Ring polarograms of $Fe(III)TPPSNa_3$ in 1 mM HCl (aq) are shown in figure (7.9).

For polarogram (a) the disc was held at 0 mV (SCE). At potentials above +850 mV, porphyrin (Fe(III)P) is oxidised to porphyrin π-radical cation ($Fe(III)P^{+\cdot}$).

For polarogram (b) the disc was held at +1000 mV (SCE). Below +850 mV the ring electrode carries a current corresponding to the reduction of $Fe(III)P^{+\cdot}$ to Fe(III)P. At potentials greater than +850 mV the ring is also oxidising Fe(III)P to $Fe(III)P^{+\cdot}$ but the ring is 'shielded' from the bulk porphyrin concentration by oxidation of porphyrin at the disc. At potentials less than +550 mV there is a further current corresponding to the reduction of free Fe(III) to Fe(II).

$Fe(III)P^{+\cdot}$ is unstable in acidic aqueous solution and the decomposition yields free Fe(III) and an electrochemically inactive porphyrin species. In 1 mM HCl, $E^{\ominus}$ Fe(II)/Fe(III) was measured as +480 mV (SCE).

In another experiment, again in 1 mM HCl, the disc was potentiostatted at +1000 mV where Fe(III)P is oxidised to $Fe(III)P^{+\cdot}$, while the ring electrode was potentiostatted at +800 mV, where $Fe(III)P^{+\cdot}$ is reduced to Fe(III)P but where Fe(III) is inactive.

Albery and Hitchman[85] have discussed the case where an electrogenerated intermediate decomposes on its way from the disc to the ring electrode by first order kinetics.

In this case:

$$\text{disc} \qquad Fe(III)P \longrightarrow Fe(III)P^{+\cdot} \tag{7.16}$$

$$\text{solution} \quad Fe(III)P^{+\cdot} \xrightarrow{k_B} \text{products} \tag{7.17}$$

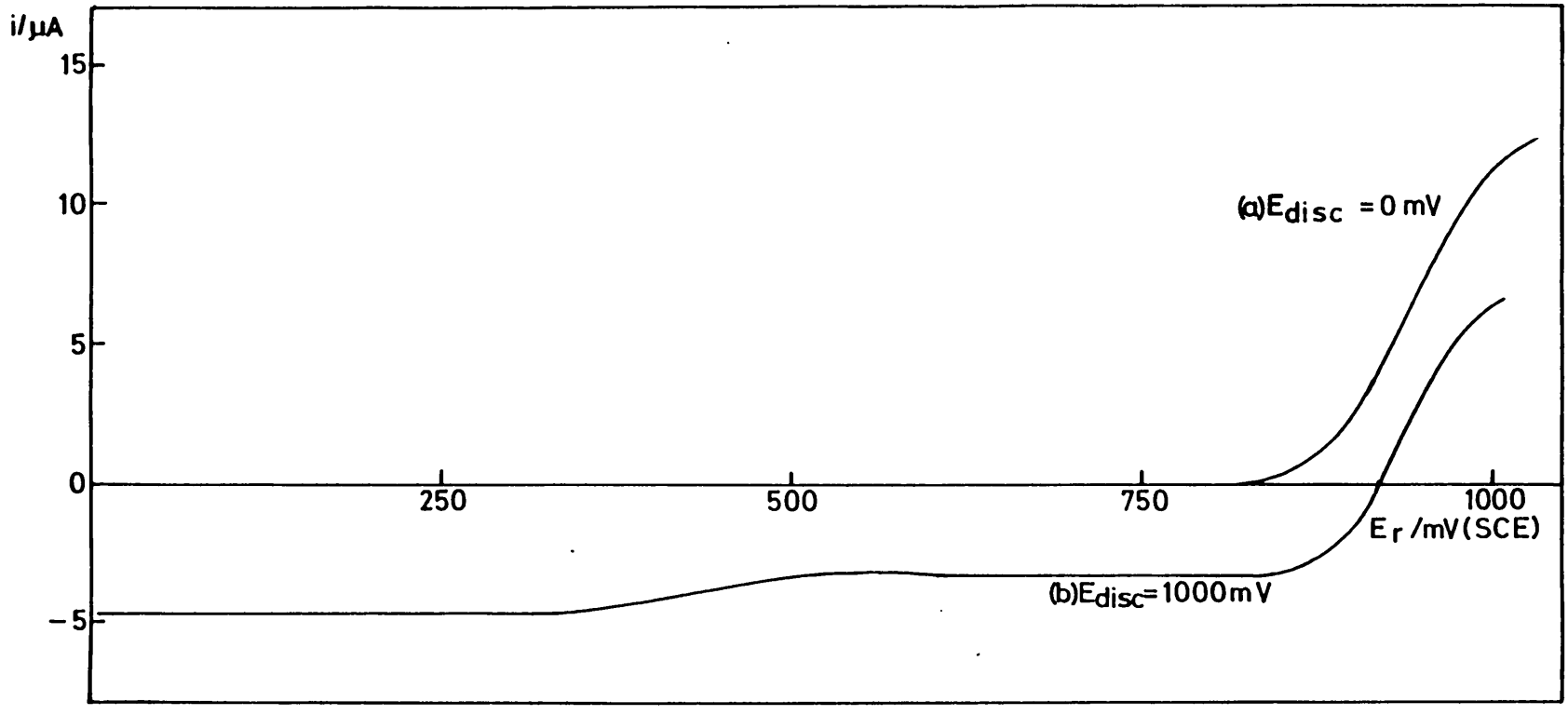

Figure 7.9. Ring polarograms of Fe(III) TPPS.

$$\text{ring} \quad Fe(III)P^{+\cdot} \longrightarrow Fe(III)P \qquad (7.18)$$

Using a theoretical plot of N_κ against κ, values of the kinetic collection efficiency were used to calculate k_B from the equation

$$\kappa^2 = 0.248\ k_B\ w^{-1}\ D^{-1/3}\ \nu^{1/3} \qquad (7.19)$$

Collection efficiencies were measured over a range of rotation speeds and a plot of κ^2 against $1/w$, according to equation (7.19) is shown in figure (7.10).

The rate constant for the decomposition reaction of $Fe(III)P^{+\cdot}$ in the bulk solution was found to be

$$k_B/s^{-1} = 0.50\ (\pm\ 0.05)\ \text{at}\ 25^oC \qquad (7.20)$$

The results of dark electrochemistry experiments using the metalloporphyrins are summarised in table (7.3).

Photoelectrochemistry of some Water-Soluble Metalloporphyrins

Photoredox reactions of some water-soluble metalloporphyrins were investigated using the ORDE technique. The systems studied are listed in table (7.4).

For many of these combinations of metalloporphyrin and quencher, no photocurrent was observed. There are three possible reasons for this:

(a) When the porphyrin contains a paramagnetic transition metal ion, the triplet lifetime is very short[86].

(b) Where the products of the electron transfer quenching reaction have opposite charges, electrostatic attraction means that the

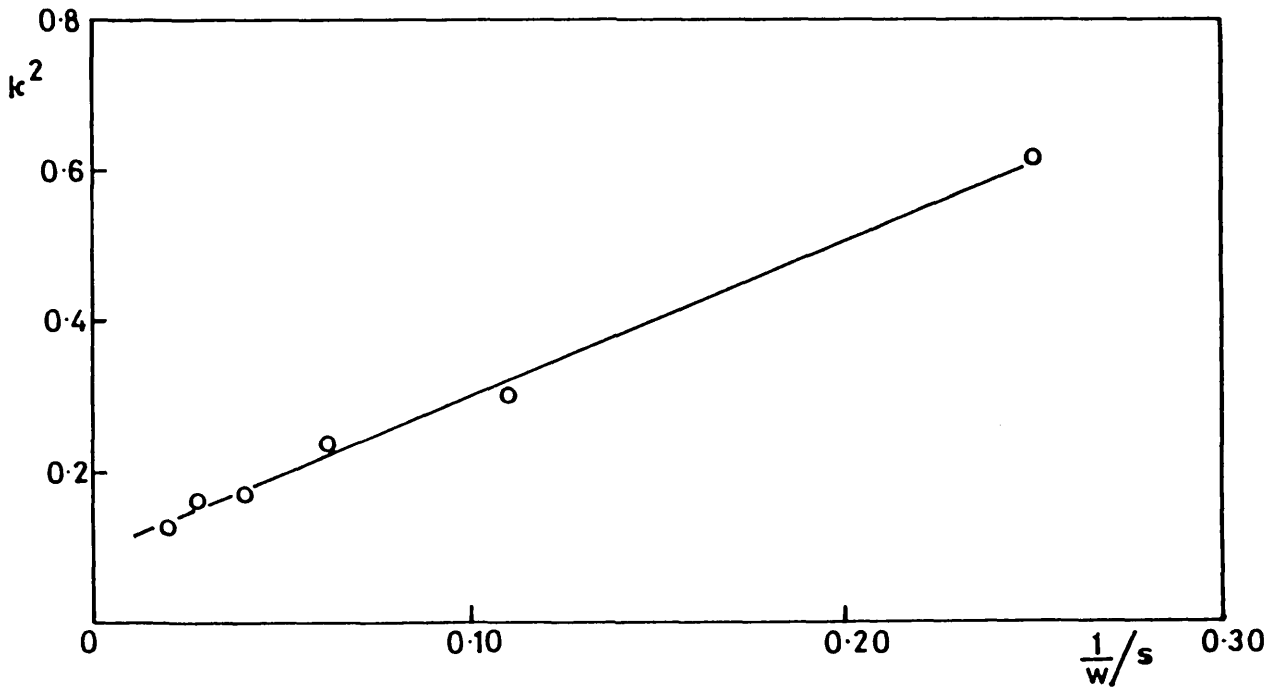

Figure 7.10. Plot of κ^2 against 1/w according to equation (7.19) for the decomposition of the Fe(III)TPPSNa_3 π-radical cation.

Table 7.3

Dark Electrochemistry of Water Soluble Metalloporphyrins

Compound	Medium	$E_{\frac{1}{2}}(1)$/mV(SCE)	$E_{\frac{1}{2}}(2)$/mV(SCE)	D/cm^2s^{-1}
$ZnTMPyPCl_4$	0.1 M Na_2SO_4 adjusted to pH 2.5	+960		$3.1x10^{-6}$
$ZnTHPyPCl_4$	0.1 M Na_2SO_4 adjusted to pH 2.5	+975		
$ZnTPPSNa_4$	1 M Na_2SO_4 + 5 mM H_2SO_4	+600	+890	
$Co(III)TPPSNa_3$	50 mM H_2SO_4	+875	+1120	$2.3x10^{-6}$
$Fe(III)TPPSNa_3$	0.5 M HCl	+925		$1.8x10^{-6}$

Table 7.4

Metalloporphyrin-quencher Systems Studied by the ORDE Technique

Metalloporphyrin	Quencher	Observation
$FeTPPS^{3-}$	Fe(III)	No photocurrent[a,b]
$FeTPPS^{3-}$	MV^{2+}	No photocurrent[a,b]
$ZnTPPS^{4-}$	MV^{2+}	No photocurrent[b]
$ZnTPPS^{4-}$	Thionine	No photocurrent[b]
$ZnTPPS^{4-}$	Fe(III)	No photocurrent[b]
$ZnTPPS^{4-}$	$[Fe(CN)_6]^{3-}$	Photocurrent observed
$ZnTMPyP^{4+}$	Fe(III)	Photocurrent observed
$ZnTHPyP^{4+}$	Fe(III)	Photocurrent observed
ZnTPSPyP	Fe(III)	No photocurrent[c]

(a) The porphyrin contains a paramagnetic transition metal and the triplet lifetime is very short[86].

(b) Electrostatic attraction between the products of the photoredox reaction means that the fraction of product species leaving the solvent cage is considerably reduced[81].

(c) Red fluorescence was observed.

fraction of products of the photoredox reaction leaving the solvent cage is considerably reduced[81].

(c) Reaction between the triplet metalloporphyrin and quencher may not be possible on thermodynamic grounds, depending on the redox potentials of these two species.

The largest photocurrents were observed for $ZnTMPyP^{4+}$ with Fe(III) as quencher and this system was chosen for further study.

7.8. ORDE Studies of the $ZnTMPyP^{4+}$/Fe(III) System

The wavelength of light used to excite the metalloporphyrin was that corresponding to the Soret absorption band at 435 nm. Measurements of photocurrent were made at the potential of zero dark current. The potential being re-adjusted with each addition of ferrous or ferric ion.

A 'map' showing the regions of [Fe(II)] and [Fe(III)] that were studied is shown in figure (7.11). The experiments at pH 1.35 are discussed in this work, experiments at pH 2.5 followed roughly the same pattern. When there was no ferrous ion added to the solution, the concentration of ferrous photogenerated from ferric was estimated to be 1×10^{-6} M and this is the value used in figure (7.11). Crosses in the diagram indicate concentrations of ferrous and ferric at which the variation of photocurrent with light intensity and rotation speed was investigated.

In agreement with other authors[72] we believe that the reaction scheme is as follows:

$$ZnTMPyP^{4+} + Fe(III) \xrightarrow{k_7} ZnTMPyP^{5+} + Fe(II) \qquad (7.21)$$

$$ZnTMPyP^{5+} + Fe(II) \xrightarrow{k_{-7}} ZnTMPyP^{4+} + Fe(III) \qquad (7.22)$$

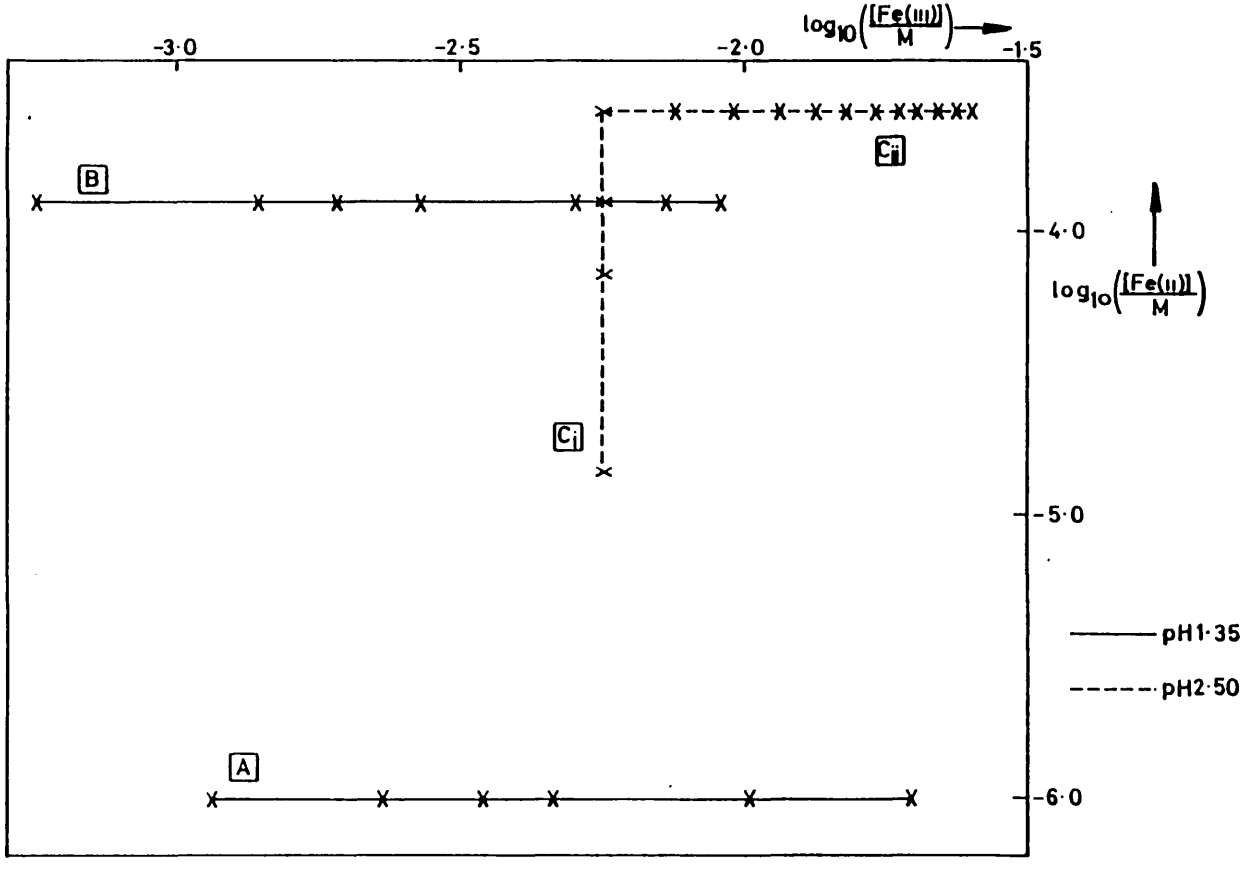

Figure 7.11. Regions of [Fe(II)] and [Fe(III)] studied by the ORDE technique.

There are two processes involved. On the one hand the forward reaction k_7 promoted by Fe(III) and on the other hand the back reaction k_{-7} promoted by Fe(II).

(1) The Forward Reaction k_7

Experiments in which [Fe(III)] was varied suggest that there is an optimum concentration of ferric at which the photocurrent is a maximum. This has been confirmed by flash photolysis[87] and by the ORDE technique at pH 2.5[88].

At low concentrations of ferric the behaviour is as expected. Increasing the concentration of quencher increases the quantum efficiency for the production of porphyrin π-radical cation and thus increases the photocurrent. This is the situation found in other photogalvanic systems e.g. the iron/thiazine system and the iron/$Ru(bpy)^{3+}$ system.

At higher concentrations of ferric the quencher reacts with excited metalloporphyrin to yield products which are not electroactive

$$P^* + Fe(III) \rightarrow ? \qquad (7.23)$$

If Fe(III) causes Stern-Volmer quenching of P* in this way ϕ, the quantum efficiency for the production of the electroactive π-radical cation will be given by

$$\phi = \frac{1}{1 + k_q[Fe(III)]} \qquad (7.24)$$

This relationship is indeed found to hold at higher concentrations of Fe(III) and so ϕ unexpectedly passes through a maximum as the ferric concentration is increased.

(2) The Back Reaction k_{-7}

A value has been reported[72] for the reverse electron transfer reaction k_{-7}

$$k_{-7}/M^{-1}\ s^{-1} = 2 \times 10^{8} \tag{7.25}$$

and this is in good agreement with our work which gives a value of

$$k_{-7}/M^{-1}\ s^{-1} = 1 \times 10^{8} \tag{7.26}$$

A typical concentration of ferrous ion used in these experiments was $[Fe(II)]/M = 2.6 \times 10^{-4}$. Under these conditions the lifetime of the porphyrin π-radical cation, $t_{\frac{1}{2}}$, given by

$$t_{\frac{1}{2}} = 1/k_{-7}[Fe(II)] \tag{7.27}$$

is about 40 μs and the kinetic length given by

$$X_k = (D/k_{-7}[Fe(II)])^{\frac{1}{2}} \tag{1.6}$$

is 1.1×10^{-5} cm.

k_{-7} is therefore so rapid that we can assume that X_k will be the shortest of the four characteristic lengths in the theory of the ORDE. The system falls into region B of figure (3.5) and the photoelectrochemical collection efficiency is given by

$$N_{h\nu} = X_k/X_\varepsilon \tag{3.53}$$

Light is trapped by the porphyrin over a distance X_ε from the working electrode but the electroactive π-radical cation cannot reach the electrode unless it is generated within the distance X_k.

ORDE experiments were conducted both with and without the addition of ferrous ion and these cases are considered separately.

(i) When no Fe(II) has been added to the solution

In this case the only ferrous present is photogenerated by the electron transfer quenching reaction. Oxidised porphyrin reacts at the ORDE but the ferrous ion cannot react there and is removed from the region of the electrode by rotation. Increasing the speed of rotation decreases the thickness of the stagnant diffusion layer next to the electrode and thus decreases the distance over which Fe(II) must diffuse to escape. Increasing the rotation speed therefore decreases the ferrous concentration near to the electrode and increases the current.

The convective diffusion equation for the ORDE, equation (3.20), can be solved[49] for the case where two photogenerated species react together and where one of the species is electroactive and the other is not. The flux of oxidised metalloporphyrin to the electrode, j is given by

$$j = D^{2/3} g^{2/3} k_{-7}^{-1/3} X_D^{-1/3} \qquad (7.28)$$

where

$$g = \phi I_o \varepsilon [ZnTMPyP^{4+}] \qquad (7.29)$$

and

$$X_D = 0.643\ \nu^{1/6} D^{1/3} w^{-1/2} \qquad (3.8)$$

Thus

$$j \propto w^{1/6} \qquad (3.9)$$

This dependence of photocurrent upon rotation speed has been observed[88] for the $ZnTMPyP^{4+}$/Fe(III) system at pH 2.5 but in the medium used for these experiments (50 mM H_2SO_4, pH 1.35) the behaviour was found to be more complex and is described later.

(ii) When Fe(II) has been added to the solution

When the concentration of photogenerated ferrous is negligible compared to the concentration of added ferrous, the distance X_k is even shorter than before the addition, and is again the shortest of the characteristic lengths. Removal of photogenerated ferrous by convection now causes an insignificant change in the ferrous concentration close to the electrode and so the photocurrent is independent of rotation speed.

7.9. Experiments at a Series of Ferric Concentrations with no Added Ferrous

Generation of the porphyrin π-radical cation is accompanied by photogeneration of ferrous ion. A value for the concentration of Fe(II) can be calculated from the rotation speed and the photocurrent at the ORDE. In this series of experiments described by line A in figure (7.11) we studied the variation of photocurrent with ferrous concentration at the electrode surface at different ferric concentrations in the range

$$1.2 \text{ mM} < [Fe(III)] < 71 \text{ mM}$$

Ferrous ions react with the oxidised porphyrin as in scheme (7.22)

$$ZnTMPyP^{5+} + Fe(II) \xrightarrow{k_{-7}} ZnTMPyP^{4+} + Fe(III) \qquad (7.22)$$

However the situation is complicated by the existence of another first order route ($k_?$) for the decomposition of $ZnTMPyP^{5+}$

$$k_\Sigma = k_? + k_{-7}[Fe(II)] \tag{7.23}$$

A steady-state current-voltage curve was obtained for the reaction of Fe(II) at the tin oxide electrode used for the ORDE experiment. A 1 mM solution of ferrous gave a limiting current of 10.0 μA at 1 Hz. This value enables us to calculate the concentration of photogenerated ferrous at the electrode surface $[Fe(II)]_0$ from equation (7.24).

$$[Fe(II)]_0 = [Fe(II)]_\infty + \frac{i_p}{i_F\, w^{\frac{1}{2}}} \tag{7.24}$$

where

$[Fe(II)]_\infty$ is the concentration of ferrous in the bulk solution ($[Fe(II)]_\infty = 0$ in this series of experiments),

i_p is the measured photocurrent,

i_F is the limiting current for a 1 M solution of Fe(II) at a rotation speed of 1 Hz on the electrode used for the ORDE experiment, and

w is the rotation speed in Hz.

Using equations (3.36) and (3.53)

$$i = i_{h\nu}\Phi X_k/X_\varepsilon \tag{7.25}$$

and from the definition of the kinetic length,

$$X_k = (D/(k_? + k_{-7}[Fe(II)]_0))^{\frac{1}{2}} \tag{7.26}$$

we find that

$$\left(\frac{\Phi}{i}\right)^2 = \left(\frac{X_\varepsilon}{\phi i_{h\nu}}\right)^2 \frac{k_? + k_{-7}[Fe(II)]_0}{D} \qquad (7.27)$$

Plots of $(\Phi/i)^2$ against $[Fe(II)]_0$ at each ferric concentration, (figures (7.12), (7.13) and (7.14)) are linear and when

$$(\Phi/i)^2 = 0, \quad [Fe(II)]_0 = -k_?/k_{-7}$$

The results of experiments at nine different ferric concentrations show a common intercept at -0.02 mM and so

$$k_{-7}/M^{-1}\ s^{-1} = 5 \times 10^4\ k_? \qquad (7.28)$$

From equation (7.27), when $[Fe(II)]_0 = 0$ we obtain the expression

$$y_{int}^{\frac{1}{2}} = X_\varepsilon\ (k_?/D)^{\frac{1}{2}}/\phi i_{h\nu} \qquad (7.29)$$

where y_{int} is the intercept on the y-axis for a particular ferric concentration, from figures (7.12), (7.13) and (7.14).

At high concentrations of added ferric ion, increasing the ferric concentration decreases ϕ, the quantum efficiency for production of the porphyrin π-radical cation. If this effect is due to Stern-Volmer quenching of the excited porphyrin, ϕ will be given by

$$\phi = \frac{1}{1 + K_q[Fe(III)]} \qquad (7.30)$$

Key for figure 7.12.

$\bar{\Phi}$	Symbol
1·00	o
0·50	∇
0·28	Δ
0·18	□
0·077	×

Key for figure 7.13.

[Fe(III)]/mM	Symbol
3·45	□
4·59	X
10·2	Δ

Figures 7.12, 7.13 and 7.14. Plots of $(\Phi/i)^2$ against $[Fe(II)]_o$ according to equation (7.27).

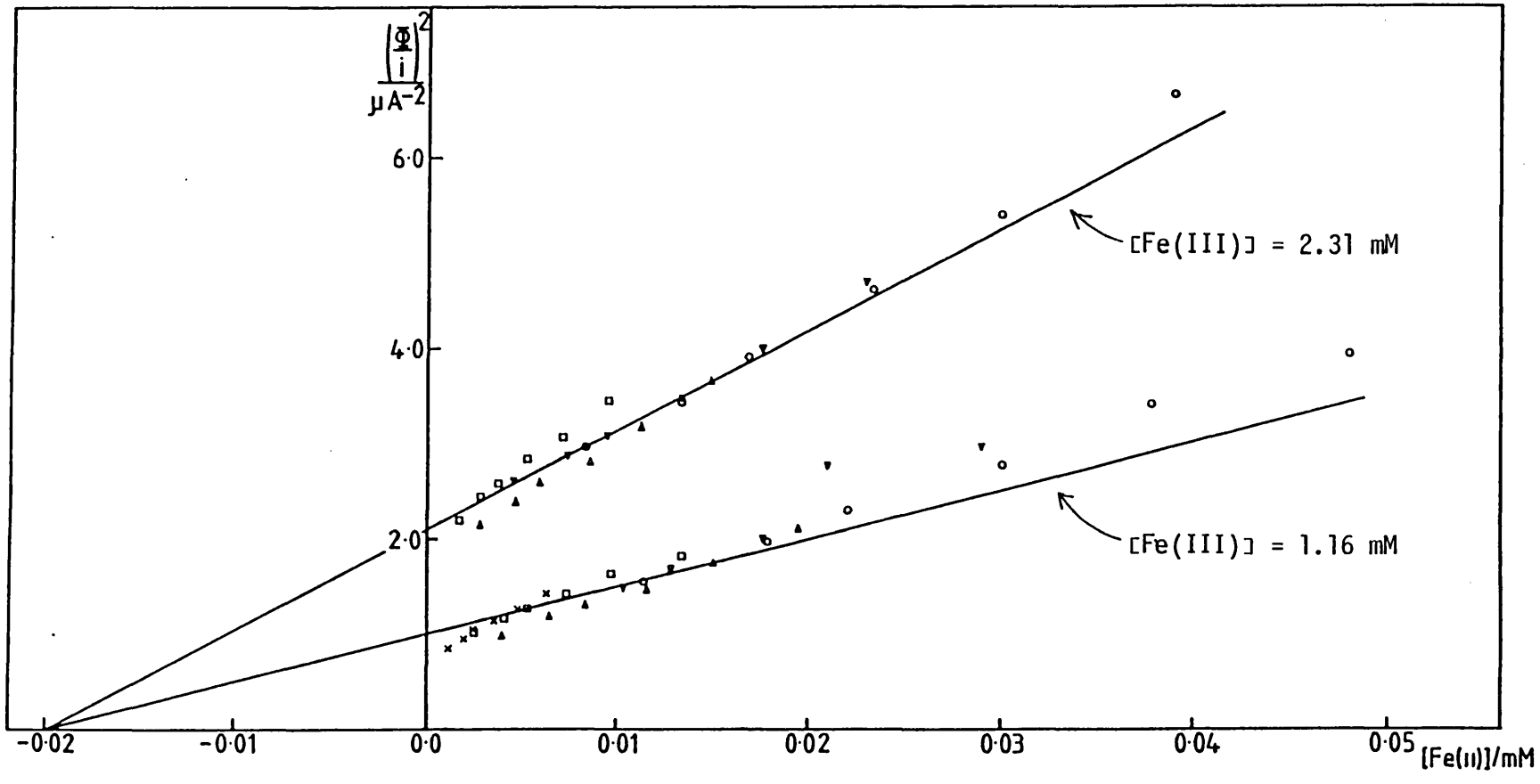
$\left(\frac{\Phi}{i}\right)^2$
μA^{-2}
6·0
4·0
2·0
-0·02
-0·01
0·0
0·01
0·02
0·03
0·04
0·05
[Fe(II)]/mM
[Fe(III)] = 2.31 mM
[Fe(III)] = 1.16 mM

Figure 7.12.

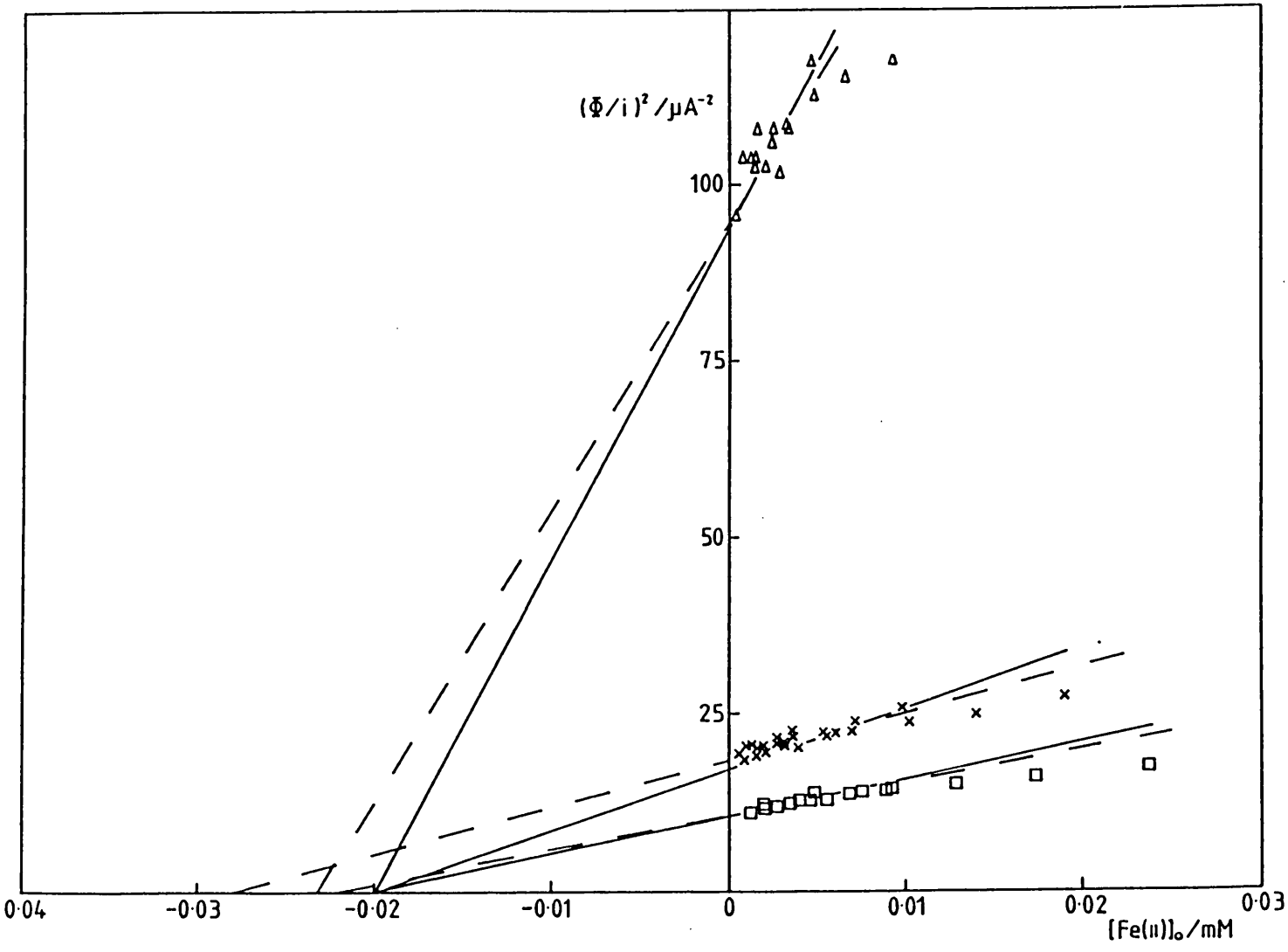

Figure 7.13.

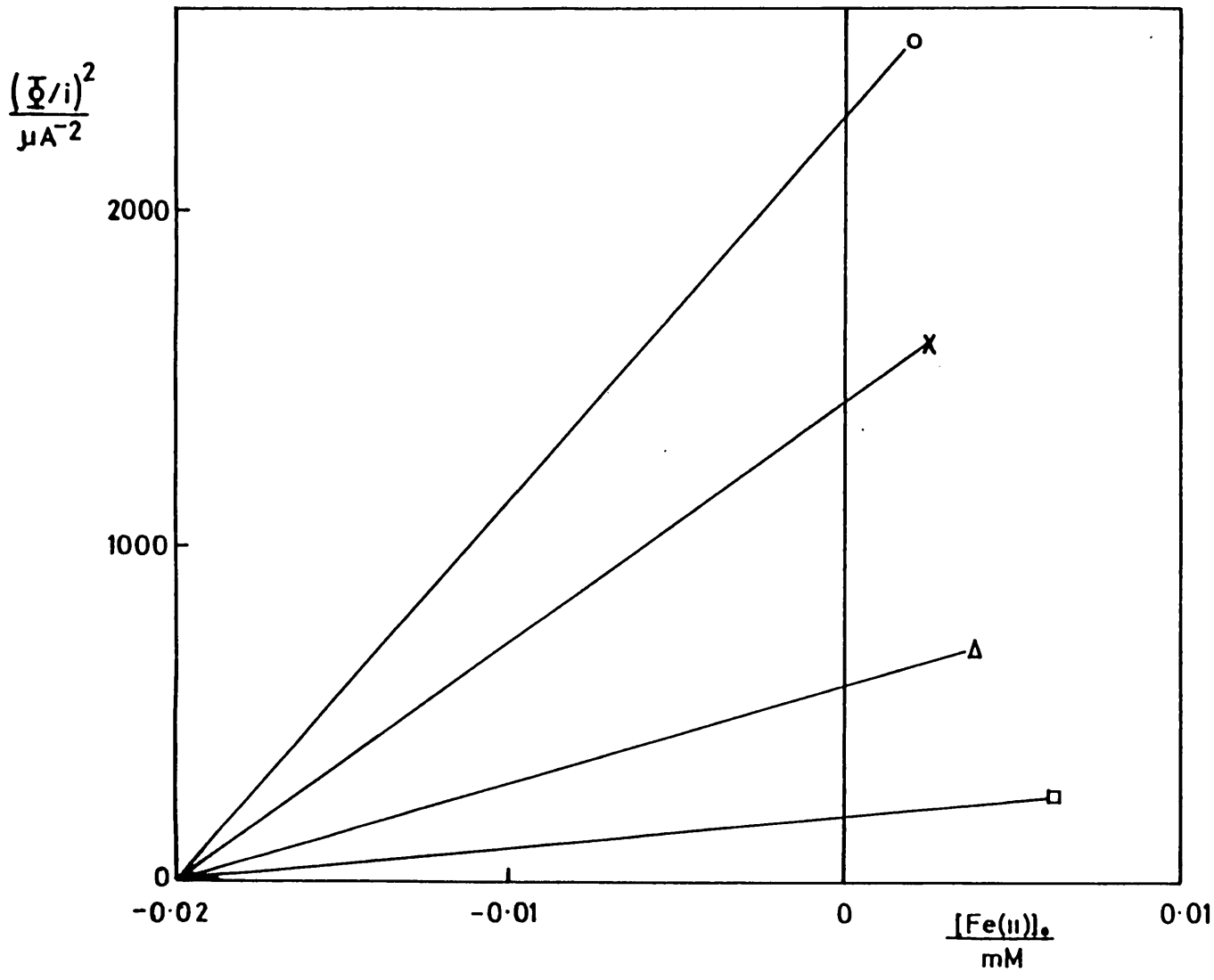

Symbol	[Fe(III)] /mM
o	71
X	45
Δ	26
□	16

Figure 7.14.

where K_q is the Stern-Volmer quenching constant. Combining equations (7.29) and (7.30) we obtain

$$y_{int}^{\frac{1}{2}} = (1 + K_q[Fe(III)])X_\varepsilon(k_?/D)^{\frac{1}{2}}/i_{h\nu} \qquad (7.31)$$

Plots of $y_{int}^{\frac{1}{2}}$ against [Fe(III)] are shown in figures (7.15) and (7.16).

These two plots give reasonable straight lines, confirming the hypothesis that ferric causes Stern-Volmer quenching of the excited state porphyrin to yield electrochemically inactive products. In this series of experiments the ferric concentration was high and $K_q[Fe(III)] > 1$. It was therefore not possible to obtain a value for the Stern-Volmer quenching constant from the negative intercept on the x-axis. However the gradient is used later to find a value for K_q.

7.10. ORDE Experiments with a Low Concentration of Added Ferrous Ion

This series of experiments is shown as line B in figure (7.11). A low concentration of ferrous ion was added to the solution ($[Fe(II)]_{added}$ = 0.126 mM) and the ferric ion concentration was varied over the range 0.56 mM to 9.2 mM.

We assume that the concentration of photogenerated ferrous will be negligible compared to the concentration of ferrous ion added. Values of Φ/i were found to be fairly constant for each ferric concentration studied (table (7.5) and figure (7.17)) and this confirms that photogenerated ferrous is unimportant under these conditions.

The range of ferric concentrations studied here was lower than that used in the previous series of experiments (line A in figure (7.11)), and enables us to calculate a value for K_q, the Stern-Volmer quenching constant

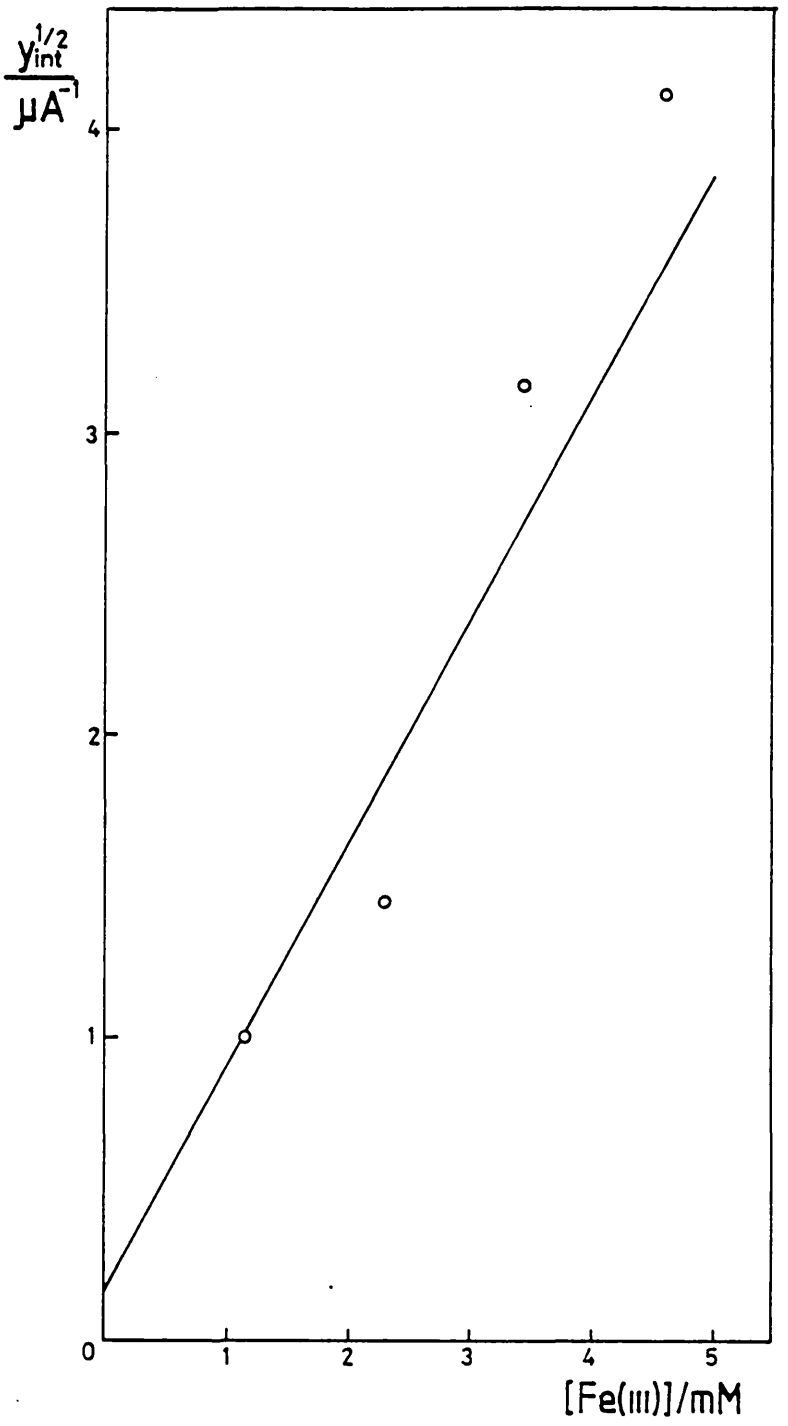

Figure 7.15. Plot of $y_{int}^{\frac{1}{2}}$ against [Fe(III)] according to equation (7.31) for the ZnTMPyP ORDE with no added ferrous.

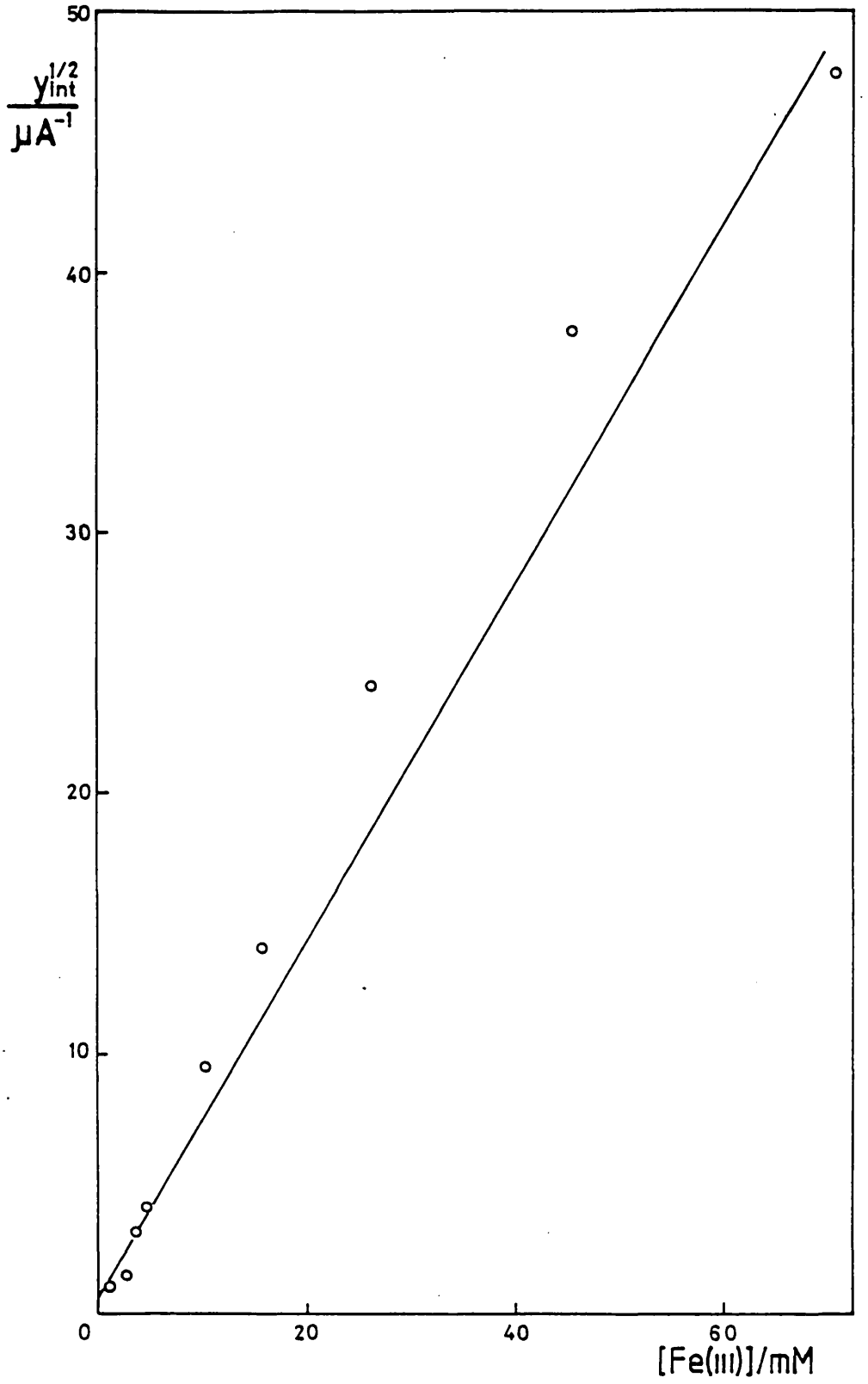

Figure 7.16. Plot of $y_{int}^{\frac{1}{2}}$ against [Fe(III)] according to equation (7.31) for the ZnTMPyP ORDE with no added ferrous.

Table 7.5

Values of Φ/i for the Series of Experiments with a Low Concentration of Added Ferrous Ion

These experiments are shown by line B in figure (7.11). Each value of Φ/i represents the average of measurements at six different electrode rotation speeds.

Φ / $\square Fe(III)\square$/mM	Φ/i / μA^{-1}			
	1	0.51	0.29	0.18
0.56	6.50	6.10	5.73	5.36
1.37	8.40		7.49	
1.90	9.80		9.33	
2.67	12.3		11.6	
5.06	21.5			
7.22	31.3	31.2	30.7	29.5
9.16	41.7	41.6	41.7	39.3

Symbol	[Fe(III)]/mM
o	0·56
X	1·37
Δ	1·90
□	2·67
◇	5·06
+	7·22
∇	9·16

Figure 7.17. Plots of photocurrent against Φ at different ferric concentrations for the ZnTMPyP ORDE.

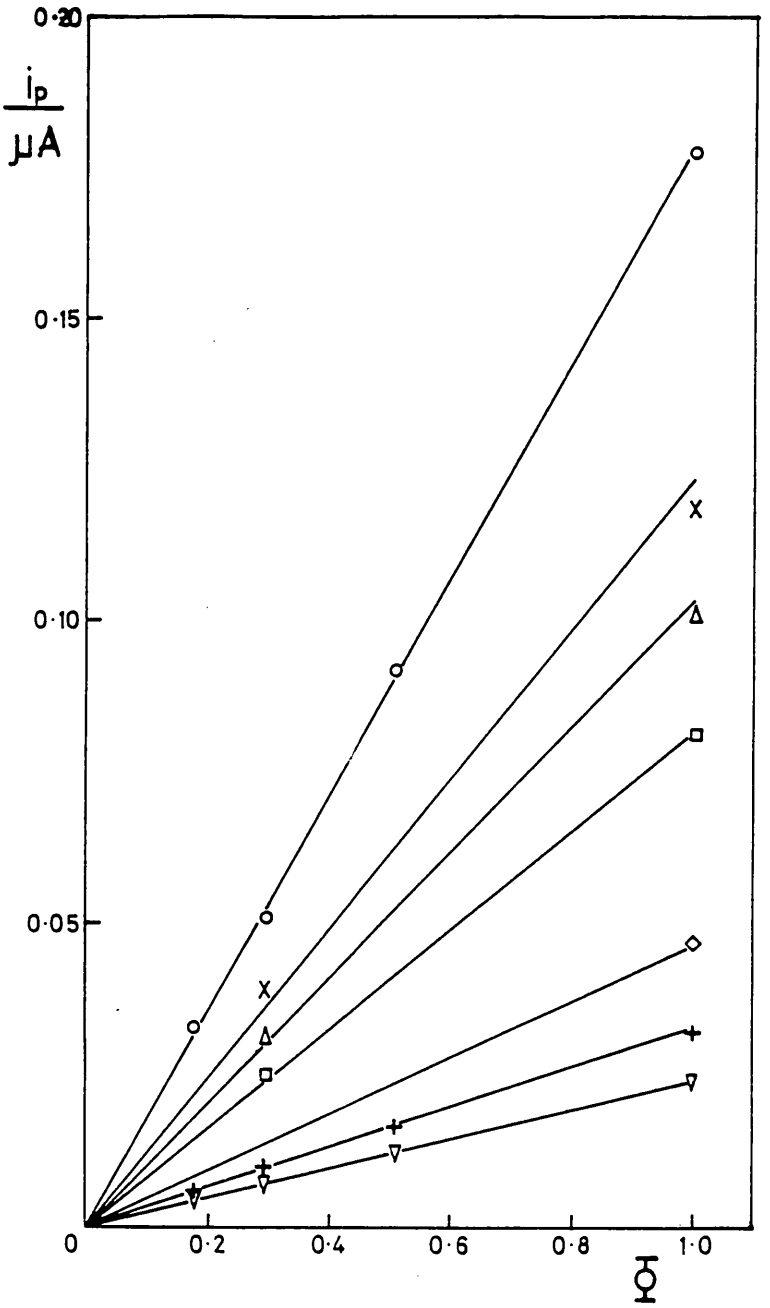

Figure 7.17.

for reaction of the excited-state porphyrin with ferric which yields electrochemically inactive products.

Combining equations (7.27) and (7.30) we obtain the expression

$$\Phi/i = X_\varepsilon(1 + K_q[Fe(III)])(k_? + k_{-7}[Fe(II)]_0/D)^{\frac{1}{2}}/i_{h\nu} \qquad (7.32)$$

A plot of Φ/i against $[Fe(III)]$ for this data (figure (7.18)) gives a good straight line with an intercept on the x-axis of

$$K_q^{-1} = 0.8\ mM^{-1} \qquad (7.33)$$

Hence

$$K_q = 1.3 \times 10^3\ M \qquad (7.34)$$

This value for the Stern-Volmer constant explains why negligible intercepts were found in figures (7.15) and (7.16) for the series of experiments with no added ferrous. In those experiments, the ferric concentrations used were too high for the intercept to be significant.

From equations (7.32) and (7.28) the gradient of the plot in figure (7.18) is given by

$$(\text{gradient}) = \frac{X_\varepsilon K_q}{i_{h\nu}} \left[\frac{k_?(1 + 5 \times 10^4[Fe(II)]_0)}{D}\right]^{\frac{1}{2}} \qquad (7.35)$$

and thus $k_?$ is given by

$$k_? = \frac{D}{1 + 5 \times 10^4[Fe(II)]_0} \left(\frac{i_{h\nu}\ (\text{gradient})}{X_\varepsilon K_q}\right)^2 \qquad (7.36)$$

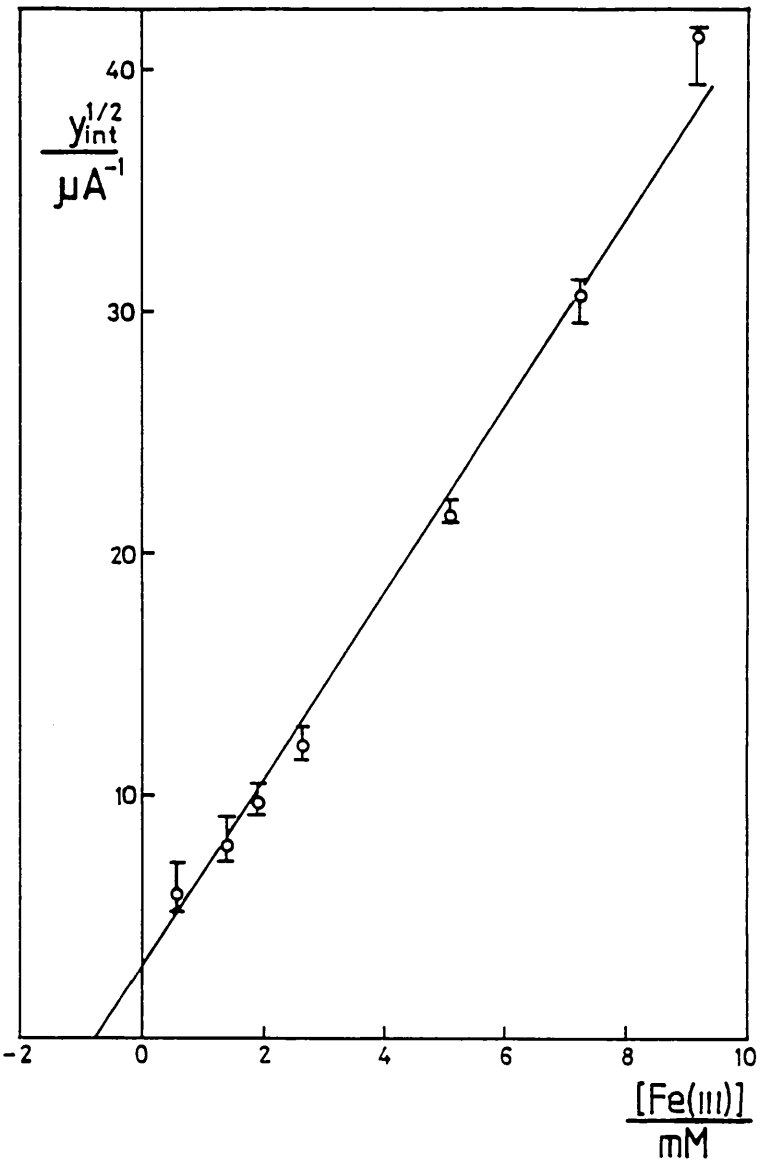

Figure 7.18. Plot of $y_{int}^{\frac{1}{2}}$ against ferric concentration according to equation (7.32) for the ZnTMPyP ORDE.

Now that a value has been found for K_q we can also obtain a value for $k_?$ from the experiments in which no ferrous ion was added to the solution. Returning to equation (7.31) and figures (7.15) and (7.16), the gradient of these plots is given by

$$\text{gradient} = X_\varepsilon K_q (k_?/D)^{\frac{1}{2}}/i_{h\nu} = 0.70 \qquad (7.37)$$

Rearranging this equation we obtain an expression for $k_?$

$$k_? = D(i_{h\nu}(\text{gradient})/X_\varepsilon K_q)^2 \qquad (7.38)$$

Using the value previously obtained for the diffusion coefficient of $ZnTMPyP^{4+}$ (equation (7.15)) $D/cm^2\ s^{-1} = 3.1 \times 10^{-6}$ we obtain the values for k_{-7} and $k_?$ given in table (7.6).

It is pleasing to note that the values for k_{-7} and $k_?$ both with, and without ferrous ions added to the solution are in good agreement and that the value for k_{-7} is similar to that reported by Harriman and Williams[72]:

$$k_{-7}/M^{-1}\ s^{-1} = 2 \times 10^8 \qquad (7.25)$$

ORDE experiments in which the concentration of Fe(III) was varied suggest that the current at the electrode (and thus the quantum efficiency for production of the π-radical cation) goes through a maximum as the ferric concentration increases. These findings have since been confirmed by flash photolysis[87] and by the ORDE technique[88] at pH 2.5. The existence of an optimum ferric concentration can be explained in terms of the following mechanism:

Table 7.6

Results for the Fe/ZnTMPyP System

	$[Fe(II)]_{added} = 0$	$[Fe(II)]_{added} = 0.13$ mM
$[ZnTMPyP^{4+}]$/mM	0.70	1.2
X_ε/cm	3.2×10^{-3}	1.9×10^{-3}
$i_{h\nu}$/μA	77	44
$k_?/s^{-1}$	1.4×10^{3}	2.1×10^{3}
$k_{-7}/M^{-1}s^{-1}$	1×10^{8}	1×10^{8}

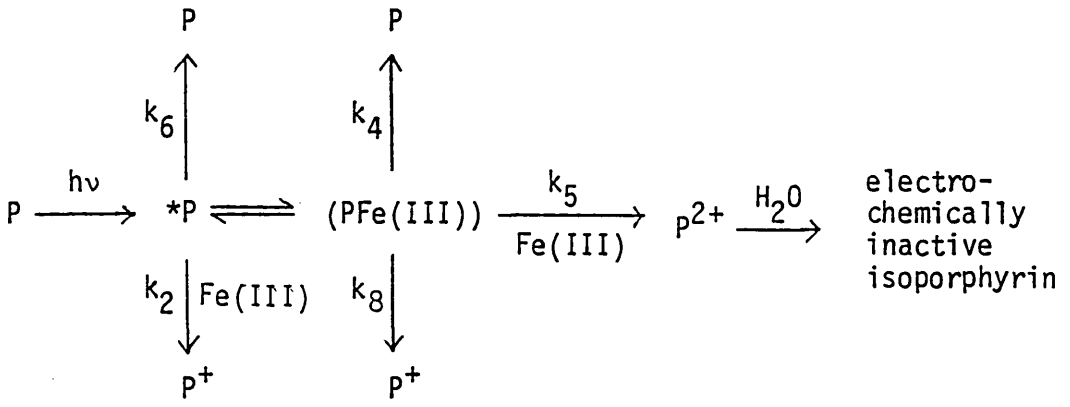

(7.39)

where P is the ground-state metalloporphyrin $ZnTMPyP^{4+}$, the triplet of which can form a complex with Fe(III). The quantum efficiency for production of the radical cation $ZnTMPyP^{5+}$ (P^+ in this notation) is given by

$$\phi = \frac{k_2[{}^*P][Fe(III)] + k_8[C]}{k_6[{}^*P] + k_2[{}^*P][Fe(III)] + k_8[C] + k_4[C] + k_5[Fe(III)][C]} \tag{7.40}$$

where [C] is the concentration of the porphyrin-ferric complex (PFe(III)), and where

$$[C] = K[{}^*P][Fe(III)] \tag{7.41}$$

Eliminating [C] and [*P] we obtain

$$\phi = \frac{k_2[Fe(III)] + k_8 K[Fe(III)]}{k_6 + k_2[Fe(III)] + k_8 K[Fe(III)] + k_4 K[Fe(III)] + k_5 K[Fe(III)]^2} \tag{7.42}$$

When [Fe(III)] is very small, the k_6 term dominates the denominator of this expression. Increasing the concentration of added ferric ion increases ϕ, and thus the current at the ORDE increases. When the solution contains a substantial concentration of ferric ion, the $k_5K[Fe(III)]^2$ term is dominant and increasing the ferric concentration decreases ϕ. This means that when the ferric concentration is high, increasing [Fe(III)] decreases the current at the electrode.

In our calculations we have assumed that k_4 is negligible and that the k_6 term is also negligible under the conditions of the experiment (i.e. the solution contains a substantial concentration of Fe(III)). In this case we have

$$\phi = 1 \Big/ \left(1 + \frac{k_5 K_q \ Fe(III)}{k_2 + k_8 K_q} \right) \tag{7.43}$$

This expression has the same form as equation (7.30) and comparing the two equations we find that

$$K_q = \frac{k_5 K}{k_2 + k_8 K} \tag{7.44}$$

where K_q is the Stern-Volmer quenching constant.

The above hypothesis is tentative and we have not characterised the products of the reaction between P* and Fe(III) at high ferric concentration. However this mechanism explains the maximum in photocurrent observed as the ferric concentration is increased in an ORDE experiment. This has important consequences for the efficiency of a porphyrin

photogalvanic cell because it reveals a further limit to the yield of electroactive products of the photoredox reaction.

7.11. Implications for a Metalloporphyrin Photogalvanic Cell

The metalloporphyrins have many attributes which make them suitable compounds for a photogalvanic cell. They are cheap, easy to synthesize and have strong absorbances in the visible region of the spectrum. Because they have long triplet state lifetimes and triplet quantum yields approaching unity they readily undergo photoredox reactions. Compared to the thiazine dyes, metalloporphyrins have a high solubility in water and so a high concentration of chromophore can be employed.

In the design of a metalloporphyrin photogalvanic cell there are however many problems to be overcome. The ZnTMPyP/Fe system requires an acidic medium to prevent the precipitation of Fe(III) as ferric hyroxide. Demetallation of the porphyrin is catalysed by protons and thus even in the dark the metalloporphyrin is unstable in solution. This tendency for porphyrins to demetallate in acidic solution restricts the range of pH at which a cell could operate.

Many metalloporphyrins, particularly anionic species, are prone to aggregation and this has important consequences for a photogalvanic cell. The rate of internal conversion from the first excited singlet state of a dimer greatly exceeds that of the corresponding monomer[71]. As was observed for the thiazine photogalvanic cell[18], useful photochemistry can only be obtained from the monomer species and so a significant amount of dimerisation severely reduces the efficiency of the cell.

In this work we have shown that for the ZnTMPyP/Fe system there is an optimum concentration of ferric required to maximise the yield of porphyrin π-radical cation. For other photogalvanic systems, e.g. those

using thiazines and $[Ru(bpy)_3]^{2+}$, increasing the concentration of quencher merely increases the yield of electroactive species until a plateau is reached. In the ZnTMPyP/Fe system, the concentration of quencher must not be too large, or the unfavourable Stern-Volmer quenching term will reduce the efficiency of the cell.

In chapter one we stated that the rate constant for the reverse electron quenching reaction should be less than 6×10^3 M^{-1} s^{-1}. However, for the ZnTMPyP/Fe system we have found that the rate constant is 1×10^8 M^{-1} s^{-1}, which is very high and much higher than for those systems using thiazine dyes. For the cell to operate efficiently there must be a sufficient concentration of Fe(II) present to pass current at the dark electrode. This requirement places a severe limitation on the power available from a metalloporphyrin photogalvanic cell as the precious porphyrin π-radical cation is rapidly removed by reaction with Fe(II), even at comparatively low concentrations of ferrous.

Harriman and Williams[72] have constructed a ZnTMPyP/Fe photogalvanic cell and have studied the effects of various parameters on the efficiency. A detailed analysis of the photogalvanic cell has been performed by Albery and co-workers[31]. An important conclusion of their work was that for a successful cell, the rate of the back reaction between the products of the photoredox reaction must be low. The very high rate of this reaction in the ZnTMPyP/Fe system is one of the major reasons why Harriman and Williams were foiled in their attempt to build an efficient cell. They found a power conversion efficiency of about 10^{-3}%.

In their paper, Harriman and Williams report the variation of photovoltage with ferric concentration. In view of our work it would be interesting to measure the effect of [Fe(III)] on the photocurrent

available from a cell. Our experiments predict that in a thin-layer cell, the photocurrent will decrease as [Fe(III)] is increased above about 10^{-4} M.

REFERENCES

1. E. Becquerel, *Compt. Rend.* 9, 145 (1939).
2. A.J. Nozik, *Ann. Rev. Phys. Chem.* 29, 189 (1978).
3. A. Heller, *Acc. Chem. Res.* 14, 154 (1981).
4. M. Matsumura, Y. Nomura and H. Tsubomura, *Bull. Chem. Soc. Jpn.* 50, 2533 (1977).
5. W. Arden and P. Fromherz, *J. Electrochem. Soc.* 127, 370 (1980).
6. M.D. Archer and M.I.C. Ferreira, *Proc. Znth. Conf. Photochem. Convers. Storage Solar Energy* 3rd, 201 (1981).
7. W.J. Albery and M.D. Archer, *J. Electroanal. Chem.* 86, 19 (1978).
8. W.J. Albery and M.D. Archer, *Nature* 270, 399 (1977).
9. W.J. Albery and M.D. Archer, *J. Electroanal. Chem.* 86, 1 (1978).
10. C.T. Lin and N. Sutin, *J. Phys. Chem.* 80, 97 (1976).
11. F.S. Fisher, Ph.D. Thesis, Oxford (1979).
12. C. Daul, O.Haas, A. Lottaz, A. von Zelensky and H.-R. Zumbrunnen, *J. Electroanal. Chem.* 112(1), 51 (1980).
13. J. Weiss, *Nature* 136, 794 (1935).
14. E. Rabinowitch, *J. Chem. Phys.* 8, 560 (1940).
15. M.D. Archer, M.I.C. Ferreira, G. Porter and C.J. Tredwell, *Nouveau Journal de Chimie* 1, 9 (1977).
16. M.I.C. Ferreira and A. Harriman, *Faraday Trans. I* 73, 1085 (1977).
17. C.G. Hatchard and C.A. Parker, *Trans. Faraday Soc.* 54, 1093 (1961).
18. W.J. Albery and A.W. Foulds, *J. Photochem.* 10, 4 (1979).
19. J.C.M. Brokken-Zijp and M.S. de Groot, *Chem. Phys. Letts.* 76, 1 (1980).
20. H.J. Conn, *Biological Stains*, Williams and Wilkins, Baltimore, MD, 7th edn. (1961).
21. W.J. Albery and A.W. Foulds, *J. Photochem.* 15, 321 (1981).
22. W.R. Bowen, *Acta. Chem. Scand.* A35, 311 (1981).

23. P.D. Wildes, N.N. Lichtin and M.Z. Hoffman, *Photochemistry and Photobiology* 25, 21-25 (1977).

24. K. Shigehara, M. Nishimura and E. Tsuchida, *Electrochimica Acta* 23, 855 (1978).

25. K. Shigehara, H. Sano and E. Tsuchida, *Macromol. Chem.* 179, 1531 (1978).

26. J. Cornelia, M. Brokken-Zijp and F.J. Reinders, British Patent No. 1 557 627 filed May 27, 1977, complete specifications published Dec. 12, 1979.

27. R. Havemann and K.G. Reimer, *Z. Phys. Chem. Leipzig* 211, 26 (1959).

28. T.L. Osif, N.N. Lichtin and M.Z. Hoffman, *J. Phys. Chem.* 82, 1778 (1978).

29. P.V. Kamat, M.D. Karkhanavala and P.N. Moorthy, *J. Phys. Chem.* 85, 810 (1981).

30. P.D. Wildes, D.R. Hobart, N.N. Lichtin, D.E. Hall and J.A. Eckert, *Solar Energy* 19, 567 (1977).

31. W.J. Albery, *Accounts of Chemical Research* 15, 142-8 (1982).

32. A.T. Chadwick, D. Phil. Thesis, Oxford (1979).

33. A.R. Hillman, D. Phil. Thesis, Oxford (1979).

34. N. Goddard, Private Communication.

35. C.C. Herrman, G.P. Perrault and A.A. Pilla, *Anal. Chem.* 40, 1173 (1968).

36. Z.M. Jarzebski and J.P. Marton, *J. Electrochem. Soc.* 123, 345c (1976).

37. P.N. Bartlett, Ph.D. Thesis, London (1981).

38. M.W. Heslop, Private Communication.

39. A.J. Bard and L.R. Faulkner 'Electrochemical Methods', Wiley, New York (1980).

40. W.J. Blaedel and L.W. Klatt, *Anal. Chem.* 38, 879 (1966).

41. J. Yamada and H. Matsuda, *J. Electroanal. Chem.* 44, 189 (1973).

42. J. Nasielski, A. Kirsch-DeMesmaker and P. Leempoel, *Electrochim. Acta.* 23, 605 (1978).

43. W.J. Albery and M.L. Hitchman, 'Ring Disc Electrodes', Oxford University Press (1971).

44. W.J. Albery, 'Electrode Kinetics', Oxford Chemistry Series (1975).

45. T. von Karman, *Z. Agew. Math. Mech.* 1, 233 (1921).

46. V.G. Levich, *Acta Physicochem. URSS*, 17, 257 (1942).

47. W.J. Albery, M.D. Archer, N.J. Field and A.W. Turner, *Disc. Faraday Soc.* 56, 28 (1973).

48. W.J. Albery, M.D. Archer and R.G. Egdell, *J. Electroanal. Chem.* 82, 199 (1977).

49. W.J. Albery, W.R. Bowen, F.S. Fisher and A.D. Turner, *J. Electroanal. Chem.* 107, 1 (1980).

50. W.J. Albery, P.N. Bartlett, W.R. Bowen, F.S. Fisher and A.W. Foulds, *J. Electroanal. Chem.* 107, 23 (1980).

51. Y. Oksawa and S. Aoyagui, *J. Electroanal. Chem.* 90, 143 (1978).

52. S.P. Perone and H.D. Drew, 'Analytical Photochemistry and Photochemical Analysis, Solids, Solutions and Polymers', ed. J.M. Fitzgerald, Marcel Dekker Inc., New York (1981), 213.

53. W.J. Albery, F.S. Fisher and C.A.E. Daul, *J. Electroanal. Chem.* 124, 189 (1981).

54. M. Abramovitz and I.A. Stegun, 'Handbook of Mathematical Functions', Dover, New York (1965).

55. W.J. Albery, P.N. Bartlett, J.P. Davies, A.W. Foulds, A.R. Hillman and F.S. Bachiller, *Farad. Discuss.* 70, 341 (1980).

56. D.E. Hall, J.A. Eckert, N.N. Lichtin and P.D. Wildes, *J. Electrochem. Soc.* 123, 1705 (1976).

57. W.J. Albery, M.G. Boutelle, P.J. Colby and A.R. Hillman, *J. Electroanal. Chem.* 133, 135 (1982).

58. R.A. Whiteker and N. Davidson, *J. Amer. Chem. Soc.* 75, 3081 (1953).

59. W.M. Clark, B. Cohen and H.D. Gibbs, *U.S. Public Health* 40, 1131 (1925).

60. F. Souto-Bachiller, Private Communication.

61. S. Wilson, Private Communication.

62. G.R. Haugen and E.R. Hardwick, *J. Phys. Chem.* 67, 725 (1963).

63. R. Bonneau and R.D.S. Stevens, *Chem. Phys. Letts.* 13, 376 (1972).

64. J. Faure, R. Bonneau, J. Jousset-Dubien, *Photochem. Photobiol.* 6, 331 (1976).

65. C.G. Hatchard and C.A. Parker, *Trans. Faraday Soc.* 57, 1093 (1961).

66. M.L. Hitchman and W.J. Albery, *Electrochim. Acta* 17, 787 (1972).

67. M.A. West, 'Creation and Detection of Excited States', ed. W.R. Ware (Marcel Dekker, New York, 1976), vol. 4.

68. G. Porter and M.A. West in 'Techniques of Chemistry', Vol. VI Part II, G.G. Hammes, Ed., Wiley-Interscience, New York, 1974, Chap. X.

69. F.W. Willets, *Progress in Reaction Kinetics* 6, 51 (1972).

70. R.V. Bensasson, E.J. Land and T.G. Truscott, 'Flash Photolysis and Pulse Radiolysis - Contributions to the Chemistry of Biology and Medicine', Pergamon Press, 1983.

71. P.G. Bowers and G. Porter, *Proc. R. Soc. London* 296, 435 (1968).

72. A. Harriman and D. Williams, *J. Electroanal. Chem.* 139, 413 (1982).

73. R.F. Pasternak, L. Francesconi, D. Raff and E. Spiro, *Inorg. Chem.* 12, 2606 (1973).

74. R.F. Pasternak, H. Lee, P. Malek and C. Spencer, *J. Inorg. Chem.* 39, 1865 (1977).

75. E.B. Fleischer, J.M. Palmer, T.S. Strivatsava and A. Chatterjee, *J. Am. Chem. Soc.* 93, 3162 (1971).

76. P. Hambright, *Inorg. Chem.* 16, 2987 (1977).

77. P. Hambright and E.B. Fleischer, *Inorg. Chem.* 9, 1757 (1970).

78. K. Kalyanasundaram and M. Neumann-Spallart, *J. Phys. Chem.* 86, 5163 (1982).

79. A. Harriman, G. Porter and P. Walters, *J. Chem. Soc., Faraday Trans. I*, 79, 1335 (1983).

80. 'Porphyrins and Metalloporphyrins', Ed. K.M. Smith, Elseveier Scientific Publishing Co. 1975, p. 609.

81. A. Harriman, G. Porter and M.C. Richoux, *J. Chem. Soc. Faraday Trans. 2*, 77, 833 (1981).

82. A.J. Bard and L.R. Faulkner, 'Electrochemical Methods, Fundamentals and Applications', J. Wiley and Sons, New York, p. 239.

83. M. Neumann-Spallart and K. Kalyanasundaram, *Z. Naturforsch* 36B, 596 (1981).

84. W.J. Albery, A.R. Hillman and S. Bruckenstein, *J. Electroanal. Chem.* 100, 687 (1979).

85. W.J. Albery and M.L. Hitchman, 'Ring-Disc Electrodes', Clarendon Press, Oxford (1971) p. 122 *et seq.*

86. J.R. Darwent, P. Douglas, A. Harriman, G. Porter and M.C. Richoux, *Coord. Chem. Revs.* 44, 83 (1982).

87. J. Porter, Private Communication.

88. Z. Shu, Private Communication.

* * * * * * *